

JSAT

Journal of Science and Agricultural Technology

e-ISSN 2730-1532, ISSN 2730-1524

J. Sci. Agric. Technol.

Vol. 4 | No. 2 | July - December 2023

<https://www.tci-thaijo.org/index.php/JSAT>

Journal of Science and Agricultural Technology



J. Sci. Agri. Technol. (2023) Vol. 4 (2)

EDITORIAL TEAM

Advisory Board

Emeritus Prof. Dr. Liang Chou Hsia,
Prof. Dr. Monchai Duangjinda,
Asst. Prof. Dr. Jutturit Thongpron,
Assoc. Prof. Dr. Wasu Pathom-aree

National Pingtung University of Science and Technology, Taiwan
Khon Kaen University, Thailand
Rajamangala University of Technology Lanna, Thailand
Chiang Mai University, Thailand

Editor-in-Chief

Assoc. Prof. Dr. Suntorn Wittayakun

Rajamangala University of Technology Lanna, Thailand

Editors

Assoc. Prof. Dr. Kecha Kuha,
Dr. Sakuntala Saijai

Rajamangala University of Technology Lanna, Thailand
Rajamangala University of Technology Lanna, Thailand

Associate Managing Editors

Asst. Prof. Dr. Rattanaporn Norarat,
Asst. Prof. Dr. Supawadee Sriyam,
Asst. Prof. Dr. Wanich Limwanich,
Asst. Prof. Dr. Nongnuch Ketui,
Asst. Prof. Dr. Tanongsak Sassa-deepaeng,
Dr. Rungrawee Thongdon-a

Rajamangala University of Technology Lanna, Thailand
Rajamangala University of Technology Lanna, Thailand

Editorial Board Members

Prof. Dr. Koichi Takaki,
Prof. Dr. Jun Ogawa,
Prof. Dr. Yoshikatsu Ueda,
Prof. Dr. A.K. Thiruvankadan,
Prof. Dr. Jatuporn Wittayakun,
Prof. Dr. Leonel Avedaño-Reyes,
Prof. Dr. Ir. Suyadi,
Prof. Dr. Ir. Yusuf Leonard Henuk,
Prof. Dr. Vincent Ru-Chu Shih,
Assoc. Prof. Dr. Dang Van Dong,
Assoc. Prof. Dr. Sanchai Prayoonpokarach,
Assoc. Prof. Dr. Saroj Ruijirawat,
Assoc. Prof. Dr. Yaowapha Jirakiattikul,
Asst. Prof. Dr. Chalermpon Yuangklang,
Asst. Prof. Dr. Panumart Rithichai,
Asst. Prof. Dr. Sasitorn Nakthong,
Dr. Chhun Tory,
Dr. Ir. Marjuki,
Dr. Julia Mayo-Ramsay,
Dr. Nguyen Van Hue

Iwate University, Japan
Kyoto University, Japan
Kyoto University, Japan
Tamilnadu Veterinary and Animal Sciences University, India.
Suranaree University of Technology, Thailand
Universidad Autónoma de Baja California, México
Brawijaya University, Indonesia
University of Sumatera Utara, Indonesia
National Pingtung University of Science and Technology, Taiwan
Fruit and Vegetable Research Institute, Hanoi, Vietnam
Suranaree University of Technology, Thailand
Suranaree University of Technology, Thailand
Thammasat University, Thailand
Rajamangala University of Technology Isan, Thailand
Thammasat University, Thailand
Kasetsart University, Thailand
Prek Leap National College of Agriculture, Cambodia
Brawijaya University, Indonesia
Department of Justice, New South Wales, Australia
Hue University of Agriculture and Forestry, Vietnam

Technical Editors

Mr. Wanchana Joobanjong,
Asst. Prof. Wiraiwan Sanchana,
Miss Paweesuda Bussayatanin

Rajamangala University of Technology Lanna, Thailand
Rajamangala University of Technology Lanna, Thailand
Rajamangala University of Technology Lanna, Thailand

Welcome message from Editor-in-Chief

Dear authors, reviewers, and readers

We are honored to present the second issue of the fourth volume of the Journal of Science and Agricultural Technology (JSAT), the official journal of the Faculty of Science and Agricultural Technology, Rajamangala University of Technology Lanna (RMUTL), Thailand. This issue includes one review article and six research articles from various institutions that contributed to this issue. The JSAT has been published in *Thai Journal Online* (ThaiJO), indexed in Google Scholar, Thai Citation Index (TCI), and Digital Object Identifier (DOI) under the National Research Council of Thailand. The journal will publish high-quality articles under an intense peer-review process with solid support from various educational institutions domestically and abroad.

As an Editor-in-Chief, I am so grateful for the support from our submitting authors, reviewers, and staff. I promise to move forward to gain international recognition, preparing for further higher index ranking. In addition, I strongly encourage researchers around the globe to submit manuscripts to share knowledge and promote the growing field of science and agricultural technology.

Best regards,

Assoc. Prof. Dr. Suntorn Wittayakun

Editor-in-Chief Journal of Science and Agricultural Technology
Faculty of Science and Agricultural Technology
Rajamangala University of Technology Lanna, Thailand.

ABOUT THE JOURNAL

Journal of Science and Agricultural Technology (JSAT) publishes original research contributions covering science and agricultural technology such as:

- Natural and applied sciences: biology, chemistry, computer science, physics, material science and related fields. Papers in mathematics and statistics are also welcomed, but should be of an applied nature rather than purely theoretical.
- Agricultural technology: plant science, animal science, aquatic science, food science, biotechnology, applied microbiology, agricultural machinery, agricultural engineering and related fields.

Furthermore, the JSAT journal aims to span the whole range of researches from local to global application.

The JSAT is published two issues a year.

Issue 1: January - June

Issue 2: July - December

Submissions are welcomed from international and Thai institutions. All submissions must be original research not previously published or simultaneously submitted for publication or submitted to other journals. Manuscripts are peer reviewed using the double-blinded review system by at least 3 reviewers before acceptance. There is no publication or processing fee.

The journal financial support is provided by Rajamangala University of Technology Lanna, Thailand.

Editorial office:

*Faculty of Science and Agricultural Technology,
Rajamangala University of Technology Lanna,
128 Huaykaew Rd., Changphuek, Muang, Chiang Mai, 50300 Thailand.
Tel/Fax: +665392 1444 Ext. 1506*

CONTENTS

	Page
Review article:	
<i>Trichoderma</i> : Biology, ecology and <i>Trichoderma</i> -plant and <i>Trichoderma</i> -pathogen interactions Payungsak Rauyaree and Tassanaporn Tadsakorn	1 - 4
Research article:	
Adsorption of methylene blue dye onto the natural liquid sugars-based carbon: Kinetic and thermodynamic Atit Wannawek, Yanee Keereeta, Pongthep Jansanthea, Watee Panthuwat, Tanongsak Sassa-deepaeng and Pusit Pookmanee	5 - 21
Influenced factors for cotton dyeing process with mangosteen leaf extract Waranya Tharawatchruk, Pat Pranamornkith, Supinan Janma, Watee Panthuwat, Narit Funsueb and Tanongsak Sassa-deepaeng	22 - 30
Accuracy of genomic breeding values estimated from simulation of the dairy cattle population of northern Thailand Sirijanya Aryuman, Nattaphon Chongkasikit, Chirawath Phatsara, Saowaluck Yammuen-art, Krasit Vasupen, Chot Rachwicha and Chalernporn Jirapanyalert	31 - 38
Effect of extraction time on the amounts of neurotransmitters and amino acids in chicken essence Sauwanit Wutthikrairat, Yi-Chen Chen, Patcharaporn Tinchan, Arsooth Sanguankiat and Sasitorn Nakthong	39 - 45
Effect of ozone micro-nano bubbles on longan shelf life extension Panadda Kidtuengkun, Preuk Choosung, Parinyawadee Sritontip and Chiti Sritontip	46 - 52
Effects of humic acid on growth and development of melon in nutrient solution culture Pimrumpa Samran, Parinyawadee Sritontip and Chiti Sritontip	53 - 57

Trichoderma: Biology, ecology and Trichoderma-plant and Trichoderma-pathogen interactions

Payungsak Rauyaree^{1*} and Tassanaporn Tadsakorn²

¹Biotechnology Research and Development Office, Department of Agriculture, Rangsit-Nakhon Nayok Road, Thanyaburi District, Pathumthani 12110, Thailand

²Plant Protection Research and Development Office, Department of Agriculture, 50 Phaholyothin Road, Ladyao, Chatuchak, Bangkok 10900, Thailand

*Corresponding author: payungsak_r@yahoo.com

Received: March 14, 2023. Revised: August 30, 2023. Accepted: October 19, 2023.

ABSTRACT

The fungal genus *Trichoderma*, belonging to the family *Hypocreaceae*, Eucaryota, Ascomycota, consists of more than 200 species and ecologically resides in most soils in the roots of plants as a rhizosphere-competent and in the part of plants as avirulent opportunistic symbionts, in the decaying woods and organic matters as saprophytes. However, to study the biology, ecology, and plant-*Trichoderma*-pathogen networking, it is essential to understand the colonization of host plant roots, plant growth promotion, root hair development, yield or crop productivity, induced systemic resistance, and prime plant defense. The objective of this review paper was to describe the *Trichoderma* functions which can attack, invade, and inhibit other types of fungi or microbes as biocontrol agents through the mechanisms called antagonistic organisms, antibiosis, nutrient and space competition, mycoparasitism, endophytic colonization, and inactivation of plant pathogen's enzymes. This review summarizes an overview of the biology, ecology, and knowledge background of *Trichoderma*-plant and *Trichoderma*-pathogen interactions.

Keywords: *Trichoderma*, biocontrol agents, *Trichoderma*-plant-pathogen interactions

INTRODUCTION

The hyphomycetes genus biocontrol agents, *Trichoderma* is a soil-well-grown or saprophyte organism (Klein and Eveleigh, 1998). The genus includes more than 200 recognized species (Samuels, 2006; Barroncelly et al., 2015). *Trichoderma* are naturally free-living organisms and abundantly found in many different substrates, living plant-animal, organic debris, and virtually most soils. The utilization of *Trichoderma* spp. resulted in many agricultural advantages such as plant physiology, productivity, and plant disease suppression. They colonize plant roots and attack other plant pathogenic fungi, recognized as biocontrol agents for controlling or reducing many important severe plant diseases. Plant roots are one of the essential parts of the plants where *Trichoderma* can be found, resulting in plant development and crop productivity (Ming et al., 2012; Pecoraro et al., 2012; Chaverri and Samuels, 2013).

Overall, the interaction of the *Trichoderma*, host plants, and pathogens includes plant nutrient sequestration, space competitions, antibiosis, cell-wall-degrading enzyme production, endophytic and rhizosphere colonization. (Benítez et al., 2004; Engelberth et al., 2003; Reino et al., 2008; Bhale and

Rajkonda 2012; Munir et al., 2014; Ranveer et al., 2018). As mentioned, even though synthetic fungicides or chemical use are widely used to control plant diseases, a potentially high risk to humans and the environment makes this biocontrol agent *Trichoderma*, even more effective. (Harman, 2006; Akrami and Yousefi, 2015).

At the molecular level, it has been found that *Trichoderma* phenolic and signaling compounds are transferred to other parts of the plants, resulting in PR gene (resistant gene production) (Yedidia et al., 2000), and the pathogenic resistance called SR (systemic acquired resistance). PR proteins (pathogenesis-related proteins) result from the PR gene (Van Loon and Van Strien, 1999; Parker, 2000; Heil and Bostock, 2002; Sallam et al., 2019).

Trichoderma can be used as a low-cost, effective, and eco-friendly alternative biofungicide to control plant diseases instead of using synthetic and toxic fungicides. (Sharma et al., 2019; Sallam et al., 2019). This makes many *Trichoderma* species beneficial microorganisms as commercial biofertilizers and biopesticides (Whipps and Lumsden, 2001; Perotto et al., 2013) and climate resilient agriculture.

Biology

Trichoderma spp. is a soil-borne or saprophyte organism (Klein and Eveleigh, 1998). The shaped-form concentric pattern is a common characteristic of *Trichoderma* spp. Natural carbon in the form of monosaccharides, disaccharides, and nitrogen sources could be utilized by this type of fungi for their growth purposes (Danielson and Davey, 1973b). The *Trichoderma* sporulation characteristic, called conidia, makes this genus grow well on both natural and artificial substrates. This is due to the light and dark responses on the particular day in which conidia will be produced in the period of daylight (Gressel and Hartmann, 1968). The germination of *Trichoderma* conidia could be easily found in various nutrient sources (Danielson and Davey, 1973c). Lewis and Papavizas (1983) reported that 75% of chlamydo-spores or fresh conidia of *Trichoderma* can be grown on agar media. One main characteristic of this fungi is to produce secondary metabolite or synthetic compounds such as terpenoids, pyrones, indolic-derived compounds, etc. (Contreras-Cornejo et al., 2016).

Ecology

The fungal *Trichoderma* can be isolated from well-degrading organic materials (Danielson and Davey, 1973a) and found in nearly all natural nutrient supplies (Cai et al., 2022). The ecology study of *Trichoderma* spp. would help to increase the information regarding this genus's lives and activities in different habitats. This will also help to increase the knowledge about population dynamics in nature, including soils, root rhizosphere, root surface, and physical, chemical, and biological environments affecting fungal lives, activities, and survives. The sporulation of *Trichoderma* called conidia grows well on both natural and artificial substrates. On the chemical substrate, Lewis and Papavizas (1983) indicated that the germination rate of fresh conidia or chlamydo-spores is 75% on agar media. The shaped-form concentric pattern is a common characteristic of *Trichoderma* spp. This is due to the responses of light and dark in the individual day in which conidia will be produced in the daylight period (Gressel and Hartmann, 1968).

Trichoderma-plant and *Trichoderma*-pathogen interactions

Trichoderma-plant interactions

According to its free-living organism characteristic, several *Trichoderma* strains induce root branching, plant root colonization, and increase

root biomass as a consequence of cell division, expansion, and differentiation by the presence of fungal auxin-like compounds (Contreras-Cornejo et al., 2016). *Trichoderma* is attracted by chemical signals released by plant roots. The initial steps of symbiosis establishment involve the attachment and penetration process. During plant-*Trichoderma* interactions, this process promotes plant growth-promoting biocontrol agents for crop plants, enhances plant fitness under biotic and abiotic stresses, alleviates environmental in plants, nutrient uptake, signaling pathways of induced disease resistance or induced-resistance in the plant, and environmental effects in soil on plants (Kuc, 2001; Colla et al., 2015; Shores et al., 2010).

The fungal genus of *Trichoderma* is also crucial due to its plant growth and performance-promoting effects, such as improved nutrient supply, mycoparasitism of plant pathogens, and priming of plant defense. *Trichoderma* is considered the filamentous fungi that can be used in agriculture PGRF or as plant growth-promoting fungi, which is essential in increasing plant defense, in controlling plant diseases or even nematodes (Hermosa et al., 2013; Stewart and Hill, 2014; Monfil and Casas-Flores, 2014; Oskiera et al., 2015). *Trichoderma* species could be used to sustain crop productivity. Many *Trichoderma* species are used as biofertilizers (Mahato et al., 2018; Ranveer et al., 2018). For example, biofertilizers use against many pathogenic fungi to increase crop growth, such as *Fusarium*, *Rhizoctonia*, *Pythium*, *Schlerotinia*, *Verticillium*, *Alternaria*, *Phytophthora* and other plant pathogenic fungi (Abu-Taleb et al., 2011, Whipps and Lumsden, 2001). They are reported to improve photosynthetic efficiency, enhance nutrient uptake, and increase crop nitrogen use efficiency. In addition, they can be used to facilitate plant adaptation and mitigate adverse effects of climate change. From the study of Colla et al. (2015), the co-cultivation of *Glomus intraradices* and *Trichoderma atroviride*, acts as a biostimulant to promote growth, yield, and nutrient uptake of vegetative crops.

Trichoderma-pathogen interactions

Trichoderma acts as plant disease control, antibiosis and secondary metabolite or volatile organic compound synthesis, mycoparasitism, and competition characteristics against various plant pathogens. The important mycoparasitic biocontrol agents against plant pathogen *Trichoderma* can inhibit growth, penetrate, and kill various fungal plant pathogens involving the hydrolytic enzymes through cell-wall-degrading enzymes (CWDE) activities (Bae et al., 2017; Mukherjee et al., 2012a).

The antibiotics and competition with pathogens (carbon and nitrogen sources, space and infection sites and soil microbial community, and enzymes responsible for secondary metabolite production and also antifungal compounds called volatile organic compounds (Guo et al., 2019; Vinale et al., 2008; Mukherjee et al., 2012b). For example, Crutcher et al. (2013) identified a putative terpene cyclase, *vir4*, is responsible for the biosynthesis of volatile terpene compounds in *T. virens*.

CONCLUSIONS

Trichoderma biology, ecology, *Trichoderma*-plant, and *Trichoderma*-pathogen interactions have been well-studied. This review paper may lead to a better understanding related to genomics and proteomics study, bioinformatics, CAZymes, comparative genome sequence analysis, CRISPR-Cas or gene editing, metabolomics, transcriptomics, and *Trichoderma* gene and protein database development. This knowledge toward the collated information will allow to gain more information in important *Trichoderma* species in the future.

REFERENCES

- Abu-Taleb, A.M., El Deeb, K., and Al-otibi, F. 2011. Assessment of antifungal activity of *Rumex vesicarius* L. and *Ziziphus spin-Christi* (L.) Willd. extracts against two phytopathogenic fungi. *Afr. J. Microbiol. Res.* 5(9): 1001–1011.
- Akrami, M., and Yousefi, Z. 2015. Biological control of Fusarium wilt of tomato (*Solanum lycopersicum*) by *Trichoderma* spp. as antagonist fungi. *BFAIJ.* 7(1): 887–892.
- Bae, S-J., Park, Y-H, Bae, H-J., Jeon, J., and Bae, H. 2017. Molecular identification, enzyme assay, and metabolic profiling of *Trichoderma* spp. *J. Microbiol. Biotechnol.* 27(6): 1157–1162.
- Baroncelli, R., Piaggesechi, G., Fiorini, L., Bertolini, E., Zapparata, A., Pè, M.E., Sarrocco, S., and Vannacci, G. 2015. Draft whole-genome sequence of the biocontrol agent *Trichoderma harzianum* T6776. *Genome Announc.* 3(3): 1–2.
- Benítez, T., Rincón, A.M., Limón, M.C., and Codón, A.C. 2004. Biocontrol mechanisms of *Trichoderma* strains. *Int. Microbiol.* 7(4): 249–260.
- Bhale, U.N., and Rajkonda, J.N. 2012. Evaluation of distribution of *Trichoderma* spp. in soils of Marathwada region of Maharashtra during 2007–2011. *J. Mycol. Plant Pathol.* 42: 505–508.
- Cai, F., Dou, K., Wang, P., Chentamara, K., Chen, J., and Druzhinina, I.S. 2022. The current state of *Trichoderma* taxonomy and species identification. In: Amaran, N., Sankaranarayanan, A., Dwivedi, M.K. and Druzhinina, I.S. (eds) *Advances in Trichoderma biology for agricultural applications*. Springer International Publishing. p.3–35.
- Chaverri, P., and Samuels, G.J. 2013. Evolution of host affiliation and substrate preference in the cosmopolitan fungal genus *Trichoderma* with evidence of interkingdom host jumps. *Evolution.* 67: 2823–2837.
- Colla, G., Roupael, Y., Di Mattia, E., El-Nakhel, C., and Cardarelli, M. 2015. Co-inoculation of *Glomus intraradices* and *Trichoderma atroviride*, acts as a biostimulant to promote growth, yield and nutrient uptake of vegetative crops. *J. Sci. Food. Agric.* 95: 1706–1715.
- Contreras-Cornejo, H.A., Macías-Rodríguez, L., Del-Val, E., and Larsen, J. 2016. Ecological functions of *Trichoderma* spp. and their secondary metabolites in the rhizosphere: Interaction with plants. *FEMS Microbiol. Ecol.* 92(4): fiw036. <https://doi.org/10.1093/femsec/fiw036>.
- Crutcher, F.K., Parich, A., Schuhmacher, R, Mukherjee, P.K., Zeilinder, S., and Kenerley, C.M. 2013. A putative terpene cyclase, *vir4*, is responsible for the biosynthesis of volatile terpene compounds in the biocontrol fungus *Trichoderma virens*. *Fungal genet. biol.* 56: 67–77.
- Danielson, R.M., and Davey, C.B. 1973a. The abundance of *Trichoderma* propagules and the distribution of species in forest soils. *Soil Biol. Biochem.* 5: 485–494.
- Danielson, R.M., and Davey, C.B. 1973b. Carbon and nitrogen nutrition of *Trichoderma*. *Soil Biol. Biochem.* 5: 505–515.
- Danielson, R.M., and Davey, C.B. 1973c. Effects of nutrients and acidity on phialospore germination of *Trichoderma in vitro*. *Soil Biol. Biochem.* 5: 517–524.
- Engelberth, J., Schmelz, E.A., Alborn, H.T., Cardoza, Y.J., Huang, J., and Tumlinson, J.H. 2003. Simultaneous quantification of jasmonic acid and salicylic acid in plants by vapor-phase extraction and gas chromatography-chemical ionization-mass spectrometry. *Anal. Biochem.* 312(2): 242–50.
- Gressel, J.B., and Hartmann, K.M. 1968. Morphogenesis in *Trichoderma*: Action spectrum of photoinduced sporulation. *Planta.* 79: 271–274.
- Guo, Y., Ghirardo, A., Weber, B., Schnitzler, J-P., Benz, J.P., and Rosenkranz, M. 2019. *Trichoderma* species differ in their volatile profiles and in antagonism toward ectomycorrhiza *Laccaria bicolor*. *Front Microbiol.* 10(891): 1–15.
- Harman, G.E. 2006. Overview of mechanisms and uses of *Trichoderma* species. *Phytopathology.* 96: 190–194.
- Heil, M., and Bostock, R.M. 2002. Induce systemic resistance (ISR) against pathogens in the context of induced resistance. *Ann. Bot.* 89: 503–512.
- Hermosa, R., Rubio, M.B., Cardoza, R.E., Nicolás, C., Monte, E., and Gutiérrez, S. 2013. The contribution of *Trichoderma* to balancing the costs of plant growth and defense. *Int. Microbiol.* 16: 69–80.
- Klein, D., and Eveleigh, D.E. 1998. Ecology of *Trichoderma*. In: Kubicek, C.P., and Harman, G.E. (eds.) *Trichoderma & Gliocladium*, Vol 1. Basic biology, taxonomy and genetics. Taylor & Francis, London p. 57–74.
- Kuc, J. 2001. Concepts and direction of induced systemic resistance in plants and its application. *Eur. J. Plant Pathol.* 107: 7–12.
- Lewis, J.A., and Papavizas, G.C. 1983. Chlamydo-spore formulation by *Trichoderma* spp. in natural substrate. *Can. J. Microbiol.* 30: 1–7.
- Mahato, S., Bhujju, S., and Shrestha, J. 2018. Effect of *trichoderma viride* as biofertilizer on growth and yield of wheat. *MJSA.* 2(2) (2018) 01–05.
- Ming, Q., Han, T.W., Zhang, Q., Zhang, H., Zheng, C., Huang, F., Rahman, K., and Qin, L. 2012. Tanshinone IIA and tanshinone I production by *Trichoderma atroviride* D16, an endophytic fungus in *Salvia miltiorrhiza*. *Phytomedicine.* 19: 330–333.

- Monfil, V.O., and Casas-Flores, S. 2014. Molecular mechanisms of biocontrol in *Trichoderma* spp. and their application in agriculture. In: Gupta V.K., Schmoll M., Herrera-Estrella A., Upadhyay, R.S. Druzhinina I., and Tuohy M.G. (eds.) Biotechnology and biology of *Trichoderma*. Elsevier, Amsterdam. p. 429–453.
- Mukherjee, M., Mukherjee, P.K., Horwitz, B.A., Zachow, Z., Berg, G., and Zeilinger, S. 2012a. *Trichoderma*-plant-pathogen interactions: Advances in genetics of biological control. Indian. J. Microbiol. 52(4): 522–529.
- Mukherjee, P. K., Horwitz, B. A., and Kenerley, C. M. 2012b. Secondary metabolism in *Trichoderma*—a genomic perspective. Microbiology. 158(Pt 1): 35–45.
- Munir, S., Jamal, Q., Bano, K., Sherwani, S.K., Abbas, M.N., Azam, S., Kan, A., Ali, S., Anees, M. 2014. *Trichoderma* and biocontrol genes: review. Sci Agric. 5: 40–45.
- Oskiera, M., Szczech, M., and Bartoszewski, G. 2015. Molecular identification of *Trichoderma* strains collected to develop plant growth-promoting and biocontrol agents. J. Hortic. Res. 23(1): 75–86.
- Parker, E.J. 2000. Signaling in plant disease resistance. In: Dickinson M. and Beynon J. (eds) Molecular plant pathology. Sheffield Academic Press, Sheffield. p. 198–217.
- Pecoraro, L., Perini, C., Persiani, A.M., Saitta, A., Sarrocco, S., Vannacci, G., Venanzoni, R., Perotto, S., Angelini, P., Bianciotto, V., Bonfante, P., Girlanda, M., Kul, T., Mello, A., Quilliam, R.S., and Jones, D.L. 2012. Evidence for specificity of culturable fungal root endophytes from the carnivorous plant *Pinguicula vulgaris* (common butterwort). Mycol Prog. 11: 583–585.
- Perotto, S., Angelini, P., Bianciotto, V., Bonfante, P., Girlanda, M., Kull, T., Mello, A., Pecoraro, L., Perini, C., Persiani, A.M., Saitta, A., Sarrocco, S., Vannacci, G., Venanzoni, R., Venturella, G., and Selosse, M.A. 2013. Interactions of fungi with other organisms. Plant Biosyst. 147:208–218.
- Ranveer, K. K., Victor, A., Yogendra, S. G., and Vivek, K. 2018. *Trichoderma*: A most common biofertilizer with multiple roles in agriculture. Biomed J Sci & Tech Res. 4(5) –2018. BJSTR.MS.ID.001107. <https://doi.org/10.26717/BJSTR.2018.04.001107>.
- Reino, J.L., Guerrero, R.F., Hernández-Galán, R., and Collado, I.G. 2008. Secondary metabolites from species of the biocontrol agent *Trichoderma*. Phytochem Rev. 7(1): 89–123.
- Sallam, N.M.A., Eraky, A.M.I. and Sallam, A. 2019. Effect of *Trichoderma* spp. on Fusarium wilt disease of tomato. Mol Biol Rep. 46: 4463–4470.
- Samuels, G.J. 2006. *Trichoderma* systematics, the sexual state, and ecology. Phytopathology. 96(2): 195–206.
- Sharma, S., Kour, D., Rana, K.L., Dhiman, A., Thakur, S., Thakur, P., Thakur, S., Thakur, N., Sudheer, S., Yadav, N., Yadav, A.N., Rastegari, A.A., and Singh, K. 2019. *Trichoderma*: Biodiversity, ecological significances, and industrial applications. In: Recent advancement in white biotechnology through fungi. Springer, Cham. p. 85–120.
- Shoresh, M., Harman, G.E., and Mastouri, F. 2010. Induced systemic resistance and plant responses to fungal biocontrol agents. Annu. Rev. Phytopathol. 48: 21–43.
- Stewart, A., and Hill, R. 2014. Applications of *Trichoderma* in plant growth promotion. In: Gupta V.K., Schmoll, M., Herra-Estrella A., Upadhyay R.S., Dru-zhinina I., and Tuohy M.G. (eds.) Biotechnology and biology of *Trichoderma*. Elsevier, Amsterdam. p. 415–428.
- Van Loon, L. C., and Van Strien., E.A. 1999. The families of pathogenesis-related proteins, their activities, and comparative analysis of PR-1 type proteins. Physiol. Mol. Plant Pathol. 55(2): 85–97.
- Vinale, F., Sivasithamparam, K., Ghisalberti, E.L., Marra, R., Woo, S.L., and Lorito, M. 2008. *Trichoderma*-plant-pathogen interactions. Soil Biol. Biochem. 40: 1–10.
- Whipps, J.M., and Lumsden, R.D. 2001. Commercial use of fungi as plant disease biological control agents: status and prospects. In: Butt, T.M., Jackson, C., and Magan, N. (eds) Fungal as biocontrol agents, problems and potential. CAB International, p 9–22.
- Yedidia, I., Benhamou, N. and Chet, I. 2000. Induction and accumulation of PR proteins activity during early stages of root colonization by the mycoparasite *Trichoderma harzianum* strain T-203. Plant Physiol. Biochem. 38: 863–873.

Adsorption of methylene blue dye onto the natural liquid sugars-based carbon: Kinetic and thermodynamic

Atit Wannawek^{1*}, Yanee Keereeta¹, Pongthep Jansanthea², Watee Panthuwat¹, Tanongsak Sassa-deepaeng^{1,3}, and Pusit Pookmanee^{4,5}

¹Faculty of Science and Agricultural Technology, Rajamangala University of Technology Lanna, Lampang 52000, Thailand

²Program in Chemistry, Faculty of Science and Technology, Uttaradit Rajabhat University, Uttaradit 53000, Thailand

³Agricultural Biochemistry Research Unit, Faculty of Science and Agricultural Technology, Rajamangala University of Technology Lanna, Lampang 52000, Thailand

⁴Department of Chemistry, Faculty of Science, Maejo University, Chiang Mai 50290, Thailand

⁵Nanoscience and Nanotechnology Research Laboratory (NNRL), Faculty of Science, Maejo University, Chiang Mai 50290, Thailand

*Corresponding author: atit_wannawek@rmutl.ac.th

Received: March 27, 2023. Revised: May 29, 2023; July 12, 2023. Accepted: October 20, 2023.

ABSTRACT

In this research, glucose-based carbon, fructose-based carbon, and sugarcane juice-based carbon materials were successfully synthesized by a simple, rapid, and one-step reaction for methylene blue adsorption. The samples were produced by the reaction of sugarcane juice with sulfuric acid. The characterization of the synthesized samples was performed by scanning electron microscopy (SEM), energy dispersive spectroscopy (EDS), Fourier Transform Infrared Spectroscopy (FTIR), and nitrogen adsorption-desorption analysis (BET). The adsorption behaviors of all samples were investigated by the determination of the adsorption capacity of methylene blue. The optimum condition for the highest adsorption capacity was at pH 7 and a contact time of 480 min. The kinetic and adsorption isotherms and thermodynamics of methylene blue on all samples were studied. Pseudo-second-order and Langmuir's isotherm were best fitted for methylene blue removal. This is indicated by chemical and monolayer adsorption. The mechanism of the adsorption process can be illustrated by the intra-particle diffusion model. A study of the thermodynamic parameters showed positive enthalpy (ΔH) and entropy (ΔS) values. This suggested that endothermic adsorption processes increased the randomness of adsorbate and adsorbent. Additionally, the negative value of Gibbs free energy (ΔG) indicated a spontaneity of adsorption. The presence of salts (NaCl and $MgCl_2$) and coexisting ions (Pb^{2+} and Zn^{2+}) cause a decrease in the adsorption efficiency.

Keywords: adsorption, carbon, sugarcane juice, sulfuric acid, methylene blue

INTRODUCTION

Wastewater discharge from chemical industries has been a continuous, long-standing problem. Mainly, dye product usage in several industries has inevitably caused environmental pollution. The dyes block the sunlight from entering the water and interrupt the ecosystem. On the other hand, some dyes are invisible and later become toxic and carcinogenic over prolonged exposure (Tuli et al., 2020). Dyes commonly used in the textile industry, such as methylene blue, congo red, remazol black, and remazol red, harm ecosystems and organisms, mainly aquatic life. This may eventually affect public health (Amran and Zaini, 2021). Methylene blue (3,7-bis(dimethylamino)-phenothiazin-5-ium chloride) (Noreen et al., 2020), thiazine cationic dye, is significant for colors manufacturing applied for paper, cotton wool, and wool. The amino group with positively charged

methylene blue is toxic to plants and animals (Aramesh et al., 2021). Therefore, the treatment of water contaminated with dyes has been focused. Currently, there are many treatment technologies for dye removal from wastewater, such as aerobic treatment systems, chemical oxidation, ozonation, sedimentation, ultrafiltration, membrane filtration, flocculation, ion exchange, biodegradation, electrochemical degradation, photocatalytic degradation, and adsorption. Some methods are, however, expensive, time-consuming, and technically complicated (Wu et al., 2021).

Adsorption technology has been proficiently developed. This method has been extensively used in wastewater treatment due to its environmentally friendly operation, high efficiency, and worthiness (Adekola et al., 2019). Various adsorbents have been studied to remove pollutants from wastewater including nanoparticles (Arab et al., 2022), nanocomposites (Khushboo et al., 2022), polymer

materials (Sattari et al., 2021), magnetic composites (Kumar et al., 2021), graphene oxide (Gautam and Hooda, 2020), graphite (Corona et al., 2021), activated carbon (Sultana et al., 2022), etc. Carbon and activated carbon (AC) are significant materials with adsorption properties due to their porosity, high surface area, and surface chemical characteristics. Therefore, there is interest in developing new carbon-based materials produced directly from plant-based materials, such as palm oil wood, palm kernel fiber, cashew nut, corncob, hazelnut husk, and others (Bello et al., 2021). The properties of these activated carbons depend on the type of raw material, operating time of the carbon process, temperature, and activating agent (Bergna et al., 2020).

NaOH, KOH (base activation), and H₂SO₄ (acid activation) are the most commonly used activating agents. In addition, the latter is a great alternative activating agent because of its efficiency of excellent methylene blue adsorption (Nizam et al., 2021). Activated carbon is produced by the chemical activation of sucrose, which is high-performance for adsorption (Bedin et al., 2016). Recently, various methods have been studied in synthesizing hydrochar and activated carbon for the adsorption of iodine and methylene blue (Genli et al., 2021).

The problem of smoke haze pollution is biomass burning (Khodmanee and Amnuaylojaroen, 2021) and charcoal/biochar production (Sparrevik et al., 2015). Using sulfuric acid during dehydration to prepare adsorption carbon is an alternative option to avoid problems caused by burning. It is well-known that carbohydrate dehydration is a simple and fast reaction (Dolson et al., 1995). For this reason, the reaction of sugar with sulfuric acid is a famous chemistry experiment. The sugar dehydration reaction for carbon film production was presented as a straightforward and rapid method (Whitener, 2016).

Natural products are relatively safe and eco-friendly products. The adsorbent carbons from solid natural products have been widely studied (Suhast et al., 2016). Natural liquid sugars-based carbon is another interesting option. Inverted sugar is present in natural liquid sugar derived from fruit (Naikwadi et al., 2010), which reacts rapidly with H₂SO₄ and reduces smoke haze pollution, especially when sugarcane juice is available throughout the country. It contains inverted sugar hydrolyzed to glucose and fructose by acidifying and can be rapidly carbonized by a dehydration reaction with H₂SO₄. Sugarcane juice has a high sugar content and can spoil quickly after extraction (Zaidan et al., 2021). Freshly squeezed sugarcane juice is easily spoiled and has a shelf life of only a few hours (Geremias-Andrade et

al., 2020). For this reason, using a nearly expired sugarcane juice is a value-added.

In this study, sugarcane juice is represented as a natural product due to its high inverted sugar content. The glucose powder-based carbons (GBC), saturated glucose solution-based carbons (GSBC), fructose powder-based carbons (FBC), saturated fructose solution-based carbons (FSBC), and sugarcane juice-based carbons (SJBC) were synthesized by a chemical reaction using concentrated H₂SO₄. All samples were characterized by SEM, EDS, FTIR, and BET analysis. The adsorption behaviors of the samples were investigated by adsorption of methylene blue dye and compared with GBC, GSBC, FBC, FSBC, and SJBC. In addition, the kinetics, adsorption isotherms, thermodynamics, effect of salts, and coexisting ions were studied.

MATERIALS AND METHODS

Materials

The sugarcane juice derived from the crushed sugarcane (*Saccharum officinarum*, Suphanburi 50) by sugarcane hydraulic press. This sugarcane was harvested from Ban Thung Ku Dai, Pong Saen Thong, Muang Lampang, Lampang Province, Thailand (18.296914, 99.432422). Glucose powder (C₆H₆O₁₂, 99.0%, Ajax Finechem Pty Ltd., Australia), fructose powder (C₆H₆O₁₂, 99.0%, Ajax Finechem Pty Ltd., Australia), and sulfuric acid (H₂SO₄, 98.0% ACL Chem Ltd., England) were used as precursors in the experiments. The pH-adjusted reagents were prepared with sodium hydroxide (NaOH, 99.0%, RCI Labscan., Thailand) and nitric acid (HNO₃, 70% Ajax Finechem Pty Ltd., Australia). Hydrochloric acid (HCl, 37.0% RCI Labscan Ltd., Thailand), potassium sodium tartarate-4-hydrate (Merck, Darmstadt), 3,5-dinitrosalicylic acid (DNS, 98% Sigma Aldrich Co., USA), and potassium hydroxide pellets (KOH, 85% Loba Chemie Ltd., India) were used for sugarcane juice hydrolyzation and sugar analysis. Sodium nitrate (NaNO₃, 99.5% RFCL Ltd., India) was employed to determine pH_{zpc} values. Sodium chloride (NaCl, 99% RCI Labscan Ltd., Thailand) and magnesium chloride (MgCl₂, 98% RCI Labscan Ltd., Thailand) were used for the study of the effect of salts on methylene blue adsorption. For the impact of coexisting ions on methylene blue adsorption, lead chloride (PbCl₂, 99% RCI Labscan Ltd., Thailand) and zinc chloride (ZnCl₂, 98% QRëC, New Zealand) were used for this study. In preparing the adsorption and kinetics study solution, methylene blue trihydrate

(C₁₆H₁₈N₃S.Cl.3H₂O, 99.0%, Himedia Laboratories Pvt Ltd., India) was used as adsorbate. All solutions in this experiment used deionized water (DI) as the solvent.

Preparation of adsorbents

The carbon material was prepared without heating (Whitener, 2016). GBC GSBC FBC and FSBC were prepared by slowly adding 50 mL of concentrated sulfuric acid to each of the large beakers, which contained 50 g of glucose powder, saturated glucose solution (50 g of glucose), 50 g of fructose powder and saturated fructose solution (50 g of fructose), respectively. The individual carbon samples were separated, washed with deionized water, and dried in a hot-air oven at 95 °C for 24 h. Similarly, SJBC was prepared by adding concentrated sulfuric acid to sugarcane juice (12% of reducing sugar) in a 2 L beaker. The carbon from this process was separated by filter paper. It was washed and dried at 95 °C for 24 h in a hot air oven. All of the carbon samples were stored in a desiccator.

Characterization

All samples are powdered and characteristically examined by SEM, EDS, FTIR, and BET techniques. The morphology was investigated using a scanning electron microscope (TESCAN-VEGA3, Czech Republic) at 5.0 kV. The chemical composition of the samples was obtained by using an energy dispersive spectroscopy (Oxford Instrument-Ultim Max 40, England) and Fourier-transform infrared spectroscopy (PerkinElmer/Spectrum RX I, UK), which were performed in wavenumber between 400 and 4000 cm⁻¹ with KBr pellets. The surface areas were calculated with the BET method. The adsorption-desorption analysis of nitrogen was carried out by using a surface area, pore volume, and pore size analyzer (Quantachrome-Autosorp 1MP, England) at an adsorber temperature of -196 °C, out gas temperature: 120 °C, outgas time 8 to 24 h and operating time 382.1 to 389.4 min. Sugarcane juice (SJ) was hydrolyzed and then analyzed for sugar content by DNS method (Wang, 2004; Texixeira and Santos, 2022). Briefly, the 1,000 µL of SJ was firstly chemically digested by adding 20 µL of concentrated HCl and then placed in a 90 °C hot water bath for 5 min. After cooling it to ambient temperature, 50 µL of 5 N KOH solution was added to neutralize the acid. The colorimetric reaction was carried out in the 5 mL test tubes using 0.5 mL of sample or reference solution (between 0.1 and 0.3 gL⁻¹ of glucose) and 0.5 mL of DNS reagent. After mixing by vortex, all samples were boiled in a 95 °C hot water bath for 5 min and cooled to ambient temperature. The absorbance was measured at 540 nm using a V-1200 spectrophotometer (Dshing Instrument Co., Ltd.,

China) with UV-Professional analysis software. All experiments were carried out in triplicates. Determination of zero-point charge (PZC) was applied to evaluate the effect of pH on the adsorption between the surface charge of adsorbent and adsorbate. The solutions of 0.1 mol/L NaNO₃ solutions 40 mL were adjusted in the initial pH values (pH_i) range of 2, 4, 6, 8, 10, and 12 using 0.1 M NaOH and 0.1 M HNO₃. 0.1 g of adsorbent was added to all solutions. The suspensions were shaken at 120 rpm for 24 h. The final solutions were separated and recorded final pH values (pH_f). The pH_{ZPC} was obtained by plotting between pH_i and ΔpH.

Adsorption studies

Effect of pH

The influence of pH was investigated by adding 0.05 g of adsorbent to the 40 mg/L of methylene blue solutions (25 mL) over the pH range from pH 2 to 9, which were adjusted by pH 0.1 M NaOH and 0.1 M HNO₃. The samples were shaken at 120 rpm for 24 h.

Effect of contact time

The effect of the contact time experiment was performed by varying contact times from 5 to 1440 min at optimum pH from effect of the pH study. Each Erlenmeyer flask contained 25 mL of fixed methylene blue concentration (40 mg/L) and 0.05 g of adsorbent. The samples were shaken at 120 rpm.

Effect of initial concentration

The Effect of the initial concentration study was operated under optimum conditions (pH of 7 and contact time 480 min) and varying initial concentrations of methylene blue from 5 to 80 mg/L. Adsorbent (0.05 g) was added to each Erlenmeyer flask containing 25 mL of methylene blue. The samples were shaken at 120 rpm.

Thermodynamic study

The effect of temperature was studied using a temperature range of 25 to 55 °C, pH of 7, and contact time of 480 min. The 0.05 g of adsorbent was added to the 40 mg/L of methylene blue solutions 25 mL. The samples were shaken at 120 rpm.

Effect of salts and coexisting ions

The effect of salt and coexisting ions was studied under optimum conditions. The impact of the salt study, the difference of NaCl (5 to 10 g/L) and MgCl₂ was added to the Erlenmeyer flask, which contained methylene blue solution (25 mL, 40 mg/L)

and 0.05 g of adsorbent. The effect of coexisting ions was performed by varying concentrations of Pb^{2+} and Zn^{2+} from 10 to 40 mg/L, which were prepared from 200 mg/L stock solutions of Pb^{2+} and Zn^{2+} , respectively. The samples were shaken at 120 rpm and a contact time of 480 min.

The final samples were centrifuged at 6,000 rpm to separate the solutions and solids. The absorbance values of the final solutions were measured by UV/Vis spectrometer (Metash V-5800, China) at wavelength 664 (Oladoye et al., 2022). The data of absorbance were used to calculate the final concentration and applied to kinetic and adsorption isotherm studies.

RESULTS AND DISCUSSION

Characterizations of the prepared adsorbents

Results of SEM and EDS

The morphology of carbons can be evaluated using SEM-analysis. The SEM photographs of all samples are shown in Figure 1. The morphology of GBC and FBC surfaces was compact, dense, layer-like, and rough, as shown in Figures 1(a) and 1(c). The characteristics of this morphology are similar to those of carbons, which were produced using an acid mixture of H_2SO_4 and H_2O_2 and analyzed by SEM technique (Chalmpes et al., 2022). The morphology of GSBC and FSBC surfaces was an agglomeration of small granules, as seen in Figures 1(b) and 1(d). This indicates that GSBC and FSBC have high surface area and are more porous than GBC and FBC, which is consistent with BET results. The surface texture (Figure 1(e)) was formed by aggregating tiny particles more compact than those of GSBC and FSBC. It is observed that SJBC has less pore size than GSBC and FSBC, as the surface area and the pore number influence adsorption. The elemental composition of all carbon samples was investigated by EDS spectroscopy, as shown in Figure 1, which consists of carbon and oxygen as the main constituents. To the EDS results, the similar O/C ratios of GBC, GSBC, FBC, FSBC, and SJBC were 0.345, 0.349, 0.378, 0.374, and 0.373, respectively. This indicates the oxygen content in the functional group. The

oxygen on the charcoal surface resulted in a negatively charged surface. This caused the attraction between the adsorbent and methylene blue through an electrostatic mechanism so that the elimination was promoted (El-Bery et al., 2022). Sulfur(S) and gold(Au) peaks remain their precursors and gold sputter coating technique of SEM, respectively.

Results of FTIR

The functional groups present in all samples were investigated by the FTIR, as shown in Figure 2. The absorbance bands peaked around 3401 cm^{-1} , corresponding to the strong O–H stretching of alcohol (Mondal and Majumder, 2019). The band located at about 2921, 1704, 1581, and 1160 cm^{-1} were assigned C–H stretching of alkane, carbonyl C=O groups of carboxylate asymmetric/symmetric stretching, C=C stretching and C–O stretching, respectively (El Maataoui et al., 2019; Marrakchi et al., 2020; Opoku et al., 2021). The absorbance peak around 1200 to 800 and 956 cm^{-1} was described as the C–C stretching and the trans-out-of-plane bending of C=C–H (Wibawa et al., 2020). The peak of about 789 and 580 cm^{-1} may be caused by carbonaceous agglomeration (Samoudi et al., 2022). The FTIR results indicated that all the samples contained carbon and oxygen, which was consistent with the results from the EDS. The peak positions of all samples are similar. It seems promising to have identical functional groups, including carboxylate and hydroxyl groups. A peak at 956 cm^{-1} was not found in GBC and GSBC. The peak was, however, observed in SJBC. This is probably because it was produced from sugarcane juice, which contains glucose and fructose.

The methylene blue dye cation (MB^+) adsorption onto all carbon samples occurred, representing the carboxyl, carboxylate, and hydroxyl groups (Wang et al., 2018). The carboxylic and hydroxyl groups become hydroxyl anion and carboxylate anion in an aqueous solution (Namal and Kalipci, 2020). These groups can actively interact with cations such as methylene blue (Dhar et al., 2021).

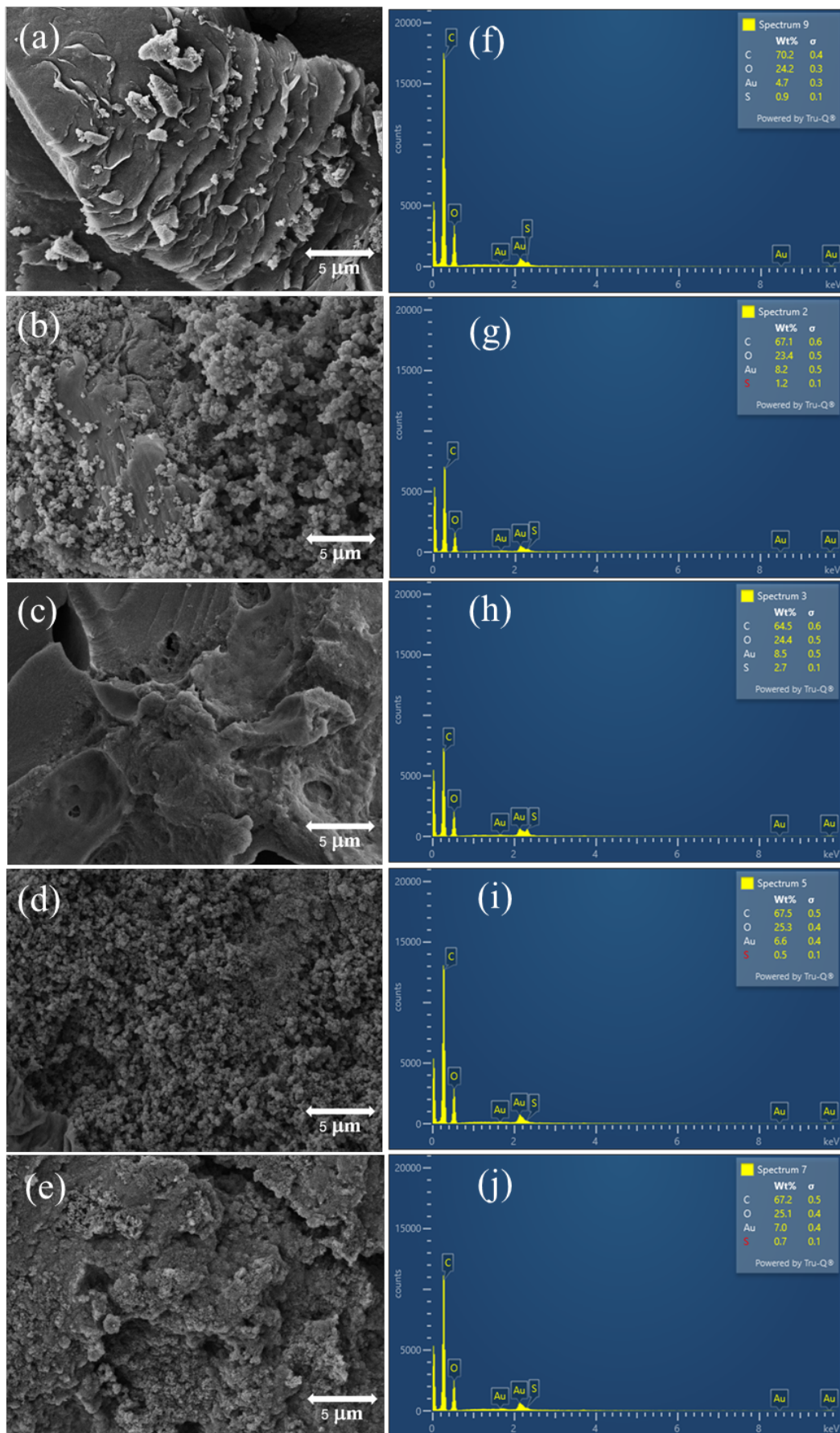


Figure 1. SEM photographs of GBC (a), GSBC (b), FBC (c), FSBC (d), and SJBC (e) and EDS results of GBC (f), GSBC (g), FBC (h), FSBC (i) and SJBC (j).

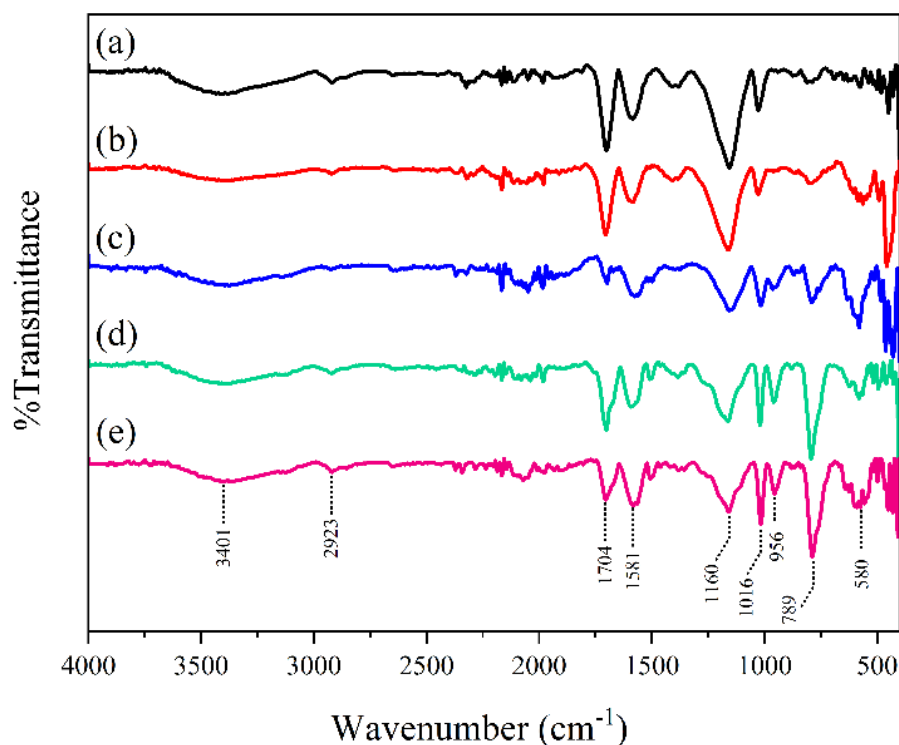


Figure 2. FTIR spectra (KBr disc) of GBC (a), GSBC(b), FBC(c), FSBC(d) and SJBC(e).

Results of nitrogen adsorption-desorption

The specific surface area (S), pore volume (V_p), and average porous radius of GBC, GSBC, FBC, FSBC, and SJBC are summarized in Table 1. After the solution process of glucose and fructose powder and hydrolysis with conc. H_2SO_4 , the specific surface area and pore volume of GSBC and FSBC were further increased compared to GBC and FBC, respectively. The specific surface area and pore volume can indicate the physical adsorption capacity of materials. The specific surface area result corresponded with SEM results, which showed

aggregation of small particles for GSBC, FSBC, and SJBC. The specific surface area of all samples is greater than that of the carbon produced by the chemical reaction (spent coffee and piranha solution), which was reported previously (10–15 m^2/g) (Chalmpes et al., 2022). The specific surface area depends on porosity, pore size distribution, shape, size, and roughness (Amador et al., 2016). The specific surface area of the particles affects the adsorption efficiency; the high specific surface area causes increased adsorption (Thang et al., 2021). However, the pore-volume and average radius of the porous also affect adsorption.

Table 1. BET constants for GBC, GSBC, FBC, FSBC, and SJBC

Adsorbent	S (m^2/g)	V_p (cm^3/g)	Average radius of porous (\AA)
GBC	24.82	0.0454	36.56
GSBC	35.98	0.0947	52.66
FBC	23.52	0.0415	35.27
FSBC	24.92	0.0783	62.87
SJBC	20.92	0.0504	48.20

Effect of pH on the adsorption of methylene blue

The effect of pH was studied within a pH range of 2 to 9 at the methylene blue concentration of 40 mg/L, 25 °C, and contact time of 24 h. As

shown in Figure 3(a), The methylene blue adsorption of all samples tended to be the same pattern. Conversely, the adsorption capacity seems to increase with an increase in pH and stabilize at $pH > 7$. The pH_{pzc} values of GBC, GSBC, FBC, FSBC, and

SJCB were determined from a final pH (pH_f) as a function of initial pH (pH_i). The pH_{pzc} value revealed the characteristic of charges on the adsorbent surface. It is indicated that when pH of the solution (pH) is higher than pH_{pzc} , the surface provides a negative charge. On the other hand, the surface shows a positive charge when pH of the solution is lower than pH_{pzc} (Zhang et al., 2021). Figure 3 suggested the point of zero charges of GBC, GSBC, FBC, FSBC, and SJCB, which were 5.4, 5.5, 5.8, 5.5, and 5.5, respectively. The adsorbent surface at $pH > pH_{pzc}$ with a negative charge was affected by electrostatic pulling between the adsorbent surface and methylene blue. Electrostatic interactions have been described on the principle of a charge density on the adsorbent surface, which is correlated with zeta potential. The deprotonation of hydroxyl and carboxyl groups will increase the negative charge density on the adsorbent.

This facilitates electrostatic interaction between the adsorbent and cation of methylene blue (Gautam and Hooda, 2020).

At low pH, the solution was obtained with high concentrations of H_3O^+ . The decreasing adsorption capacity was detected due to the competition of positive ion effect between H_3O^+ and methylene blue (Zhou et al., 2018). The electrostatic repulsion between methylene blue, a cationic dye, and the adsorbent surface increased due to the increase in the H_3O^+ concentration (Alver et al., 2020). However, when $pH < pH_{pzc}$ is considered, the surface of the adsorbent becomes positively charged. This induces an electrostatic repulsion on the free H_3O^+ ions in the solution and the cation of methylene blue (Gautam and Hooda, 2020).

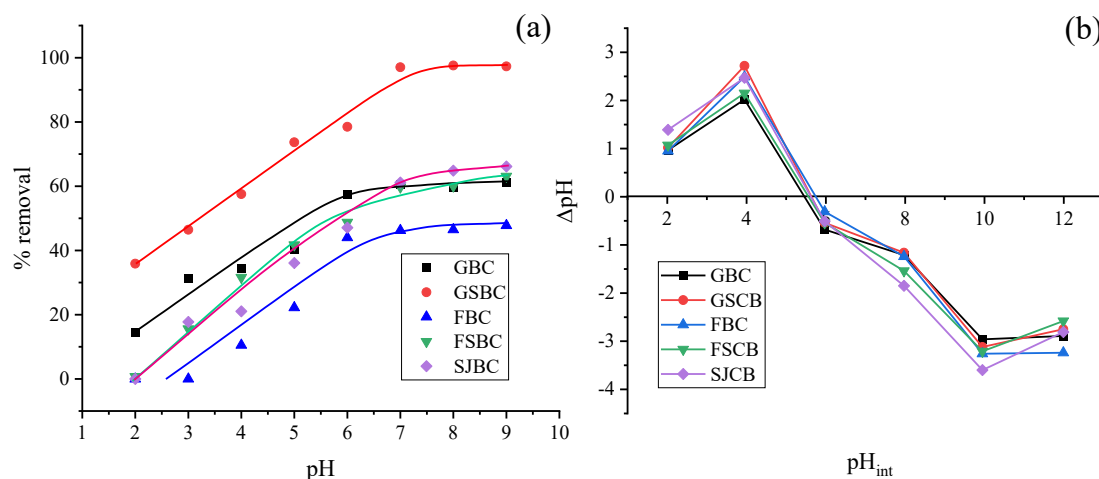


Figure 3. Effect of pH (a), pH_{pzc} determination curve of GBC, GSBC, FBC, FSBC and SJCB (b).

Effect of contact time and initial concentration of adsorbents

The effect of contact time at different contact times of 5, 10, 20, 30, 40, 50, 60, 120, 240, 360, 480, and 1440 min was investigated at the methylene blue concentration of 40 mg/L, pH of 7 and 25 °C. The percent removal of methylene blue is shown in Figure 4(a). It was found that the trend of methylene blue adsorption to all adsorbents was in the same pattern. The methylene blue was adsorbed rapidly in 0 to 50 min due to the fact that all samples consisted of abundant free adsorption sites and the electrostatic interaction effect between molecules of the adsorbates and adsorption sites on the adsorbent (Lyu et al., 2020). After a while, the adsorption sites were filled with methylene blue. The gradual increase of the methylene blue adsorption was shown

for 50 to 240 min due to the decrease of adsorption sites and the repulsion of methylene blue in solution and methylene blue adsorbed on the adsorption sites (Nkutha et al., 2020). A slower adsorption rate was observed for 240–360 min afterward because the adsorption sites were nearly filled with methylene blue molecules. After 360 min, the adsorption of methylene blue was continuing. However, the process was occurred at a lower rate and prolonged before entering an equilibrium. Therefore, this study assumed that at 480 min, the adsorption occurred close to an equilibrium point to reduce the study time length for other adsorption-affected factors. However, the adsorption had entered equilibrium, and the treatment would later no longer be able to eradicate methylene blue.

A study of initial concentrations was conducted under varying concentrations of methylene blue. The different initial concentrations of 5, 10, 20, 30, 40, 50, 60, 70, and 80 mg/L of all samples were examined at 25 °C, pH of 7, with a contact time of 480 min. Figure 4(b) shows that the amount of removed methylene blue varies with different initial concentrations. The adsorption capacity of methylene blue on all samples was the same pattern. It increased as the initial concentration increased, and it eventually became stable. The

higher initial concentration resulted in a higher amount of removed methylene blue was observed. This is due to the driving force generated by increasing solute, which is sufficient to overcome the mass transfer resistance between the solid and liquid phases. This will remain stable after reaching equilibrium. However, the adsorption capacity decreased at the initial 70 mg/L concentration. This may be due to a repulsion between methylene blue on the adsorbent surface and methylene blue in a solution.

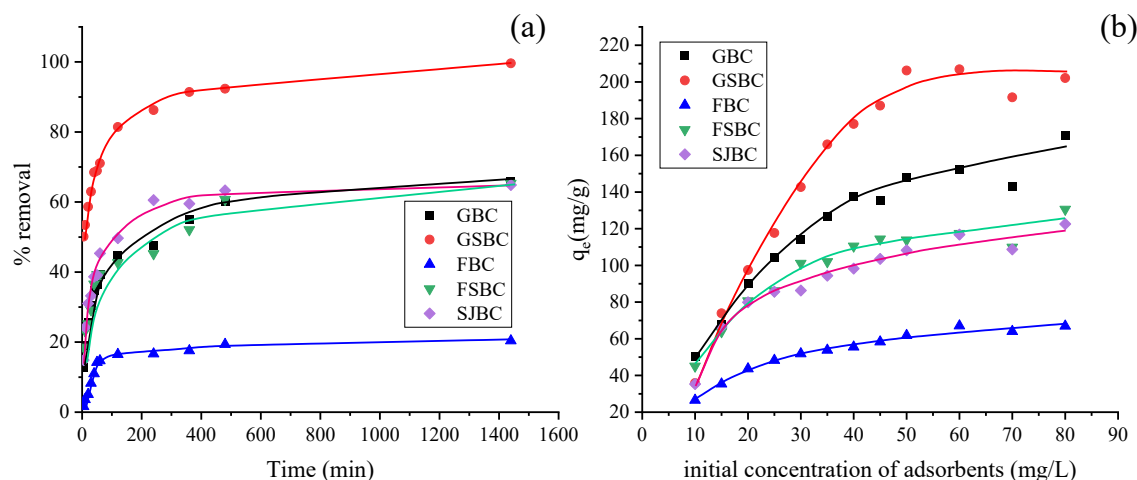


Figure 4. Effect of contact time (a) and initial concentration of methylene blue removal (b).

Kinetic study

The contact time data of methylene blue adsorption onto all adsorbents were used to study adsorption kinetic. The pseudo-first-order, pseudo-second-order, and intra-particle diffusion models were evaluated by equations (1), (2), and (3), respectively (Badri et al., 2020; Tran et al., 2020).

$$\log(q_e - q_t) = \log(q_e) - \frac{k_1}{2.303} t \quad (1)$$

$$\frac{t}{q_t} = \frac{1}{k_2 q_e^2} + \left(\frac{1}{q_e}\right) t \quad (2)$$

$$q_t = k_{ip} t^{1/2} + C \quad (3)$$

Where t , q_e , and q_t are contact time, adsorption capacity (mg/g) at equilibrium, and at a time “ t ,” respectively. The k_1 , k_2 , and k_{ip} represent the rate constant of pseudo-first-order, pseudo-second-order, and intra-particle diffusion models. The C is maintaining the boundary layer thickness. The data were plotted for the three models, shown in Figure 5, and the obtained kinetic parameters were

summarized in Table 2. The methylene blue adsorption on all adsorbents follows the pseudo-second-order model, which was fitted due to the calculated value (q_{cal}) high approximation with the experimental data (q_{exp}) and better linearity (high R^2) than the pseudo-first-order model. Therefore, the pseudo-second-order model was suitable to explain better the adsorption kinetics of methylene blue adsorption by GBC, GSBC, FBC, FSBC, and SJBC. The pseudo-second-order model can be used for predicting adsorption capacity. The expected value is similar to those of the experiments. The pseudo-second-order model demonstrated a chemisorption process involving electrostatic force and valence forces (Sahoo and Prelot, 2020). For SJBC, the adsorption capacity values obtained from the experiment and the pseudo-second-order model were 135.1 and 133.4 mg/g. However, the intra-particle diffusion model showed the potential control rate and diffusion mechanism of the adsorption process. This indicated intra-particle diffusion during the adsorption process. The parameters are given in Table 3. The two steps of adsorption were illustrated as the intra-particle diffusion model. The slope of

the line for the first step occurred at 5 to 60 min ($t^{1/2}$, 2.24 to 7.75 $\text{min}^{1/2}$). This suggested that methylene blue is rapidly adsorbed on the surface of the adsorbent. The second step occurred approximately 120 min and 1440 min ($t^{1/2}$, 11.0 to 37.9 $\text{min}^{1/2}$). The particles were diffused within the adsorbent. The slope was increased gradually, as well as the adsorption, until equilibrium. This is a progressive

and speed-limiting step of the intra-particle diffusion process. The experimental results were similar to those from the adsorption of methylene blue by Coal-based activated carbon reported by Wang et al. (2022), which showed a rapid adsorption rate in the first step and a decreasing rate in the second step model.

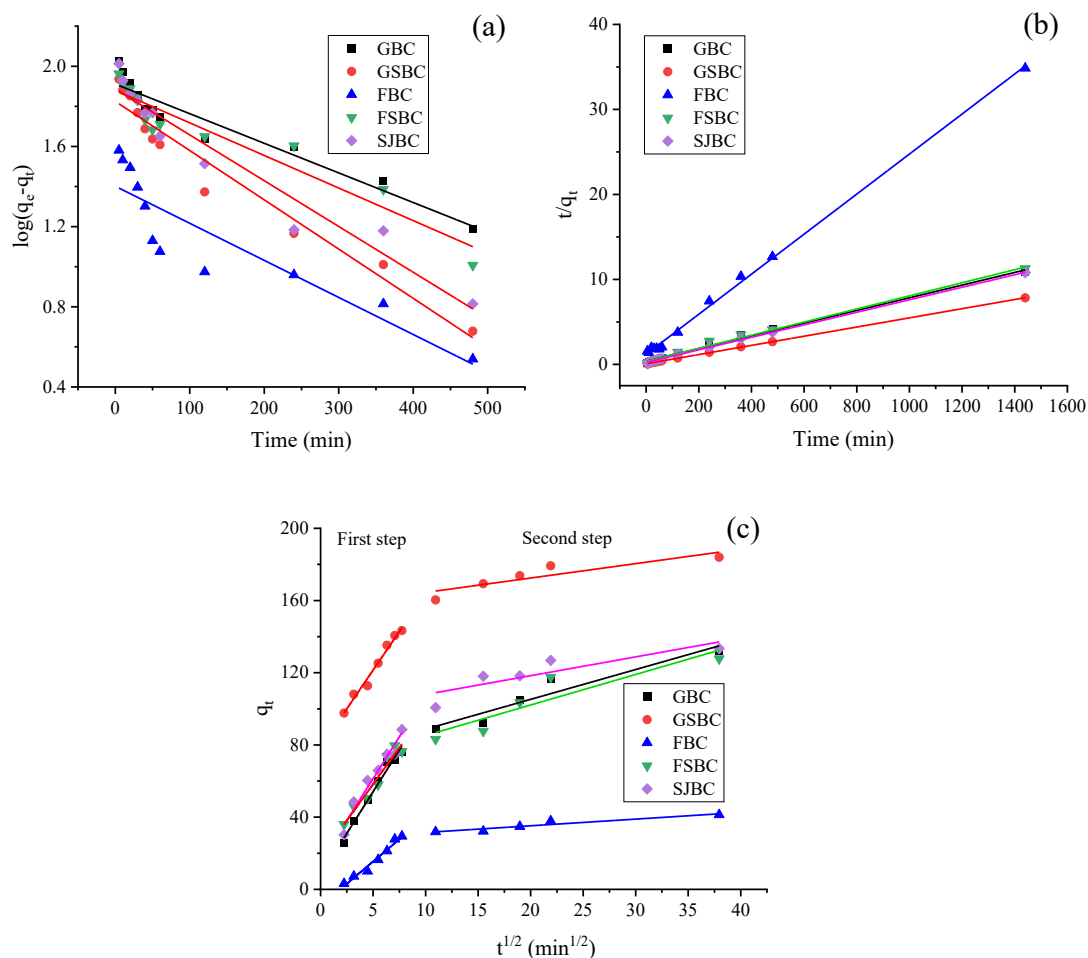


Figure 5. Kinetic plots of methylene blue removal for the pseudo-first-order (a), pseudo-second-order (b), and intra-particle diffusion (c).

Table 2. The obtained kinetic parameters for the adsorption of methylene blue onto GBC, GSBC, FBC, FSBC, and SJBC using pseudo-first and pseudo-second-order models

Adsorbents	Parameters							
	Pseudo-first-order				Pseudo-second-order			
	k_1 (L/min)	$q_e^{(cal)}$ (mg/g)	$q_e^{(exp)}$ (mg/g)	R^2	$k_2 \times 10^{-4}$ (g/mg min)	$q_e^{(cal)}$ (mg/g)	$q_e^{(exp)}$ (mg/g)	R^2
GBC	0.0035	81.51	132.0	0.9198	2.81	117.6	132.0	0.9907
GSBC	0.0058	66.87	184.0	0.9551	3.61	185.2	184.0	0.9998
FBC	0.0041	25.21	41.30	0.8119	4.67	42.4	41.3	0.9982
FSBC	0.0037	75.88	127.8	0.9086	1.68	129.9	127.8	0.9943
SJBC	0.0053	76.93	133.4	0.9432	2.31	135.1	133.4	0.9994

Table 3. Intra-peptide diffusion parameters for the adsorption of methylene blue onto GBC, GSBC, FBC, FSBC, and SJBC

Adsorbents	Parameters					
	First step			Second step		
	k_{ip} (mg/g min ^{1/2})	C	R ²	k_{ip} (mg/g min ^{1/2})	C	R ²
GBC	0.0035	81.51	0.9198	2.81	117.6	0.9907
GSBC	0.0058	66.87	0.9551	3.61	185.2	0.9998
FBC	0.0041	25.21	0.8119	4.67	42.4	0.9982
FSBC	0.0037	75.88	0.9086	1.68	129.9	0.9943
SJBC	0.0053	76.93	0.9432	2.31	135.1	0.9994

Adsorption isotherms study

The adsorption isotherms were studied at 25 °C, pH of 7, and contact time of 480 min. The concentrations of methylene blue were 10, 15, 20, 25, 30, 35, 40, 50, 60, 70, and 80 mg/L, respectively. Figure 6(a) shows that the adsorption of methylene blue was a rapid process at the first step due to the presence of abundant active sites (carboxylate and hydroxyl groups) evident in the FTIR result. The adsorption capacity was constant when it reached the equilibrium state. Adsorption isotherms of solids

were related to the amount of adsorption and the concentration of a solution. The Langmuir isotherm is relevant to homogeneous sites and monolayer adsorption, a definite position, and several adsorbed molecules, and the adsorbed molecules can adsorb only one molecule. The Freundlich isotherm can be used for heterogeneous surfaces, which is multilayer adsorption (Kalam et al., 2021). The Langmuir and Freundlich isotherms were interesting and shown in equations (4) and (5) (Rehman et al., 2021; Rheima et al., 2021).

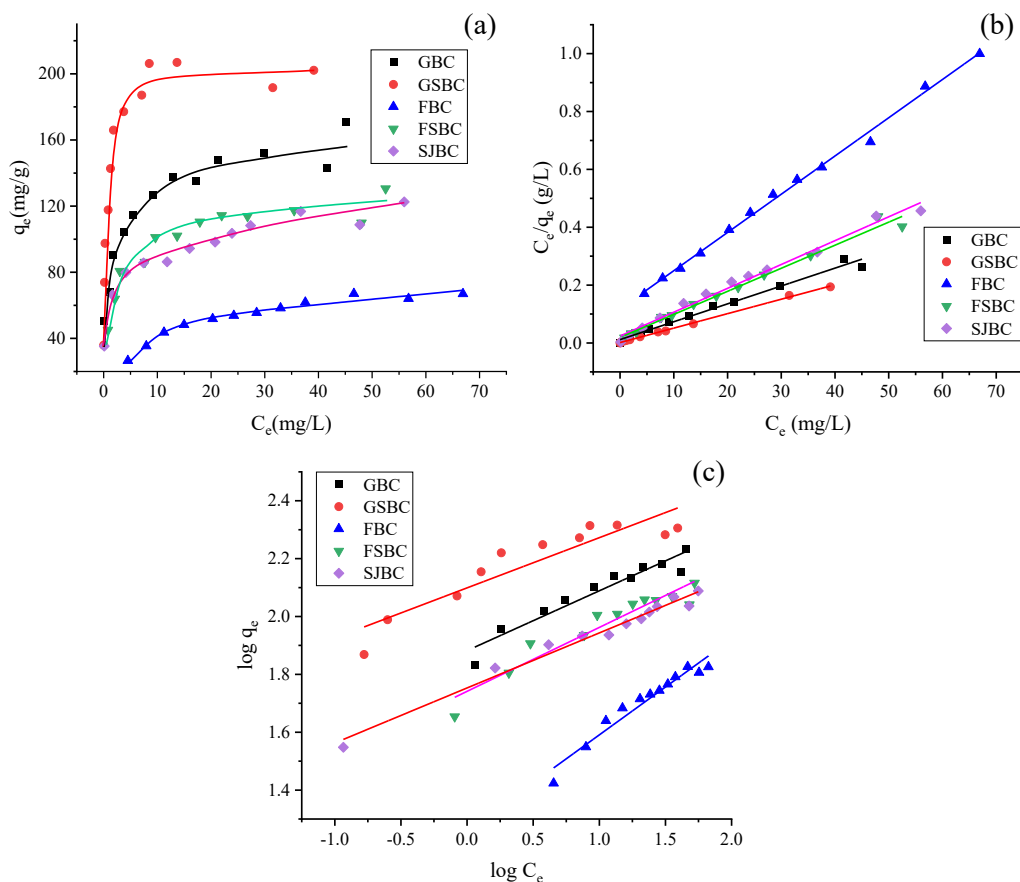


Figure 6. Adsorption isotherm of methylene blue removal (a), Langmuir (b), and Freundlich isotherm (c).

$$\frac{C_e}{q_e} = \frac{1}{q_m b} + \frac{C_e}{q_m} \quad (4)$$

$$\log q_e = \log K_F + \frac{1}{n} \log C_e \quad (5)$$

Where q_m is the maximum adsorption capacity (mg/g), C_e represents the methylene blue concentration at equilibrium, and b and K_F are the Langmuir and Freundlich constant, respectively. The Langmuir constant (b) refers to the adsorbate and surface interaction. The large value of b presents a strong interaction between the adsorbate and the adsorbent. The small b value presents a weak interaction. The n is the adsorption intensity used for the trend prediction of adsorption. If $n = 1$, the adsorption isotherm is a linear line; $n < 1$ refers to poor adsorptive potential, and $n > 1$ refers to the possibility of adsorption; titled $(1/n)$ with a small value is related to the adsorbent-adsorbent bonding (Shikuku et al., 2021).

The adsorption isotherm is the relative adsorption capacity and concentration of residual adsorbent in solution at equilibrium. The Langmuir and Freundlich isotherms are shown in Figures 6(b) and 6(c). The parameters obtained from both isotherms are shown in Table 4. The adsorptions of methylene blue onto GBC, GSBC, FBC, FSBC, and SJBC were fitted with Langmuir isotherm with higher R^2 . These results showed that this adsorption was monolayer adsorption on a homogeneous surface. Table 4 showed that the maximum adsorption of GSBC (200.0 mg/g) was higher than other adsorbents due to the high specific surface area

(Table 1). However, a specific surface area was not the only factor affecting the adsorption; pore structures and functional groups were also involved (Wang et al., 2023). The adsorption capacity increases with the pore size of the adsorbent (Roslan et al., 2022). For the similar surface areas of FBC and FSBC, the latter showed greater values than those of FBC when a pore volume and average radius of porous were considered, as shown in Table 1. The effect of pore volume can also explain methylene blue adsorption capacity between FBC and SJBC. All these values affected the adsorption. The result was similar to the experiments of Goyal et al. (2004) for the insignificantly different surface areas and adsorption capacities. It was claimed that this may be due to the differences in the microporous and chemical properties of the carbon surface (Goyal et al., 2004). However, the maximum adsorption capacity of SJBC is 121.9 mg/g, which is lower than GSBC. This is because of the number of void volumes or pores caused by coagulation. The particles of SJBC aggregated tightly so that fewer pores were introduced. The minimum adsorption capacity for FBC was shown due to the small surface area and low porosity, which corresponded to Figure 1 and Table 1.

The adsorption capabilities of methylene blue onto different adsorbents are shown in Table 5. Non-activated carbon comparisons revealed that all samples fell within the competitive range. For further study, improving its quality could be able to adsorb similar to or better than other types of activated carbon.

Table 4. The determined parameters from Langmuir and Freundlich isotherms for the adsorption of methylene blue onto GBC, GSB, FBC, FSBC, and SJBC

Adsorbents	Parameters					
	Langmuir isotherm			Freundlich isotherm		
	b (L/min)	q_m (mg/g)	R^2	K_F (mg/g)(L/mg) ^{1/n}	n	R^2
GBC	0.549	161.3	0.9858	76.23	4.836	0.9219
GSBC	7.143	200.0	0.9975	125.60	5.764	0.8491
FBC	0.112	75.8	0.9964	18.20	3.022	0.9458
FSBC	0.423	125.0	0.9876	55.12	4.525	0.9120
SJBC	0.323	121.9	0.9883	56.64	5.258	0.9783

Table 5. Adsorption capacities of methylene blue

Precursor	Activation reagent	Adsorption capacity (mg/g)	Sources
Rubber seeds	H ₂ SO ₄	769.23	Nizam et al., 2021
Sucrose spherical carbon	KOH	704.2	Bedin et al., 2016
Un-sieved sugarcane bagasse	Water	148.8	El-Bery et al., 2022
Ackee apple pod	ZnCl ₂	47.17	Bello et al., 2021
Deglat Beida stones	NaOH	163.67	Gherbia, et al., 2019
Chickpea stalk	ZnCl ₂	105	Genli et al., 2021
Chickpea stalk hydrochar	None	45	Genli et al., 2021
<i>Magnolia Grandiflora</i> Linn leaf biochar	None	78.6	Ji et al., 2019
cosmetics industry, sewage sludge, Biochar	None	51.1	Ribeiro et al., 2021
Seaweed-based biochars	None	175	Güleç et al., 2022
Biochar from cocoa shell	None	163.5	Prabu et al., 2020
GBC	None	161.3	This study
GSBC	None	200.0	This study
FBC	None	75.8	This study
FSBC	None	125.0	This study
SJBC	None	122.0	This study

Thermodynamics study

The thermodynamics study used the methylene blue concentration of 40 mg/L at a pH of 7, contact time of 480 min, and temperatures of 25, 35, 45, and 50°C, respectively. Thermodynamic parameters, including enthalpy change (ΔH), entropy change (ΔS), and Gibbs free energy change (ΔG), are considerable for a better understanding of the effect of temperature on the adsorption process. This could be revealed if processes occur naturally (Estrada et al., 2021). For adsorption, it is already known that ΔH depends on electrostatic and Van der Waals interactions. Additionally, ΔS depends on hydrophobic interactions (Yoshida et al., 2020). The correlation of ΔG , ΔH , and ΔS is represented by equations (6), (7), and (8) (Liyanaarachchi et al., 2023; Tran, 2022).

$$\Delta G = \Delta H - T\Delta S \quad (6)$$

$$\ln K = -\frac{\Delta H}{RT} + \frac{\Delta S}{R} \quad (7)$$

$$K = \frac{q_e}{C_e} \quad (8)$$

The values of ΔH and ΔS can be obtained from the slope and intercept of the Van't Hoff plots as illustrated in Fig. 7. with $\ln K$ on the Y-axis versus $1/T$ on X-axis. R (8.314 J/mol K) is the gas constant, K is the equilibrium constant correlated with the Langmuir equation (Liu, 2009), and T (K) is the absolute temperature of the solution.

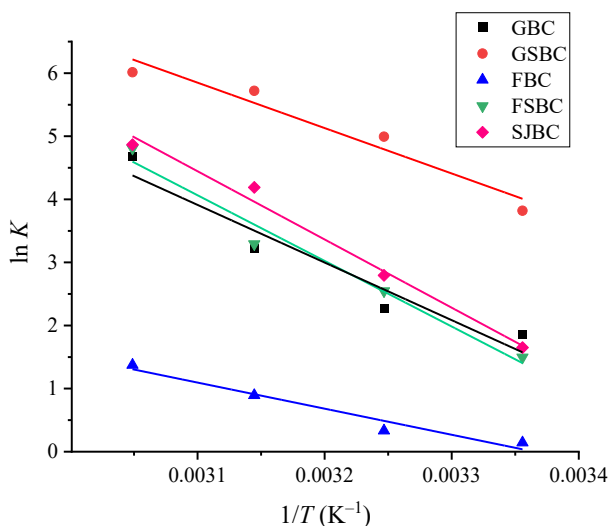


Figure 7. Van't Hoff plot of methylene blue removal by GBC, GSBC, FBC, FSBC, and SJBC.

From Table 6, the R^2 values of GBC, GSBC, FBC, FSBC, and SJBC were 0.9284, 0.9461, 0.9574, 0.9746 and 0.9881, respectively. The ΔH values of all samples were positive. This indicates that adsorption was an endothermic process. A positive value of ΔS represented a great affinity of MB^+ towards the adsorbent and increased randomness at the solid–solution interface (Tongpoothorn et al., 2020). ΔG was a negative value. It indicated that the adsorption capacity of MB^+ onto all samples could occur spontaneously. Basically, ΔH values of physisorption and chemisorption range from 2.1 to 20.9 kJ/mol and 80 to 200 kJ/mol, respectively (Amel et al., 2021).

The ΔH values of methylene blue adsorption for all samples represent the chemisorption process. This corresponded to the results of the pseudo-second-order model, which was similar to the experimental results of Liyanaarachchi et al. (2023). The ΔG values of physisorption and chemisorption range from 0 to -20.9 kJ/mol and -80 to -400 kJ/mol. However, it was reported that the activity coefficient

affected the calculation of ΔG from the Langmuir equilibrium constant. This needs to be strictly considered due to the effect of the activity coefficient of a high-concentration solution (Liu, 2009). Tran (2022) reported that physisorption or chemisorption must depend on the magnitude of standard enthalpy change rather than standard Gibbs's free energy change.

Table 6. Thermodynamic parameters for the adsorption of methylene blue onto GBC, GSB, FBC, FSBC, and SJBC.

Adsorbents	ΔH (kJ/mol)	ΔS (J/mol K)	ΔG (kJ/mol)			
			25 °C	35 °C	45 °C	55 °C
GBC	75.95	267.96	-3.95	-6.63	-9.30	-11.98
GSBC	59.84	234.12	-9.97	-12.31	-14.65	-16.99
FBC	34.39	115.71	-0.11	-1.27	-2.43	-3.58
FSBC	86.47	301.87	-3.53	-6.55	-9.57	-12.59
SJBC	89.90	315.65	-4.21	-7.37	-10.52	-13.68

Effect of salt and existing ion

Salt and existing ions were investigated since most natural water, such as groundwater, canal water, seawater, and most wastewater, consists of several types of salt or ions. The type and concentration of salts or ions depend on the source and quality of the water. These may influence the adsorption of methylene blue. SJBC will be used to investigate the effects of salt and existing ions on methylene blue adsorption. This is because SJBC provided similar results of adsorption isotherm, kinetic, and thermodynamic effects. Besides, SJBC is produced for general purposes at a lower cost than GBS, GSBC, FBC, and FSBC, which are made from pure substances. The effect of salt was studied using a concentration of methylene blue of 40 mg/L under pH of 7, contact time of 480 min, and 25 °C. The initial concentrations of NaCl and MgCl₂ were 5, 10, 15, and 20 g/L, respectively. It was found that increasing the concentration of NaCl and MgCl₂ decreased the adsorption capacity of methylene blue, as shown in Figure 8(a). The increasing salt

concentration decreased the electrostatic attraction and electrostatic repulsion. The adsorption capacity is generally slightly increased when the ionic strength increases. As the experimental result, the adsorption capacity of methylene blue meanwhile decreased when the ionic strength increased. Consequently, the electrostatic attraction between methylene blue and SJBC was reduced and resulted in the adsorption capacity (Wang et al., 2022). From the experiment, it can be seen that Mg²⁺ had showed more effect on methylene blue adsorption than Na⁺ because of the effect of ionic strength. A decrease of active sites on the adsorbent and the active concentration of methylene blue occurred when the ionic strength increased. This is due to the interaction between positive and negative charges decreased. Therefore, at the same concentration of Mg²⁺ and Na⁺, the effect of Mg²⁺ on adsorption capacity was greater than those of the latter, as theoretically expected. This might be because of the increased number of cations of Mg²⁺, which can methylene blue cation adsorption (Guo et al., 2014).

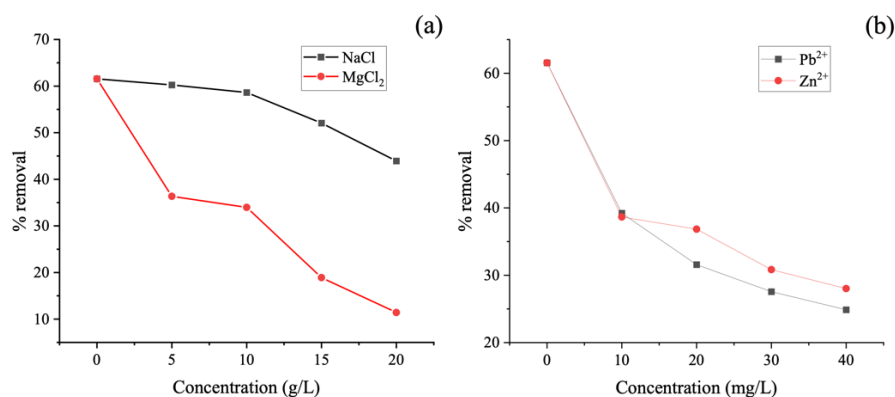


Figure 8. Effect of salt (a) and effect of coexisting ions (b) for methylene blue removal.

The coexisting ion was studied using 40 mg/L of methylene blue at pH 7, 25 °C, and a contact time of 480 min. The initial concentrations of Pb²⁺ and Zn²⁺ were 10, 20, 30, and 40 mg/L, respectively. From Figure 8(b), the decrease in methylene blue adsorption of SJBC resulted from adsorption competition between the metal ions with methylene blue, as corresponded to the previous results of Ebadollahzadeh and Zabihi (2020) and Eltaweil et al. (2023). The existence of Pb²⁺ would affect the adsorption of methylene blue compared to Zn²⁺. This is because Pb²⁺ can be better adsorbed. As previously reported, Pb²⁺ can be better absorbed on biochar than Zn²⁺ due to its lower binding energy (Zhao et al., 2020). The binding energies of Pb²⁺ and Zn²⁺ adsorbed on biochar were reported to be 139 and 1022 eV (Trakal et al., 2014; Gan et al., 2015). The binding energy of adsorption is related to the bond energy between the adsorbed molecule and the adsorbent (Yazaydin and Thompson, 2009).

Although SJBC suggested less adsorption capacity of methylene blue than GSBC and FSBC in this study, sugarcane juice is a cheaper precursor than pure glucose and fructose. SJBC can be substantially manufactured and used. Nonetheless, enhancing SJBC efficiency for further study could result in higher adsorption. The carbon from the rapid reaction of sugarcane juice with concentrated sulfuric acid can be used for the cation adsorption technique. Moreover, SJBC can also be applied to other adsorption applications such as antibiotics (Wang et al., 2020), methane (Shi et al., 2015), organic pollutants (Li et al., 2019), etc. or the use of other sugars in the synthesis of carbon (Tuli et al., 2020), such as sucrose (Choi and Park, 2015), white sugar (Xiao et al., 2020), molasses wastewater, etc.

CONCLUSIONS

SJBC was synthesized by rapid hydrolysis of sugarcane juice using concentrated sulfuric acid to produce adsorbent adsorption. It was found that the surface area of GBC and FBC was smooth and almost non-porous. On the other hand, synthesized GSBC, FSBC, and SJBC prepared from concentrated sulfuric acid and a solution suggested an aggregation of small particles, which affected the methylene blue adsorption. The adsorption kinetic study indicates that the adsorption of methylene blue onto all samples was performed under the pseudo-second-order model, which provided similar calculated and experimental q_e values. A study of the intra-particle diffusion model showed that the adsorption process occurred in two steps. The first step was rapid adsorption of methylene blue onto all the sample's surface. The second step was a slow diffusion within

the adsorbent pore. The Langmuir model fits the methylene blue adsorption behavior onto all samples. This indicated a monolayer adsorption. GSBC, GBC, FSBC, SJBC, and FBC adsorption capacities were 200.0, 161.3, 125.0, 121.9, and 75.8 mg/g, respectively. The solution-produced GSBC and FSBC had more adsorption capacity of methylene blue than the powder-made GBC and FBC, respectively. The thermodynamic parameters represent the endothermic adsorption processes, the disorder and randomness at the solid-solution interface, and the spontaneity of adsorption. The values of ΔH and the pseudo-second-order model suggest that chemisorption is involved. Salts and metal ions that occurred during the process would negatively affect the methylene blue adsorption of SJBC. Using a solution such as sugarcane juice to convert into charcoal for adsorption by dehydration can remove methylene blue, which is the development of adsorbents from liquid natural products to remove other contaminants.

ACKNOWLEDGMENTS

The study was supported by Rajamangala University of Technology Lanna, Lampang. The authors sincerely thank the Department of Industrial Chemistry, Faculty of Science, Chiang Mai University, Chemistry Program, Faculty of Science, and Science and Technology Service Centre, Faculty of Science, Maejo University for analytical instruments support.

REFERENCES

- Adekola, F. A., Ayodele, S. B., and Inyinbor, A. A. 2019. Activated biochar prepared from plantain peels: Characterization and Rhodamine B adsorption data set, Chemical Data Collections. 19: 100170. <https://doi.org/10.1016/j.cdc.2018.11.012>.
- Alver, E., Metin, A. Ü., and Brouers, F. 2020. Methylene blue adsorption on magnetic alginate/rice husk bio-composite, International Journal of Biological Macromolecules. 154: 104–113. <https://doi.org/10.1016/j.ijbiomac.2020.02.330>.
- Amador, C., and Martin de Juan, L. 2016. Chapter 19 – Strategies for structured particulate systems design. In: Computer Aided Chemical Engineering. Elsevier. p.509–579.
- Amel, H., Yeddou-Mezenner, N., and Lounis, A. 2021. Eco-Friendly scolymus hispanicus for the Removal of Basic Blue 41, Iranian Journal of Chemistry and Chemical Engineering. 40(2): 511–523. <https://doi.org/10.30492/ijcce.2020.38019>.
- Amran, F., and Zaini, M. A. A. 2021. Sodium hydroxide-activated Casuarina empty fruit: Isotherm, kinetics and thermodynamics of methylene blue and congo red adsorption, Environmental Technology & Innovation. 23: 101727. <https://doi.org/10.1016/j.eti.2021.101727>.
- Arab, C., El Kurdi, R., and Patra, D., 2022. Zinc curcumin oxide nanoparticles for enhanced adsorption of congo red: kinetics and adsorption isotherms study, Materials Today Chemistry. 23: 100701. <https://doi.org/10.1016/j.mtchem.2021.100701>.

- Aramesh, N., Bagheri, A. R., and Bilal, M. 2021. Chitosan-based hybrid materials for adsorptive removal of dyes and underlying interaction mechanisms, *International Journal of Biological Macromolecules*. 183: 399–422. <https://doi.org/10.1016/j.ijbiomac.2021.04.158>.
- Badri, A., Alvarez-Serrano, I., Luisa López, M., and Ben Amara, M. 2020. Sol-gel synthesis, magnetic and methylene blue adsorption properties of lamellar iron monophosphate $\text{KMgFe}(\text{PO}_4)_2$. *Inorganic Chemistry Communications*. 121: 108217. <https://doi.org/10.1016/j.inoche.2020.108217>.
- Bedin, K. C., Martins, A. C., Cazetta, A. L., Pezoti, O., and Almeida, V. C. 2016. KOH-activated carbon prepared from sucrose spherical carbon: Adsorption equilibrium, kinetic and thermodynamic studies for Methylene Blue removal. *Chemical Engineering Journal*. 286: 476–484. <https://doi.org/10.1016/j.ccej.2015.10.099>.
- Bello, M. O., Abdus-Salam, N., Adekola, F. A., and Pal, U. 2021. Isotherm and kinetic studies of adsorption of methylene blue using activated carbon from ackee apple pods. *Chemical Data Collections*. 31: 100607. <https://doi.org/10.1016/j.cdc.2020.100607>.
- Bergna, D., Hu, T., Prokkoala, H., Romar, H., and Lassi, U. 2020. Effect of some process parameters on the main properties of activated carbon produced from peat in a lab-scale process, *Waste and biomass valorization*. 11(6): 2837–2848. <https://doi.org/10.1007/s12649-019-00584-2>.
- Chalmpes, N., Baikousi, M., Giousis, T., Rudolf, P., Salmas, C. E., Moschovas, D., Avgeropoulos, A., Bourlinos, A. B., Tantis, I., Bakandritsos, A., Gournis, D., and Karakassides, M. A. 2022. Biomass waste carbonization in piranha solution: A route to hypergolic carbons? *Micro*. 2(1): 137–153. <https://doi.org/10.3390/micro2010009>
- Choi, Y. K., and Park, S. J. 2015. Preparation and characterization of sucrose-based microporous carbons for increasing hydrogen storage, *Journal of Industrial and Engineering Chemistry*. 28: 32–36. <https://doi.org/10.1016/j.jiec.2015.02.012>.
- Corona, R. R. B., Sad, C. M. S., da Silva, M., Lopes, D. L., Leite, J. S. D., de F. Viegas, G. M., Gonçalves, G. R., Filgueiras, P. R., and de Castro, E. V. R. 2021. Adsorption of anionic surfactant in graphite oxide: A study for treatment of laundry wastewater, *Journal of Environmental Chemical Engineering*. 9(6): 106858. <https://doi.org/10.1016/j.jece.2021.106858>.
- Dhar, L., Hossain, S., Rahman, M. S., Quraishi, S. B., Saha, K., Rahman, F., and Rahman, M. T. 2021. Adsorption mechanism of methylene blue by graphene oxide-shielded Mg-Al-layered double hydroxide from synthetic wastewater. *The Journal of Physical Chemistry A*. 125(4): 954–965. <https://doi.org/10.1021/acs.jpca.0c09124>.
- Dolson, D. A., Battino, R., Letcher, T. M., Pegel, K. H., and Revaprasadu, N. 1995. Carbohydrate dehydration demonstrations. *Journal of Chemical Education*. 72(10): 927–929 <https://doi.org/10.1021/ed072p927>.
- Ebadollahzadeh, H., and Zabihi, M. 2020. Competitive adsorption of methylene blue and Pb (II) ions on the nano-magnetic activated carbon and alumina. *Materials Chemistry and Physics*. 248: 122893. <https://doi.org/10.1016/j.matchemphys.2020.122893>.
- El Maataoui, Y., Mrabet, M., Maaroufi, A., and Abdelmalek, D. 2019. Spiramycin adsorption behavior on activated bentonite, activated carbon and natural phosphate in aqueous solution. *Environmental Science and Pollution Research*. 26: 15953–15972. <https://doi.org/10.1007/s11356-019-05021-4>.
- El-Bery, H. M., Saleh, M., El-Gendy, R. A., Saleh, M. R., and Thabet, S. M., 2022. High adsorption capacity of phenol and methylene blue using activated carbon derived from lignocellulosic agriculture wastes. *Scientific Reports*. 12(1): 5499. <https://doi.org/10.1038/s41598-022-09475-4>.
- Eltaweil, A. S., Abd El-Monaem, E. M., El-Subruiti, G. M., Ali, B. M., Abd El-Latif, M. M., and Omer, A. M. 2023. Graphene oxide incorporated cellulose acetate beads for efficient removal of methylene blue dye; isotherms, kinetic, mechanism and co-existing ions studies. *Journal of Porous Materials*. 30(2): 607–618. <https://doi.org/10.1007/s10934-022-01347-6>.
- Estrada, A. K. C., Lozano, F. C., and Díaz, R. A. L. 2021. Thermodynamics and kinetic studies for the adsorption process of methyl orange by magnetic activated carbons. *Air, Soil and Water Research*. 14: 11786221211013336. <https://doi.org/10.1177/11786221211013336>.
- Gan, C., Liu, Y., Tan, X., Wang, S., Zeng, G., Zheng, B., Li, T., Jiang, Z., and Liu, W. 2015. Effect of porous zinc-biochar nanocomposites on Cr(VI) adsorption from aqueous solution. *RSC Advances*. 5(44): 35107–35115. <https://doi.org/10.1039/C5RA04416B>.
- Gautam, D., and Hooda, S. 2020. Magnetic graphene oxide/chitin nanocomposites for efficient adsorption of methylene blue and crystal violet from aqueous solutions. *Journal of Chemical & Engineering Data*. 65(8): 4052–4062. <https://doi.org/10.1021/acs.jced.0c00350>.
- Genli, N., Şahin, Ö., Baytar, O., and Horoz, S. 2021. Synthesis of activated carbon in the presence of hydrochar from chickpea stalk and its characterization. *Journal of Ovonic Research*. 17(2): 117–124.
- Geremias-Andrade, I. M., Rocheto, A. C., Gallo, F. A., and Petrus, R. R. 2020. The shelf life of standardized sugarcane juice stored under refrigeration. *Food Science and Technology*. 40(1): 95–101. <https://doi.org/10.1590/fst.33918>.
- Gherbia, A., Chergui, A., Yeddou, A. R., Selatnia, A., and Nadjemi, B., 2019. Removal of methylene blue using activated carbon prepared from date stones activated with NaO. *Global Nest Journal*. 21(3): 374–380. <https://doi.org/10.30955/gnj.002913>.
- Goyal, M., Singh, S., and Bansal, R. 2004. Equilibrium and Dynamic Adsorption of methylene blue from aqueous solutions by surface modified activated carbons. *Carbon letters*. 5.
- Güleç, F., Williams, O., Kostas, E. T., Samson, A., Stevens, L. A., and Lester, E. 2022. A comprehensive comparative study on methylene blue removal from aqueous solution using biochars produced from rapeseed, whitewood, and seaweed via different thermal conversion technologies. *Fuel*. 330: 125428. <https://doi.org/10.1016/j.fuel.2022.125428>.
- Guo, J. Z., Li, B., Liu, L., and Lv, K. 2014. Removal of methylene blue from aqueous solutions by chemically modified bamboo. *Chemosphere*. 111: 225–231. <https://doi.org/10.1016/j.chemosphere.2014.03.118>.
- Ji, B., Wang, J., Song, H., and Chen, W. 2019. Removal of methylene blue from aqueous solutions using biochar derived from a fallen leaf by slow pyrolysis: Behavior and mechanism. *Journal of Environmental Chemical Engineering*. 7(3): 103036. <https://doi.org/10.1016/j.jece.2019.103036>.
- Kalam, S., Abu-Khamsin, S. A., Kamal, M. S., and Patil, S. 2021. Surfactant adsorption isotherms: A Review, *ACS Omega*. 6(48): 32342–32348. <https://doi.org/10.1021/acsomega.1c04661>.
- Khodmanee, S., and Amnuaylojaroen, T. 2021. Impact of biomass burning on ozone, carbon monoxide, and nitrogen dioxide in northern Thailand. 9: 641877. <https://doi.org/10.3389/fenvs.2021.641877>.
- Khushboo, Kaur, M., and Jeet, K. 2022. Mechanistic insight into adsorption and photocatalytic potential of magnesium ferrite-bentonite nanocomposite. *Journal of Photochemistry and Photobiology A: Chemistry*. 425: 113717. <https://doi.org/10.1016/j.jphotochem.2021.113717>.

- Kumar, R., Bhattacharya, S., and Sharma, P. 2021. Novel insights into adsorption of heavy metal ions using magnetic graphene composites. *Journal of Environmental Chemical Engineering*. 9(5): 106212. <https://doi.org/10.1016/j.jece.2021.106212>.
- Li, K., Zhou, M., Liang, L., Jiang, L., and Wang, W. 2019. Ultrahigh-surface-area activated carbon aerogels derived from glucose for high-performance organic pollutants adsorption. *Journal of Colloid and Interface Science*. 546: 333–343. <https://doi.org/10.1016/j.jcis.2019.03.076>.
- Liu, Y. 2009. Is the free energy change of adsorption correctly calculated?. *Journal of Chemical & Engineering Data*. 54(7): 1981–1985. <https://doi.org/10.1021/jc800661q>.
- Liyanaarachchi, H., Thambiliyagodage, C., Lokuge, H., and Vigneswaran, S. 2023. Kinetics and thermodynamics study of methylene blue adsorption to sucrose- and urea-derived nitrogen-enriched, hierarchically porous carbon activated by KOH and H₃PO₄. *ACS Omega*. 8: 16158–16173. <https://doi.org/10.1021/acsomega.3c00339>.
- Lyu, R., Zhang, C., Xia, T., Chen, S., Wang, Z., Luo, X., Wang, L., Wang, Y., Yu, J., and Wang, C. 2020. Efficient adsorption of methylene blue by mesoporous silica prepared using sol-gel method employing hydroxyethyl cellulose as a template. *Colloids and Surfaces A: Physicochemical and Engineering Aspects*. 606: 125425. <https://doi.org/10.1016/j.colsurfa.2020.125425>.
- Marrakchi, F., Hameed, B. H., and Bouaziz, M. 2020. Mesoporous and high-surface-area activated carbon from defatted olive cake by-products of olive mills for the adsorption kinetics and isotherm of methylene blue and acid blue 29. *Journal of Environmental Chemical Engineering*. 8(5): 104199. <https://doi.org/10.1016/j.jece.2020.104199>.
- Mondal, S., and Majumder, S. K. 2019. Honeycomb-like porous activated carbon for efficient copper (II) adsorption synthesized from natural source: Kinetic study and equilibrium isotherm analysis. *Journal of Environmental Chemical Engineering*. 7(4): 103236. <https://doi.org/10.1016/j.jece.2019.103236>.
- Naikwadi, P. M., Chavan, U. D., Pawar, V. D., and Amarowicz, R., 2010. Studies on dehydration of figs using different sugar syrup treatments. *Journal of Food Science and Technology*. 47(4): 442–445. <https://doi.org/10.1007/s13197-010-0073-6>.
- Namal, O. O., and Kalipci, E. 2020. Adsorption kinetics of methylene blue removal from aqueous solutions using potassium hydroxide (KOH) modified apricot kernel shells. *International Journal of Environmental Analytical Chemistry*. 100(14): 1549–1565. <https://doi.org/10.1080/03067319.2019.1656721>.
- Nizam, N. U. M., Hanafiah, M. M., Mahmoudi, E., Halim, A. A., and Mohammad, A. W. 2021. The removal of anionic and cationic dyes from an aqueous solution using biomass-based activated carbon. *Scientific Reports*. 11(1): 8623. <https://doi.org/10.1038/s41598-021-88084-z>.
- Nkutha, C. S., Shooto, N. D., and Naidoo, E. B. 2020. Adsorption studies of methylene blue and lead ions from aqueous solution by using mesoporous coral limestones. *South African Journal of Chemical Engineering*. 34: 151–157. <https://doi.org/10.1016/j.sajce.2020.08.003>.
- Noreen, S., Khalid, U., Ibrahim, S. M., Javed, T., Ghani, A., Naz, S., and Iqbal, M. 2020. ZnO, MgO and FeO adsorption efficiencies for direct sky Blue dye: equilibrium, kinetics and thermodynamics studies. *Journal of Materials Research and Technology*. 9(3): 5881–5893. <https://doi.org/10.1016/j.jmrt.2020.03.115>.
- Oladoye, P. O., Ajiboye, T. O., Omotola, E. O., and Oyewola, O. J., 2022. Methylene blue dye: Toxicity and potential elimination technology from wastewater. *Results in Engineering*. 16: 100678. <https://doi.org/10.1016/j.rineng.2022.100678>.
- Opoku, B. K., Isaac, A., Micheal, A. A., Bentum, J. K., and Muyoma, W. P. 2021. Characterization of chemically activated carbons produced from coconut and palm kernel shells using SEM and FTIR analyses. *American Journal of Applied Chemistry*. 9(3): 90–96.
- Prabu, D., Kumar, P. S., Vardhan, K. H., Sathish, S., Raju, A., and Mathew, J. 2020. Adsorptive elimination of methylene blue dye from aquatic system using biochar produced from cocoa shell. *Desalination and Water Treatment*. 2020: 366–378. <https://doi.org/10.5004/dwt.2020.26197>.
- Rehman, M. U., Manan, A., Uzair, M., Khan, A. S., Ullah, A., Ahmad, A. S., Wazir, A. H., Qazi, I., and Khan, M. A. 2021. Physicochemical characterization of Pakistani clay for adsorption of methylene blue: Kinetic, isotherm and thermodynamic study. *Materials Chemistry and Physics*. 269: 124722. <https://doi.org/10.1016/j.matchemphys.2021.124722>.
- Rheima, A. M., Mahmood, R. S., Hussain, D. H., and Abbas, Z. S. 2021. Study the adsorption ability of alizarin red dye from their aqueous solution on synthesized carbon nanotubes. *Digest Journal of Nanomaterials and Biostructures*. 16(1): 11–18.
- Ribeiro, M. R., de Moraes Guimarães, Y., Silva, I. F., Almeida, C. A., Silva, M. S. V., Nascimento, M. A., da Silva, U. P., Varejão, E. V., dos Santos Renato, N., Teixeira, A. P. d. C., and Lopes, R. P. 2021. Synthesis of value-added materials from the sewage sludge of cosmetics industry effluent treatment plant. *Journal of Environmental Chemical Engineering*. 9(4): 105367. <https://doi.org/10.1016/j.jece.2021.105367>.
- Roslan, F. A. S., Harun, N. Y., Hezam, A. A., Saeed, R. M. R., Mannikam, S. D., and Al-Qadami, E. H. H., 2022. Methylene blue removal using palm oil mill effluent sludge-derived adsorbent. *Chemical Engineering Transactions*. 91: 589–594. <https://doi.org/10.3303/CET2291099>.
- Sahoo, T. R., and Prelo, B. 2020. Chapter 7- Adsorption processes for the removal of contaminants from wastewater: the perspective role of nanomaterials and nanotechnology. In: *Nanomaterials for the detection and removal of wastewater Pollutants*. Elsevier. p.161–222.
- Samoudi, B., Bendaou, O., Hanafi, I., Asselman, A., and Haboubi, K. 2022. FTIR and raman spectroscopy study of soot deposits produced in the infrared multiphoton dissociation of vinyl bromide. *Journal of Spectroscopy*. 2022: 9942870. <https://doi.org/10.1155/2022/9942870>.
- Sattari, A., Ramazani, A., Aghahosseini, H., and Aroua, M. K. 2021. The application of polymer containing materials in CO₂ capturing via absorption and adsorption methods. *Journal of CO₂ Utilization*. 48: 101526. <https://doi.org/10.1016/j.jcou.2021.101526>.
- Shi, J., Li, W. B., and Li, D. 2015. Rapidly reversible adsorption of methane with a high storage capacity on the zeolite templated carbons with glucose as carbon precursors. *Colloids and Surfaces A: Physicochemical and Engineering Aspects*. 485: 11–17. <https://doi.org/10.1016/j.colsurfa.2015.08.026>.
- Shikuku, V. O., and Mishra, T. 2021, Adsorption isotherm modeling for methylene blue removal onto magnetic kaolinite clay: a comparison of two-parameter isotherms. *Applied Water Science*. 11(6): 103. <https://doi.org/10.1007/s13201-021-01440-2>.
- Sparrevik, M., Adam, C., Martinsen, V., Jubaedah, and Cornelissen, G. 2015. Emissions of gases and particles from charcoal/biochar production in rural areas using medium-sized traditional and improved “retort” kilns. *Biomass and Bioenergy*. 72: 65–73. <https://doi.org/10.1016/j.biombioe.2014.11.016>.

- Suhas, Gupta, V. K., Carrott, P. J. M., Singh, R., Chaudhary, M., and Kushwaha, S., 2016. Cellulose: A review as natural, modified and activated carbon adsorbent. *Bioresource Technology*. 216: 1066–1076. <https://doi.org/10.1016/j.biortech.2016.05.106>.
- Sultana, M., Rowan, M. H., Sabrin, M., Rahaman, M. H., and Alam, S. M. N. 2022. A review on experimental chemically modified activated carbon to enhance dye and heavy metals adsorption. *Cleaner Engineering and Technology*. 6: 100382. <https://doi.org/10.1016/j.clet.2021.100382>.
- Texeira, G.G., and Santos, P. M. 2022. Simple and cost-effective approaches for quantification of reducing sugar exploiting digital image analysis. *Journal of Food Composition and Analysis*. 113 (2022): 104719. <https://doi.org/10.1016/j.jfca.2022.104719>.
- Thang, N. H., Khang, D. S., Hai, T. D., Nga, D. T., and Tuan, P. D. 2021. Methylene blue adsorption mechanism of activated carbon synthesized from cashew nut shells. *RSC Advances*. 11(43): 26563–26570. <https://doi.org/10.1039/D1RA04672A>.
- Tongpoothorn, W., Somboon, T., and Sriuttha, M. 2020. The utilization of Napier grass stems for Cd(II) ions removal from aqueous solution: Process optimization studies using response surface methodology. *Naresuan University Journal: Science and Technology*. 28(3): 46–62. <https://doi.org/10.14456/nujst.2020.25>.
- Trakal, L., Bingöl, D., Pohorelý, M., Hruška, M., and Komárek, M. 2014. Geochemical and spectroscopic investigations of Cd and Pb sorption mechanisms on contrasting biochars: Engineering implications. *Bioresource Technology*. 171: 442–451. <https://doi.org/10.1016/j.biortech.2014.08.108>.
- Tran, H. N. 2022. Improper estimation of thermodynamic parameters in adsorption studies with distribution coefficient K_D (q_e/C_e) or Freundlich constant (K_F): Considerations from the derivation of dimensionless thermodynamic equilibrium constant and suggestions. *Adsorption Science & Technology*. 2022: 5553212. <https://doi.org/10.1155/2022/5553212>.
- Tran, H. V., Hoang, L. T., and Huynh, C. D. 2020. An investigation on kinetic and thermodynamic parameters of methylene blue adsorption onto graphene-based nanocomposite. *Chemical Physics*. 535: 110793. <https://doi.org/10.1016/j.chemphys.2020.110793>.
- Tuli, F. J., Hossain, A., Kibria, A. K. M. F., Tareq, A. R. M., Mamun, S. M. M. A., and Ullah, A. K. M. A. 2020. Removal of methylene blue from water by low-cost activated carbon prepared from tea waste: A study of adsorption isotherm and kinetics. *Environmental Nanotechnology, Monitoring and Management*. 14: 100354. <https://doi.org/10.1016/j.enmm.2020.100354>.
- Wang, B., Lan, J., Bo, C., Gong, B., and Ou, J. 2023. Adsorption of heavy metal onto biomass-derived activated carbon: review. *Royal Society of Chemistry*. 13: 4275-4302. <https://doi.org/10.1039/D2RA07911A>.
- Wang, B., Xu, X., Tang, H., Mao, Y., Chen, H., and Ji, F. 2020. Highly efficient adsorption of three antibiotics from aqueous solutions using glucose-based mesoporous carbon. *Applied Surface Science*. 528: 147048. <https://doi.org/10.1016/j.apsusc.2020.147048>.
- Wang, J., Ma, J., and Sun, Y. 2022. Adsorption of methylene blue by coal-based activated carbon in high-salt wastewater. *Water*. 14(21): 3576.
- Wang, N. S. 2004. Experimental No.9D Sucrose assay by the dinitrosalicylic colorimetric method. <https://user.eng.umd.edu/~nsw/ench485/lab9d.htm>
- Wang, S. N., Li, P., Gu, J. J., Liang, H., and Wu, J. H. 2018. Carboxylate-functionalized sugarcane bagasse as an effective and renewable adsorbent to remove methylene blue. *Water Science and Technology*. 2017(1): 300–309. <https://doi.org/10.2166/wst.2018.113>.
- Whitener, J. K. E. 2016. Rapid synthesis of thin amorphous carbon films by sugar dehydration and dispersion. *AIMS Materials Science*. 3(4): 1309–1320. <https://doi.org/10.3934/mat.2016.4.1309>.
- Wibawa, P. J., Nur, M., Asy'ari, M., and Nur, H. 2020. SEM, XRD, and FTIR analyses of both ultrasonic and heat-generated activated carbon black microstructures. *Heliyon*. 6(3): e03546. <https://doi.org/10.1016/j.heliyon.2020.e03546>.
- Wu, K. H., Huang, W. C., Hung, W. C., and Tsai, C. W. 2021. Modified expanded graphite/Fe₃O₄ composite as an adsorbent of methylene blue: Adsorption kinetics and isotherms. *Materials Science and Engineering: B*. 266: 115068. <https://doi.org/10.1016/j.mseb.2021.115068>.
- Wu, Q., Dong, S., Wang, L., and Li, X. 2021. Single and competitive adsorption behaviors of Cu²⁺, Pb²⁺ and Zn²⁺ on the biochar and magnetic biochar of Pomelo peel in aqueous solution. *Water*. 13(6): 868.
- Xiao, W., Garba, Z. N., Sun, S., Lawan, I., Wang, L., Lin, M., and Yuan, Z. 2020. Preparation and evaluation of an effective activated carbon from white sugar for the adsorption of rhodamine B dye. *Journal of Cleaner Production*. 253: 119989. <https://doi.org/10.1016/j.jclepro.2020.119989>.
- Yazaydin, A. O., and Thompson, R. W. J. E. S. 2009. Computing adsorbate/adsorbent binding energies and Henry's law constants from molecular simulations. *Environmental Engineering Science*. 26: 297–303. <https://doi.org/10.1089/EES.2008.0025>
- Yoshida, Y., Shimada, T., Ishida, T., and Takagi, S. 2020. Thermodynamic study of the adsorption of acridinium derivatives on the clay surface. *RSC Advances*. 10: 21360–21368. <https://doi.org/10.1039/D0RA03158E>.
- Zaidan, N. L., Mohamad-Fuzi, S. F., Hailan, I. M., Roshidi, A. A., Kormin, F., Abu-Bakar, M. F., and Sabran, S. F. 2021. Physicochemical and sensory characteristics of treated sugarcane juice, In: IOP Conference Series: Earth and Environmental Science, International Conference on Biodiversity, Melaka, 4-5 November 2020. IOP Publishing, Philadelphia. p.012073.
- Zhang, Y., Xu, J., Li, B., Xie, Z., Li, X., Tang, J., and Fan, S. 2021. Enhanced adsorption performance of tetracycline in aqueous solutions by KOH-modified peanut shell-derived biochar. *Biomass Conversion and Biorefinery*. <https://doi.org/10.1007/s13399-021-02083-8>.
- Zhao, M., Dai, Y., Zhang, M., Feng, C., Qin, B., Zhang, W., Zhao, N., Li, Y., Ni, Z., Xu, Z., Tsang, D. C. W., and Qiu, R. 2020. Mechanisms of Pb and/or Zn adsorption by different biochars: Biochar characteristics, stability, and binding energies. *Science of the Total Environment*. 717: 136894. <https://doi.org/10.1016/j.scitotenv.2020.136894>.
- Zhou, Q., Liao, B., Lin, L., Qiu, W., and Song, Z. 2018. Adsorption of Cu(II) and Cd(II) from aqueous solutions by ferromanganese binary oxide-biochar composites. *Science of the Total Environment*. 615: 115–122. <https://doi.org/10.1016/j.scitotenv.2017.09.220>.

Influenced factors for cotton dyeing process with mangosteen leaf extract

Waranya Tharawatchruk¹, Pat Pranamornkith¹, Supinan Janma¹, Watee Panthuwat¹, Narit Funsueb¹ and Tanongsak Sassa-deepaeng^{1,2*}

¹Faculty of Science and Agricultural Technology, Rajamangala University of Technology Lanna, Lampang 52000, Thailand

²Agricultural Biochemistry Research Unit, Faculty of Science and Agricultural Technology, Rajamangala University of Technology Lanna, Lampang 52000, Thailand

*Corresponding author: tanongsaks@rmutl.ac.th

Received: November 6, 2023. Revised: December 16, 2023. Accepted: December 16, 2022.

ABSTRACT

This current study investigated the aqueous extracts of mangosteen leaves for dyeing cotton fabric with various mordants to develop color shadings. Freshly prepared extracts were subjected to preliminary phytochemical screening. It was found that mangosteen leaf extract revealed the presence of pH in the range of 6.0–7.6 and the content of phenolic compound, flavonoid, reducing sugar, and tannin in the range of 0.32–1.10 GAE/mg DW, 0.70–2.97 QE/mg DW, 0.91–7.15 mg/mL and 17.5–24.79 ECGC/mg DW, respectively. This might be responsible for the reduced properties. The three times repetition of 80 g/L extract with mordant was found to be the most satisfying, characterized by using colorimetric characteristics (CIE L*a*b*). It can be concluded that mangosteen leaf extract has a high potential for fabric dyeing and might be a promising low-cost reducing agent for developing green dyeing for clothing in the near future.

Keywords: mangosteen leaves, cotton dyeing, mordants

INTRODUCTION

Natural dyes have been used since ancient times. They are currently showing a significant trend towards their popularity. Natural dyes provide more significant advantages than synthetic dyes, which cause environmental and health impacts. The application areas of the colors are numerous, including clothing, cosmetics, pharmaceutical, food industry, medicine, etc. Natural colors can be mainly obtained from minerals, animals, and plants. Most of the mineral dyes are inorganic metal salt and metal oxides. They can be categorized in terms of their colors. Animal dyes are extracted from the dried bodies of insects. Compared to the others, plant dye extracts are a high-potential source as they are commonly and abundantly found. Also, the colorants can be extracted from several plant parts, including leaves, barks, fruits, seeds, roots, etc. (Yusuf et al., 2017) by conventional and modern methods, which depend on their applications (Yadav et al., 2023).

Mangosteen or *Garcinia mangostana* L. (Thai; Mang-Khut), a small evergreen fruit tree in the family Clusiaceae, is widely grown and consumed in tropical countries at a low cost. It was reported that total phenolic, flavonoid, tannins, and saponins were rich in leaves (Suhartati et al., 2019). These components contributed to reducing properties measured using 2,2-diphenyl-1-picrylhydrazyl (DPPH) reducing ability assay as indicated by Sassa-

deepaeng et al. (2019). Interestingly, the extract also shows antibacterial properties against *Pseudomonas aeruginosa*, which causes various diseases, such as skin infections (Suhartati et al., 2019). Thus, the newly challenged plant might be used in this experiment as a reducing agent and dye.

As indicated by Azeem et al. (2019), it was found that mordanting treated cotton fabrics with iron (II) sulfate and tannic acid developed darker shades. To investigate the effect of mordants on color shadings, the natural materials were selected, based on reported high tannin content, for testing, such as alum, carandas-plum fruits, tea, guava leaf, raw banana peel, neem tree bark, and chemicals were also chosen such as ash calcium hydroxide, FeSO₄, and CuSO₄. Alum has been used as mordant for natural dyeing for many decades as well as our previous report that carandas-plum fruit possessed the excellent reducing properties for traditional cotton fabrics dyeing with indigo from *Strobilanthes cusia* (Nees) Kuntze (Pranamornkith et al., 2022). Tea is also used as a traditional mordant for dyeing, as reported by Triwiswara and Indrayani (2020). Guava leaf is a good source of tannin, according to the report of Mailoa et al. (2013), while raw banana peel was also reported as a tannin resource by Aroonsrimorakot and Whangchai (2019). Many publications indicated that Neem tree bark comprises tannin in the aqueous extracts (Bhagwat et al., 2020; Islas et al., 2020). For using Ca(OH)₂, FeSO₄, and CuSO₄, it was documented by Azeem et al. (2019) and Indrianingsih et al. (2021).

According to the information provided, the researchers are interested in researching the use of mangosteen leaf extract for dyeing cotton fabric. The concentrations of mangosteen leaves were varied from 40, 80, 120, and 160 g/L for the extraction process. The CIE L* a* b* technique observed the optimal concentration after the dyeing process. The chemical composition of the mangosteen leaf extract solution was examined. The effect of different mordants on the color shade of dyed cotton was studied.

MATERIALS AND METHODS

Materials

The cotton fabric and alum were purchased from a local store. Mangosteen leaves were collected from Na-Ku-Ha village, Amphoe Muang, Phrae province, northern Thailand. Natural mordants such as Carandas-plum, tea, guava leaves, raw banana peel, and neem trees were obtained locally from Amphoe Muang, Lamphang province, northern Thailand. Iron (II) sulfate (FeSO_4) was commercially provided by Gammaco (Thailand) Co., Ltd., Copper (II) sulfate (CuSO_4) was purchased from Ajax Finechem Pty Ltd., Australia.

Methods

Dye extraction from mangosteen leaves

Collected mangosteen leaves were air-dried at ambient temperature for a few months with a moisture content of 50%. Dried leaves were extracted by immersing 40, 80, 120, and 160 g of dried leaves in a liter of water, respectively. Each concentration's crude dye extraction solutions were boiled using a cooking gas burner for 30 minutes. The crude dye extraction solution samples were then separated into two portions. One portion was further used for chemical characterization, and the other was for dyeing.

Identification of mangosteen leaves extracted dye

The crude dye extraction solution was filtered with filter paper (Whatman No. 1) and used for the following determination:

UV-Visible spectral characteristic

The crude dye extraction solution samples were diluted 100-fold for characterization by UV-visible spectroscopy. The spectrophotometer (Biochrome, S50-S80) measured in the range of 200 to 800 nm to obtain spectra.

Phenolic compound content

The quantification of total phenolic content (TPC) in water extracts was conducted in triplicate employing the Folin-Ciocalteu reagent. The formation of a blue complex resulting from electron transfer was monitored using a UV-Vis spectrophotometer (Dshing Instrument Co., Ltd., China) following the procedure outlined by Singleton and Rossi (1965). Specifically, 20 μL of the extract was combined with 100 μL of FC reagent (Merck, Damstadt, Germany) in 1,980 μL of deionized water, followed by a 5-minute incubation at room temperature. Subsequently, 300 μL of a 7% solution of Na_2NO_3 (Univar, Ajax Finechem, Australia) was introduced and vigorously mixed before a 60-minute incubation in darkness at room temperature. Ultimately, the absorbance was measured at 765 nm. The TPC values were expressed as micrograms of gallic acid equivalent per milligram of dry weight of the extract, determined through linear regression analysis utilizing gallic acid standards at concentrations ranging from 0 to 25 $\mu\text{g}/\text{mL}$.

Flavonoid content

The determination of flavonoid content (FC) was conducted in triplicate using the aluminum trichloride (AlCl_3) colorimetric method as described initially by Christ and Müller (1960), with adaptations to accommodate 96-well microplates, as outlined by Yodthong et al. (2020). In this procedure, a 20 μL aliquot of the ethanolic solution of each extract or various concentrations of quercetin was combined with 75 μL of deionized water, followed by the addition of 25 μL of a 5% NaNO_2 solution (Univar, Ajax Finechem, Australia) within a microplate. Following a 5-minute incubation at ambient temperature, 25 μL of a 10% AlCl_3 solution (Lobachemie, India) was introduced, and the mixture was further incubated for 6 minutes under the same conditions. Subsequently, 100 μL of a 1M NaOH solution (Merck KGaA, Germany) was added, and the reaction was allowed to continue for 60 minutes in the absence of light before measuring the absorbance at 405 nm using a microplate reader (Biobase EL-10A China). The flavonoid content was expressed as micrograms of quercetin (Sigma-Aldrich, Germany) equivalent (QE) per milligram of dry weight of the extract.

Tannin content

The content of tannin also had a direct impact on the reducing properties of the sample. To quantify the tannin content (TC), the vanillin assay was performed in triplicate, following the procedure outlined initially by Broadhurst and Jones (1978),

with adaptations to minimize reagent volume and consequently reduce the generation of hazardous waste. Specifically, 250 μL of the extract was combined with 450 μL of a 1% vanillin solution (Merck, Germany) in methanol (QR $\ddot{\text{C}}$, New Zealand). After a 5-minute incubation at room temperature without light, the mixture was vigorously mixed with 300 μL of concentrated hydrochloric acid (QR $\ddot{\text{C}}$, New Zealand) and allowed to incubate for 30 minutes in darkness. Subsequently, the solution turned red, and this change was detectable at 500 nm using a UV-Vis spectrophotometer (Dshing Instrument Co., Ltd., China). The tannin content was expressed as micrograms of Epigallocatechin gallate (Sigma–Aldrich, Germany) equivalent (EE) per milligram of dried weight of the extract.

Saponin

A total of 5 mL of an ethanolic extract was vigorously agitated with 5 mL of distilled water within a test tube and subsequently subjected to warming in a water bath maintained at 39 ± 1 °C for 10 minutes. The observation of a persistent honeycomb froth formation for 10 minutes served as an indicative marker for the presence of saponins in accordance with the criteria defined by Harborne (1998).

Reducing sugar

Reducing sugar was determined by the DNS method, which was adjusted by Saqib and Whitney (2011). DNS reagent was prepared by mixing 3,5-dinitro salicylic acid (DNS) solution (2.5 g in 100 mL of 1 M NaOH) with the heated dissolved sodium potassium tartrate solution (75 g in 125 mL of distilled water). The volume of the mixing solution was then adjusted to 500 mL with distilled water. DNS reagent 1 mL was added to 0.1 mL crude dye extraction solution samples and adjusted to the final volume of 4 mL with distilled water. The tube was heated in boiling water for 5 minutes. The absorbance was measured at 540 nm. The standard measurement was performed using 2 mM glucose as a reducing sugar standard.

Dyeing process

Cotton fabrics were soaked in hot crude extracted dye solution for 30 min with a ratio of fabric 20 g: 1 L of liquor. Dyed cotton fabrics were brought to squeeze until damp and mordanted with calcium hydroxide solution (5% w/v). The fabrics were eventually washed and air-dried.

Dyeing repetition

The dyeing repetition was carried out for five treatments: one-time, two-time, three-time, four-time, and five-time repeated dyeing.

Mordanting process

Different mordants were used, including alum, Carandas-plum (*Carissa carandas* L.) fruit, tea, guava leaf, raw banana peel, Neem tree (*Azadirachta indica*) bark, ash, calcium hydroxide solution at the concentration of 5% w/v and FeSO_4 , and CuSO_4 at the concentration of 10 mg/L. After the dyeing process with the crude dye extraction solution, the damped dyed fabrics were soaked and squeezed in each mordant for 5 minutes. All dyed fabrics were then washed and air-dried.

Color measurement and fastness test

The color coordinates CIE $L^* a^* b^*$ values of all dyed clothes were measured by HunterLab, ColorQuest XE model. The dyed clothes were tested and evaluated for colorfastness to washing.

RESULTS AND DISCUSSION

The powder of mangosteen leaves was prepared by drying fresh leaves at ambient temperature for months until the moisture content dropped to 50%. To make a fine powder, dried leaves were ground and sieved. The obtained powder has a light brown color, and the crude dye extraction solution has a dark brown color (Figure 1).



Figure 1. Sample preparation.

Property and chemical composition analysis

The extract prepared by dissolving mangosteen leaf (ML) powder in various concentrations in hot DI water showed a pH value in the range of 6.0 to 7.6. It might result from the high composition of tannic acid, as indicated in Figure 2 and Table 1. However, the results also show that the ML-extract consisted of other organic acids such as tannins, saponin, and phenolic compounds, as reported by Alsultan et al. (2017), which contributed to the decrease of the extract pH. Among these compounds, tannins are an important component of the dyeing process as they can act as a natural mordant to sustain the color of matter permanently. As reported by Sassa-deepening et al. (2019), it was

found that the aqueous extract of mangosteen leaves possessed high reducing properties. To investigate the source molecules of reducing power, the total phenolic content (TPC) assay was conducted using the Folin-Ciocalteu colorimetric method. The highest TPC of plant aqueous extracts was found gradually with increasing concentration. This indicates ML-extract had a high ability to reduce Folin-Ciocalteu

reagent. In addition, ML extract also exhibited the highest flavonoid content and reducing sugar, which contributes to the reducing properties. Therefore, ML extract might be an excellent tentative plant for using traditional cotton fabrics dyeing with mordants. To characterize the composition of the ML extracts, the UV-Vis spectra of the extract were recorded by spectrophotometry and shown in Figure 2.

Table 1. Property and chemical composition of extracted dyes from mangosteen leaves

Extracted dyes (g/L)	Phenolic compounds (GAE/mg DW)	Flavonoid (QE/mg DW)	Tannin (ECGC /mg DW)	Reducing sugar (g/L)	pH	Saponin
40	0.32	0.70	17.57	0.91	7.6	–
80	0.69	1.64	20.39	4.19	6.8	+
120	0.85	2.48	22.29	5.47	6.4	++
160	1.10	2.97	24.79	7.15	6.0	++

– = N.D. + = mild positive. ++ = strong positive.

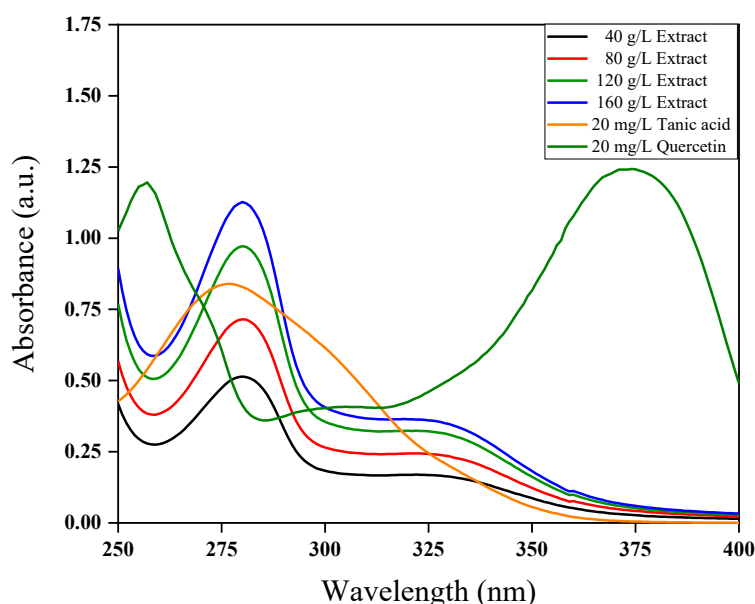


Figure 2. UV-Vis spectra of extract dyes from mangosteen leaves at different concentrations.

The characteristic color of ML extract could be the consequence of the presence of the major compounds. Tannin and quercetin are transparent in the visible region (Grasel et al., 2016). Therefore, Figure 2 shows the absorption spectra of those compounds generated during the analysis of the aqueous extract at various concentrations of ML extract (40–160 g/L). It was found that the strong absorption at 280 nm was obtained from aqueous solutions. The result is supported by the founding of Grigsby et al. (2013), who documented that the major peaks of tannic acid and tannin derivatives were observed in the UVB (285–315 nm). Unfortunately, UV-visible spectra for quercetin (spectrum) exhibited two absorption bands at 256 and 374 nm were not detected. From the UV data ML-extracted, it can be

stated that there was a tannin-related compound present in the dye extract.

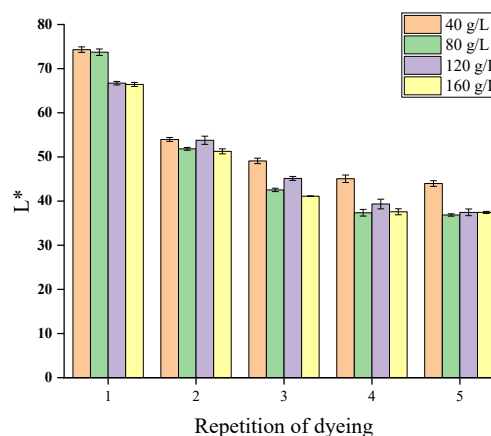


Figure 3. The lightness value (L^*) of ML-extract.

The color of the dyed samples is given in CIE Lab coordinates (L^* , a^* , b^*): L^* corresponding to the brightness (100 = white, 0 = black), a^* to the red-green coordinate (+ve = red, -ve = green or blue) and b^* to the yellow-blue coordinate (+ve = yellow, -ve = green). From Figure 3, it was found that the ML-extract at a concentration of 80 g/L shows the effective cost with efficiency for dyeing due to the saturated perceptual darkness on cotton fabric at the third repetition. However, the a^* value was also considered, and the result is shown in Figure 4.

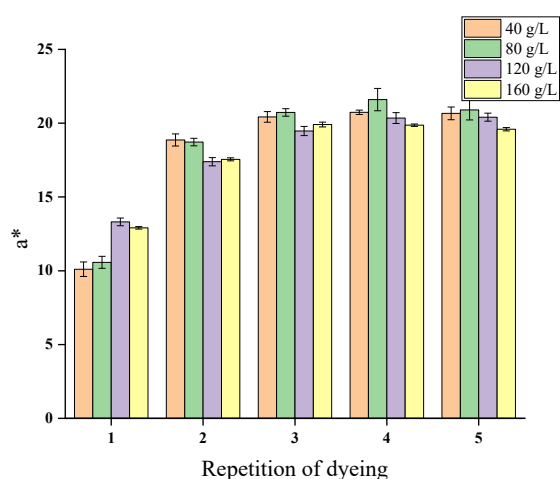


Figure 4. The green-magenta opponent color value (a^*) of ML-extract.

The a^* value, represented as a red and green scale, runs from 0 to 60. From the data, it can be seen that cotton fabric dyed three times repetition at a concentration of 80 g/L without mordant revealed the highest a^* value of 20.73 ± 0.25 .

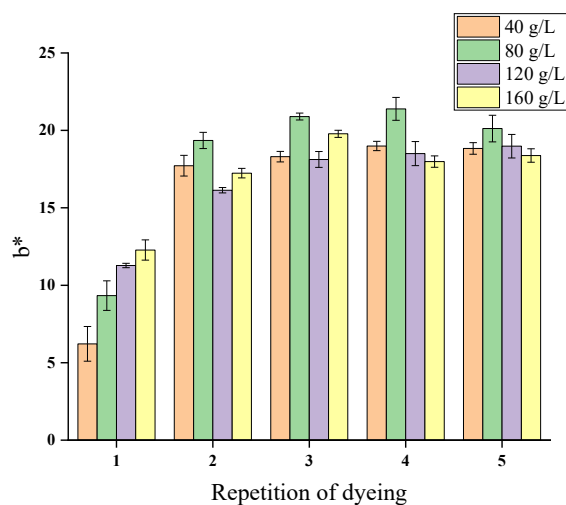


Figure 5. The blue-yellow opponents' value (b^*) of ML-extract.

The b^* notation represents the chromatic color in the direction of blue and yellow. A positive value of b^* ($+b^*$) from 0 to 60 and a negative value of b^* ($-b^*$) from 0 to -60. The average value of b^* in this study was 20.89 ± 0.22 (Figure 5). Therefore, it is clear that cotton fabric dyed three times of repetition at a concentration of 80 g/L is a suitable condition for further study on the mordanting step.

Dyeing cotton with extract dyes from mangosteen leaves

In Table 2, the cotton dyeing process with various concentrations of ML-extract at 40, 80, 120, and 160 g/L showed that the lightness value (L^*) decreased with higher concentrations. This represents the effect of the dye's concentration on the shades of dyed fabrics. It was obviously seen that the higher the dye uptake, the darker yellow-brown shade of the fabric color appeared. This evident was confirmed by an increase of the blue-yellow coordinate (b^*) in the first round of dyeing repetition, particularly.

Dyeing repetition has been reported to darken the color of the fabric and reinforce the fabric's dyed color (Suciatmih, 2020). In this study, it caused a deep brown color on the fabric sample (Table 2). The decrease of the L^* value of 1–5 dyeing repetitions was observed and illustrated that the frequency of dyeing applied affected the intensity of the brown color. This is due to the high negative charge in the tannin compound, which is contained dominantly in mangosteen leaves, as well as in its peels, which reacted favorably with the Ca^{2+} atom in a mordant compound. The $Ca(OH)_2$ solution, as a mordant compound in this case, plays an important role in the link between fabric fiber and dyes (Kusumawati et al., 2017).

Color fastness

Table 3 revealed the result of color fastness of dyed cotton fabrics with mangosteen leaves to washing. It provided promising lightfastness results with the good to excellent range of 4–5. The fabric samples, after washing repetition 5 times, showed non-significant color variations when subjected to wash fastness according to the lightness value (L^*).

Table 2. Dyeing cotton with extract dyes from mangosteen leaves at different concentration

Extracted dyes (g/L)	Dyeing repetition				
	1	2	3	4	5
40	 L* 74.30 a* 13.44 b* 6.22	 L* 53.97 a* 18.86 b* 17.72	 L* 49.10 a* 20.42 b* 18.30	 L* 45.06 a* 20.74 b* 18.99	 L* 43.97 a* 20.66 b* 18.84
80	 L* 73.73 a* 10.57 b* 9.33	 L* 51.84 a* 18.72 b* 19.35	 L* 42.54 a* 20.73 b* 20.89	 L* 37.36 a* 21.60 b* 21.39	 L* 36.86 a* 20.90 b* 20.12
120	 L* 66.71 a* 13.31 b* 11.28	 L* 53.78 a* 17.39 b* 16.14	 L* 45.13 a* 19.47 b* 18.12	 L* 39.33 a* 20.35 b* 18.50	 L* 37.55 a* 20.41 b* 18.98
160	 L* 66.43 a* 12.91 b* 12.28	 L* 51.26 a* 17.55 b* 17.24	 L* 41.11 a* 19.91 b* 19.78	 L* 37.57 a* 19.87 b* 17.99	 L* 37.44 a* 19.59 b* 18.38

Table 3. Color fading of cotton-dyed washing

Items	Repetition of washing				
	1	2	3	4	5
Dyed clothes					
L* a* b*	L* 45.86 a* 17.19 b* 16.31	L* 43.81 a* 17.81 b* 18.40	L* 42.35 a* 18.23 b* 18.67	L* 45.75 a* 17.45 b* 16.43	L* 45.66 a* 17.47 b* 16.64
Grey scale	5	5	5	4-5	4-5

Table 4. Color strength of ML-extract dyed cotton fabrics with mordants

Mordants	pH	Cotton fabrics	Color		
			L*	a*	b*
1. None	6.9		71.01	10.98	8.52
2. Alum	3.3		80.23	2.59	9.94
3. Carandas-plum (<i>Carissa carandas</i> L.) fruit	3.4		80.83	4.32	7.19
4. Tea	6.3		79.15	1.79	14.99
5. Guava leaf	6.6		78.64	3.30	12.37
6. Raw banana peel	7.4		77.13	6.91	3.05
7. Neem tree (<i>Azadirachta indica</i>) bark	7.6		72.85	9.45	7.46
8. Ash	9.5		73.25	8.25	5.44
9. Ca(OH) ₂	11.8		67.21	11.81	10.96
10. FeSO ₄	5.8		61.73	5.56	-1.86
11. CuSO ₄	5.6		66.44	8.65	10.27

The analysis results show that there were differences between the types of mordanting agents (Table 4). The lowest pH value was found in alum solution, while the highest pH value was detected in $\text{Ca}(\text{OH})_2$. It seems that a higher pH can develop darker color shades of ML-extract. The dye solution of ML-extract using FeSO_4 as a mordanting agent has the lowest brightness level of 61.730.12 while using Carandas-plum as a mordanting agent has a brightness level of 80.83 ± 0.23 . The variation of chemicals ferrous sulfate as a mordanting agent seems to be more affected by color darkening compared to those bio-mordants. As reported by Mongkholrattanasit et al. (2015), copper sulfate and ferrous sulfate, mordants are well known for their ability to form coordination complexes to readily chelate with the dye. The darker color shades by mordanting with tannic acid indicated strong interactions of this mordant with dye molecules to form an insoluble complex that firmly attached to cotton fabric (Ali, et al. 2010), while metal ions constituted a firm bonding with dye molecules as well as cotton fabric ultimately approaching towards maximum color strength as discussion by Bouatay et al. (2016). The fabric dyed using ML-extract under $\text{Ca}(\text{OH})_2$ as mordant has the highest* value of 11.810.26, while fabric dyed under tea as mordanting agent provided a* value of 1.79 ± 0.06 , indicating $\text{Ca}(\text{OH})_2$ was proper mordant in this study. The average value of b^* was in the range of -1.864 to 14.99. ML-extract dye solution with tea has the highest b^* value, while FeSO_4 possesses the lowest value of b^* . The results obtained from the measurement of b^* notation revealed the variations of green and yellowish green in the sample. The greater value of b^* indicated the more yellow sample color. Based on the data in Table 4, it can be indicated that ML-extract natural dyes generated many shades under mordant use.

CONCLUSIONS

In summary, mangosteen leaves extracted with hot water are suitable for use in the dyeing process. The 80 g/L of ML extract provided the dark-brown color of the cotton fabric caused by contained phytochemical compounds. Dyed cotton fabric with mordants showed many shades, including brown-grey, pale brown, yellow-brown, and yellow colors. Therefore, ML-extract has a high potential in traditional cotton fabric dyeing. This presents a promising low-cost natural dye for green dyeing fabric in the near future.

ACKNOWLEDGMENTS

The authors would like to thank the agricultural biochemistry research unit for supporting facilities and partial financial support. We are also grateful for the color measurement instrument of the Department of Food Science and Food Technology, Faculty of Science and Agricultural Technology, Rajamangala University of Technology Lanna Lampang.

REFERENCES

- Ali, A., Ali, S., Saleem, H., and Hussain, T. 2010. Effect of tannic acid and metallic mordants on the dyeing properties of natural dye extracted from *Acacia nilotica* bark. *Asian Journal of Chemistry*. 22(9): 7065–7069.
- Alsultan, Q.M.N., Sijam, K., Rashid, T.S., Ahmad, K.B., and Awla, H.K., 2017. Investigation of phytochemical components and bioautography of *Garcinia mangostana* L. methanol leaf extract. *Journal of Experimental Agriculture International*. 15 (3): 1–7.
- Aroonsrimorakot, S. and Whangchai, N. 2019. The Application of tannin extract from plants to reduce the concentration of arsenic. *International Journal of Agricultural Technology*. 15(2): 207–214.
- Azeem, M., Iqbal, N., Mir, R.A., Adeel, S., Batool, F., Kkan, A.A., and Gul, S. 2019. Harnessing natural colorants from algal species for fabric dyeing: a sustainable eco-friendly approach for textile processing. *Journal of Applied Phycology*. 31: 3941–3948. <https://doi.org/10.1007/s10811-019-01848-z>.
- Bhagwat, V.C. and Kadam V.B 2020. Phytochemical profile of *Azadirachta indica* A. Juss. and *Melia azedarach* Linn., *Journal of Drug Delivery and Therapeutics*. 10(2):180–183. <http://dx.doi.org/10.22270/jddt.v10i2.3944>.
- Bouatay, F., Meksi, N., Adeel, S., Salah, F. and Mhenni, F. 2016. Dyeing behavior of the cellulosic and jute fibers with cationic dyes: Process development and optimization using statistical analysis. *Journal of Natural Fibers*. 13(4): 423–436. <https://doi.org/10.1080/15440478.2015.1043685>
- Broadhurst, R. and Jones W. T. 1978. Analysis of condensed tannins using acidified vanillin. *Journal of the Science of Food and Agriculture*. 29(9): 788–94.
- Christ, B. and Müller, K. H. 1960. Zur serienmäßigen bestimmung des gehaltes an flavonol-derivaten in drogen. *Archiv der Pharmazie*. 293 (12): 1033–1042.
- Grasel, F. S., Ferrão, M. F., and Wolf, C. R. 2016. Ultraviolet spectroscopy and chemometrics for the identification of vegetable tannins, *Industrial Crops and Products*. 91: 279–285. <https://doi.org/10.1016/j.indcrop.2016.07.022>.
- Grigsby, W., Bridson, J., Lomas, C., and Elliot, J-A. 2013. Esterification of condensed tannins and their impact on the properties of poly (lactic acid). *Polymers*. 5(2): 344–360. <https://doi.org/10.3390/polym5020344>.
- Harborne, A.J. 1998. *Phytochemical methods: A guide to modern techniques of plant analysis*. 3rd ed. Chapman and Hall, London.
- Indrianingsih, A.W., Rosyida, V. T., Darsih, C., and Apriyana, W. 2021. Antibacterial activity of *Garcinia mangostana* peel-dyed cotton fabrics using synthetic and natural mordants. *Sustainable Chemistry and Pharmacy*, 21, 100440, <https://doi.org/10.1016/j.scp.2021.100440>.

- Islas, J. F., Acosta, E., G-Buentello, Z., Delgado-Gallegos, J. L., Moreno-Treviño, M.G., Escalante, B., and Moreno-Cuevas, J. E. 2020. An overview of Neem (*Azadirachta indica*) and its potential impact on health. *Journal of Functional Foods*. 74: 104171. <https://doi.org/10.1016/j.jff.2020.104171>.
- Kusumawati, N., Santoso, A. B., Sianita, M. M., and Muslim, S. 2017. Extraction, characterization, and application of natural dyes from the fresh mangosteen (*Garcinia mangostana* L.) peel. *International Journal on Advanced Science Engineering Information Technology*. 7(3): 878–884.
- Mailoa, N. M., Mahendradatta, M., Laga, A., and Djide, N. 2013. Tannin extract of guava leaves (*Psidium Guajava* L) variation with concentration organic solvents. *International Journal of Scientific and Technology Research*. 2:106–110.
- Mongkhohrattanasit, R., Saiwan, C., Rungruangkitkrai, N., Punrattanasin, N., Sriharuksa, K., Klaichoi, C., and Nakpathom, M. 2015. Ecological dyeing of silk fabric with lac dye by using padding techniques. *The Journal of The Textile Institute*. 106 (10): 1106–1114. <https://doi.org/10.1080/00405000.2014.976957>.
- Pranamornkith, P., Tharawatchruk, W., Panthuwat, W., Chaiwongsar, S., Yodthong, W., and Sassa-deepaeng, T. 2022. Utilization of *Carissa carandas* Linn. aqueous extracts as reducing agent for traditional cotton fabrics dyeing with indigo from *Strobilanthes cusia* Nees. *Journal of Science and Agricultural Technology*. 3(2): 12–18. <https://doi.org/10.14456/jsat.2022.7>.
- Saqib, A. A. N. and Whitney, P. J. 2011. Differential behaviour of the dinitrosalicylic acid (DNS) reagent towards mono- and di-saccharide sugars. *Biomass Bioenergy*. 35 (11): 4748–4750.
- Sassa-deepaeng, T., Yodthong, W., and Khamphira, T. 2019. Green synthesized copper nanoparticles and their anti-bacterial properties against bullfrog multidrug resistant gram negative bacteria. *Veterinary Integrative Sciences*. 17(1): 33–49.
- Singleton, V. and Rossi, J. 1965. Colorimetry of total phenolic compounds with phosphomolybdic-phosphotungstic acid reagents. *American Journal of Enology and Viticulture*. 16: 144–158.
- Suciatmih. 2020. Effect of Dyeing Repetition and Color Reinforcement Materials on Color Formation of Cloth by Mixed Fungi Dyes. *IOP Conference Series: Earth and Environment Science*. 572: 1–9.
- Suhartati, R., Apriyani, F., Khunsnul, Virgianti, D. P. and Fathurohman, M. 2019. Antimicrobial activity test of mangosteen leaves ethanol extract (*Garcinia mangostana* Linn) against *Pseudomonas aeruginosa* bacteria. *Journal of Physics: Conference Series*. 1179: 012167. <https://doi.org/10.1088/1742-6596/1179/1/012167>.
- Triwiswara, M. and Indrayani, L. 2020. Utilization of black tea waste as natural batik dyes on cotton and silk. *IOP Conference Series: Earth and Environment Science*. 456: 012051. <https://doi.org/10.1088/1755-1315/456/1/012051>.
- Yadav, S., Tiwari, K. S., Gupta, C., Tiwari, M. K., Khan, A., and Sonkar, S. P. 2023. A brief review on natural dyes, pigments: Recent advances and future perspectives. *Results in Chemistry*. 5: 1–17.
- Yodthong, W., Chaiwongsar, S., Wanachantararak, P., Keereeta, Y., Panthuwat, W., Saovapha, B., and Sassa-deepaeng, T. 2020. Influence of different extraction solvents on antioxidant and antityrosinase activities of *Morus alba* Linn. leave extract. *Journal of Science and Agricultural Technology*. 1(1): 7–17. <https://doi.org/10.14456/jsat.2020.2>.
- Yusuf, M., Shabbir, M., and Mohammad, F. 2017. Natural colorants: Historical, processing and sustainable prospects. *Natural Products and Bioprospecting*. 7: 123–145. <https://doi.org/10.1007/s13659-017-0119-9>.

Accuracy of genomic breeding values estimated from simulation of the dairy cattle population of northern Thailand

Sirijanya Aryuman^{1*}, Nattaphon Chongkasikit¹, Chirawath Phatsara¹, Saowaluck Yammuen-art¹, Krasit Vasupen², Chot Rachwicha¹ and Chalernporn Jirapanyalert³

¹Department of Animal and Aquatic Sciences, Faculty of Agriculture, Chiang Mai University, Chiang Mai 50100, Thailand

²Department of Animal Science, Faculty of Agricultural Innovation and Technology, Rajamangala University of Technology Isan, Nakhon Ratchasima 30210, Thailand

³Northern Institute of Vocational Education in Agriculture, Tak 63180, Thailand

*Corresponding author: Sirijanya_aryuman@cmu.ac.th

Received: November 5, 2023. Revised: December 19, 2023. Accepted: December 20, 2023.

ABSTRACT

Accuracy is of significant importance in animal breeding, as it directly impacts the response to selection. The objectives of this study were to estimate the accuracy of genomic breeding values (GEBV) from a simulated population of the dairy cattle population of northern Thailand, which has exhibited an increasing trend from the past to the present. Data were simulated using a calibration set (CS) of 2,000 and 3,000 animals, heritability (h^2) ranging from 0.05 to 0.50, and the number of SNPs at 20K and 40K. The GEBV was estimated using BLUP under animal model, and the accuracy was estimated by the correlation between GEBV and TBV from the simulation. The accuracy of GEBV ranged from 0.0870 to 0.8761. The CS of 3,000 animals was higher than the CS of 2,000 animals. Additionally, it was observed that the accuracy of the low h^2 trait was unstable and lower than the high h^2 trait, and the accuracy between 20K and 40K of SNPs was similar, with the highest values being 0.8761 and 0.8189, respectively. This study showed the CS of 3,000 animals and SNPs 40K would be appropriate for estimating GEBV.

Keywords: accuracy, dairy cattle, GEBV, calibration set, simulated

INTRODUCTION

Dairy cattle breeding aims to improve the efficiency and productivity of dairy cattle by selecting animals with desirable traits. Estimated Breeding Value (EBV) was used to predict the genetic value of a trait in an individual animal based on the Best Linear Unbiased Prediction Method (BLUP; Henderson, 1975). Genomic Selection (GS; Meuwissen et al., 2001) was developed for use in dairy cattle breeding by using genetic markers distributed throughout the genome to estimate genomic breeding value (GEBV) (Guarini et al., 2019). The GEBV is the predicted genetic value of an individual animal based on genomic information and is calculated using statistical models that incorporate the animal's genotypic data as well as information on the inheritance and expression of the trait of interest (Hayes et al., 2010). The GEBV can be used in breeding programs to make selection decisions for individual animals. The animals with the highest GEBV for these traits can be selected as sires and dams for the next generation to improve the overall genetic potential of the population (de los Campos et al., 2013; García-Ruiz et al., 2022).

The accuracy of GEBV depends on many factors, such as the historical population, CS, h^2 of the

trait, the number of single nucleotide polymorphisms (SNPs), linkage disequilibrium (LD), minor allele frequency (MAF), quantitative trait loci (QTL), and the relatedness between the CS and validation set (VS) (VanRaden et al., 2008; Goddard, 2009; Daetwyler et al., 2010; Wientjes et al., 2013). Corbin et al. (2010) reported that historical population data reveal genetic diversity and patterns of genetic variation in populations, which can help in selection planning. Hayes et al. (2009) and Hickey et al. (2011) reported that large CS led to greater genetic diversity. This leads to a more accurate assessment of the influence of markers, especially for traits with a complex genetic structure. Similarly, Meuwissen et al. (2016) reviewed the literature on GS in animal breeding and highlighted the importance of combining genotypic and phenotypic information to improve the accuracy of genomic predictions. The authors also emphasized the need to account for the genetic architecture of the trait being predicted and the effects of population structure and environmental factors. The group of animals consists of a group of animals with a known phenotype (calibration set; CS) and an unknown phenotype or progeny group (validation set; VS). Data simulation is a prevalent method. It can be used to study the methods for estimating GEBV, the factors affecting GEBV, and

the accuracy of GEBV in different populations. It can apply the results to real data by adjusting environmental factors or other fixed factors to obtain GEBV and accuracy. However, there are many factors affecting GEBV and accuracy estimation. The number of CS and SNPs is important for different populations and traits (h^2). Therefore, the objective of this study was to estimate the accuracy and study the trend of changes in accuracy within the dairy cattle population of northern Thailand, considering different levels of CS, h^2 , and SNPs. This study will provide information on the selection and planning of dairy cattle breeding for the future.

MATERIALS AND METHODS

Data Simulation

This study uses dairy cattle population data collected from the dairy cattle data of northern Thailand from 1964 to 2020 to be used as a historical population (location of Chiang Mai, the latitude and longitude were 18° N and 98° E, respectively). It simulated the data from two groups of animals: a reference group of animals with known phenotypes (calibration set; CS) of 2 levels, 2,000 and 3,000 animals, and a group of animals with unknown phenotypes (validation set; VS). In the VS group are the offspring born from the CS group. The QMSim package (Sargolzaei and Schenkel, 2009; Scheper, 2016; Mehdi and Flavio, 2019) was used to simulate all animals at two levels of SNPs, 20,000 (20K) and 40,000 (40K), at MAF of 0.05 and 10 levels of h^2 of 0.05, 0.10, 0.15, 0.20, 0.25, 0.30, 0.35, 0.40, 0.45, and 0.50, as shown in Table 1. Phenotypic and genotypic data, SNPs, and true breeding value (TBV) from the data simulation were determined by the h^2 of the trait without environmental factors or fixed effects.

Estimation of Genomic Breeding Values (GEBV)

The SNPs obtained from the simulation are used to create the genomic relationship matrix (G matrix) to estimate the GEBV of the trait determined by h^2 in the CS and VS using BLUP (Best Linear Unbiased Prediction) under the Animal model.

$$y = 1\mu + Zu + e$$

Where y = vector of observation

μ = the overall mean

u = vector of random animal effects

Z = design matrix relates records to random animal effects

e = vector of random residual errors

Generally, the mixed model equation (MME) is as follows:

$$\begin{bmatrix} \hat{b} \\ \hat{u} \end{bmatrix} = \begin{bmatrix} X'X & X'Z \\ Z'X & Z'Z + \alpha G^{-1} \end{bmatrix}^{-1} \begin{bmatrix} X'y \\ Z'y \end{bmatrix}$$

Where $\alpha = \frac{\sigma_e^2}{\sigma_u^2}$

G = genomic relationship matrix

Table 1. Base parameters used in the simulations

Parameters	
Historical population	
No. of animals in the 0 generation	1,252
No. of animals in the 10 th generation	35,844
No. of animals in the 20 th generation	70,724
Current population	
Replacement ratio for sires	0.50
Replacement ratio for dams	0.25
Criteria for selection/culling	Age
Heritability (h^2)	0.05, 0.10, 0.15, 0.20, 0.25, 0.30, 0.35, 0.40, 0.45, 0.50
Genome	
No. of chromosome	30
number of markers (1 K = 1,000 SNPs)	20K and 40K
Minor allele frequency (MAF)	0.05

Accuracy of Genomic Breeding Values (GEBV)

The accuracy of GEBV was calculated from the correlation between GEBV in the CS and VS and True Breeding Value (TBV) (Takeda et al., 2021).

RESULTS

Accuracy of genomic breeding values (GEBV)

This study showed the accuracy of GEBV under simulated data from the dairy cattle population

of northern Thailand, as shown in Table 2. It was found that the accuracy ranged from 0.0870 to 0.8761. The accuracy of CS and VS ranges from 0.0870 to 0.8761 and 0.1278 to 0.7015, respectively.

Table 2. Accuracy of genomic breeding values (GEBV)

SNP	h ²	Rep.	2,000 animals				3,000 animals			
			Calibration set		Validation set		Calibration set		Validation set	
			\bar{X}	SE	\bar{X}	SE	\bar{X}	SE	\bar{X}	SE
20K	0.05	10	0.0870	0.1064	0.1656	0.0669	0.0890	0.0259	0.1752	0.0304
	0.10	10	0.3849	0.0846	0.3426	0.0367	0.3676	0.0475	0.3408	0.0589
	0.15	10	0.4596	0.0323	0.2267	0.1726	0.5339	0.0794	0.4625	0.0713
	0.20	10	0.4116	0.1185	0.3637	0.0336	0.5986	0.0081	0.5181	0.0170
	0.25	10	0.6990	0.0647	0.4790	0.0665	0.6589	0.0248	0.4241	0.0620
	0.30	10	0.6560	0.0401	0.4169	0.0182	0.7356	0.0331	0.5200	0.0591
	0.35	10	0.7512	0.0379	0.5560	0.0351	0.7256	0.0685	0.6189	0.0438
	0.40	10	0.8154	0.0264	0.6238	0.0554	0.8185	0.0345	0.5659	0.0316
	0.45	10	0.7781	0.0530	0.5729	0.0956	0.8305	0.0269	0.6398	0.0491
	0.50	10	0.8084	0.0865	0.5179	0.2223	0.8761	0.0082	0.7015	0.0273
40K	0.05	10	0.1837	0.0889	0.1278	0.0652	0.1883	0.1051	0.2282	0.1275
	0.10	10	0.3480	0.1088	0.2924	0.0631	0.3014	0.0567	0.1917	0.0415
	0.15	10	0.3892	0.0799	0.3141	0.0296	0.6573	0.0398	0.4956	0.0371
	0.20	10	0.5796	0.0761	0.4036	0.0913	0.6808	0.0277	0.5532	0.0445
	0.25	10	0.6038	0.0761	0.4693	0.0428	0.7218	0.0333	0.5433	0.0455
	0.30	10	0.7029	0.0500	0.4407	0.1540	0.7579	0.0318	0.5765	0.0704
	0.35	10	0.7931	0.0165	0.5600	0.0368	0.8189	0.0092	0.6483	0.0271
	0.40	10	0.7460	0.0511	0.5963	0.0563	0.7589	0.0231	0.5660	0.0293
	0.45	10	0.8359	0.0179	0.6209	0.0300	0.8274	0.0125	0.6048	0.0337
	0.50	10	0.8306	0.0220	0.5761	0.0449	0.8039	0.0301	0.5805	0.0488

SNPs = single nucleotide polymorphism, h² = heritability, Rep. = replication.

Effect of Calibration set (CS) on the accuracy of genomic breeding values (GEBV)

The accuracy of GEBV under the CS in 2,000 and 3,000 animals with 20K SNPs was similar in both sizes. The accuracy of the CS of 3,000 animals and the VS from the CS of 3,000 animals had the highest values of 0.8761 and 0.7015, respectively. The accuracy of the CS of 2,000 animals and the VS from the CS of 2,000 animals had the highest values

of 0.8154 and 0.6238, respectively (Figure 1). Similarly, with the number of SNPs at 40K, the accuracy for both sizes was similar. The accuracy of the CS of 3,000 animals and the VS from the CS of 3,000 animals had the highest values of 0.8189 and 0.6483, respectively. The CS of 2,000 animals and the VS from the CS of 2,000 animals had the highest values of 0.7931 and 0.5963, respectively, as shown in Figure 2.

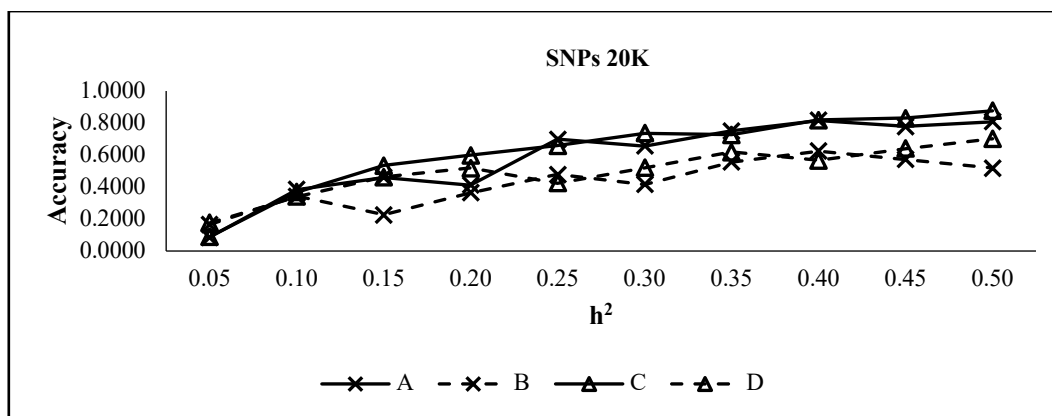


Figure 1. Accuracy of genomic breeding values (GEBV) of CS of 2,000 and 3,000 animals, and number of SNPs 20K. (A = accuracy of CS of 2,000 animals, B = accuracy of VS from CS of 2,000 animals, C = accuracy of CS of 3,000 animals, D = accuracy of VS from CS of 3,000 animals).

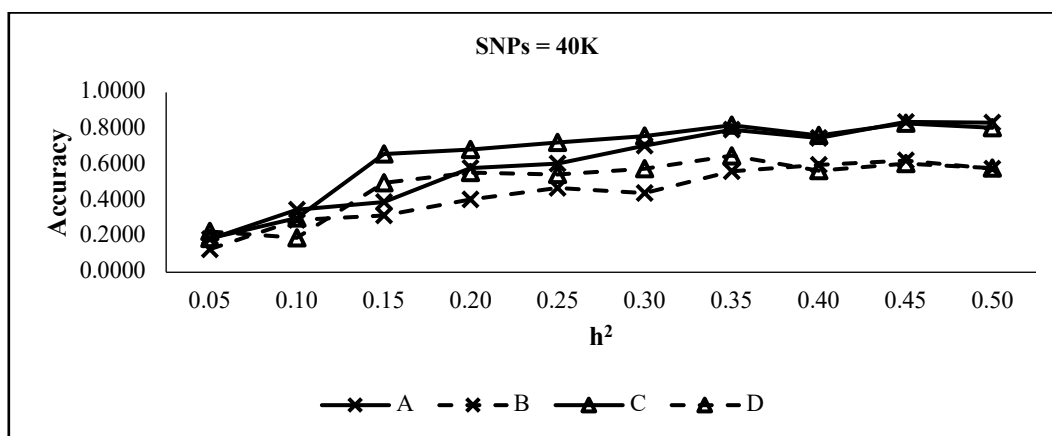


Figure 2. Accuracy of genomic breeding value (GEBV) of CS of 2,000 and 3,000 animals and number of SNPs 40K. (A = accuracy of CS of 2,000 animals, B = accuracy of VS from CS of 2,000 animals, C = accuracy of CS of 3,000 animals, D = accuracy of VS from CS of 3,000 animals).

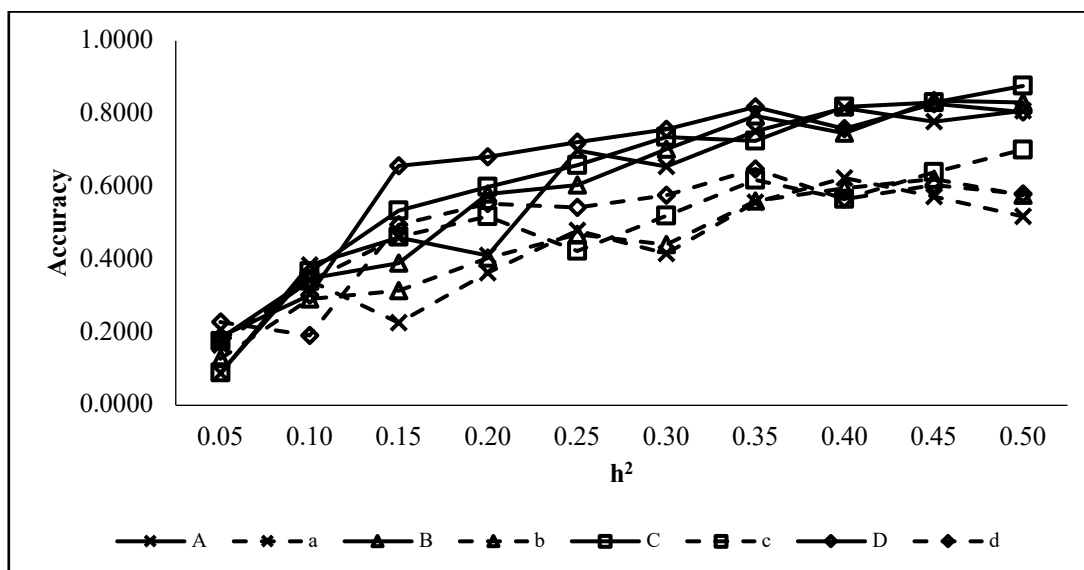


Figure 3. Accuracy of genomic breeding value (GEBV) at different levels of heritability (h^2). (A = accuracy of CS of 2,000 animals and 20K SNPs, a = accuracy of VS from CS of 2,000 animals and 20K SNPs, B = accuracy of CS of 2,000 animals and 40K SNPs, b = accuracy of VS from CS of 2,000 animals and 40K SNPs, C = accuracy of CS of 3,000 animals and 20K SNPs, c = accuracy of VS from CS of 3,000 animals and 20K SNPs, D = accuracy of CS of 3,000 animals and 40K SNPs, d = accuracy of VS from CS of 3,000 animals and 40K SNPs).

Effect of heritability (h^2) on the accuracy of genomic breeding values (GEBV)

The effect of h^2 on the accuracy of GEBV was found to increase and remain constant when h^2 increased (Figure 3). The accuracy of GEBV in the CS of 3,000 animals and the VS from the CS of 3,000 animals were highest in the h^2 at 0.45 and 0.35, respectively; and with a group of 2,000 animals, it had the highest h^2 of 0.45 for both CS and VS.

Effect of number of SNPs on the accuracy of genomic breeding values (GEBV)

The effect of the number of SNPs on the accuracy of GEBV, it was found that the number of SNPs 20K and 40K in the CS of 2,000 animals had the highest values of 0.8154 and 0.7931, and in the VS from the CS of 2,000 animals, the values were 0.6238 and 0.5963, respectively. And, at the CS of 3,000 animals, the highest values were 0.8761 and 0.8189, and in the VS from the CS of 3,000 animals, the highest values were 0.7015 and 0.6483 at the number of SNPs 20K and 40K, respectively (Figure 4 and 5).

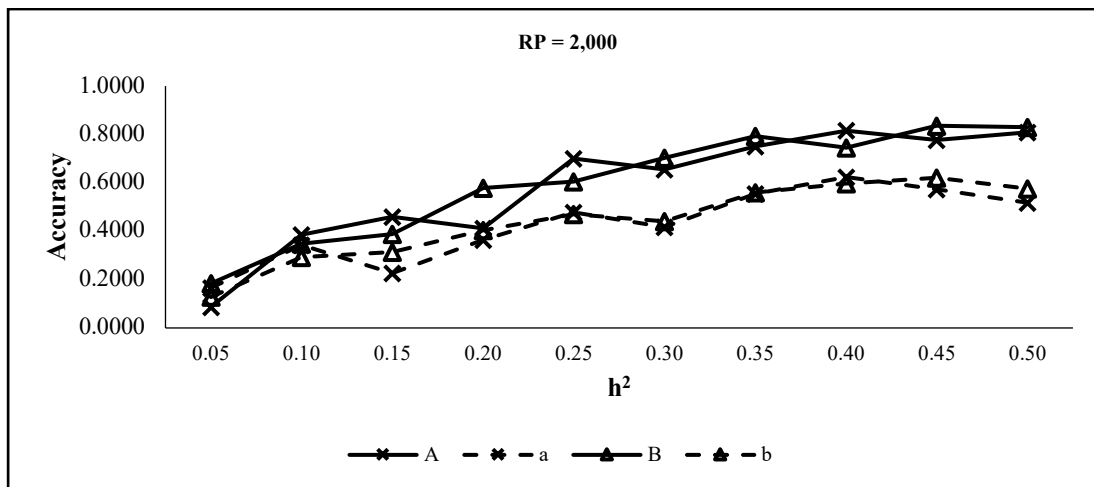


Figure 4. Accuracy of GEBV at the number 20K and 40K of SNPs of CS of 2,000 animals.

(A = accuracy of CS 2,000 animals on 20K SNPs, a = accuracy of VS from CS 2,000 animals on 20K SNPs, B = accuracy of CS 2,000 animals on 40K SNPs, b = accuracy of VS from CS 2,000 animals on 40K SNPs).

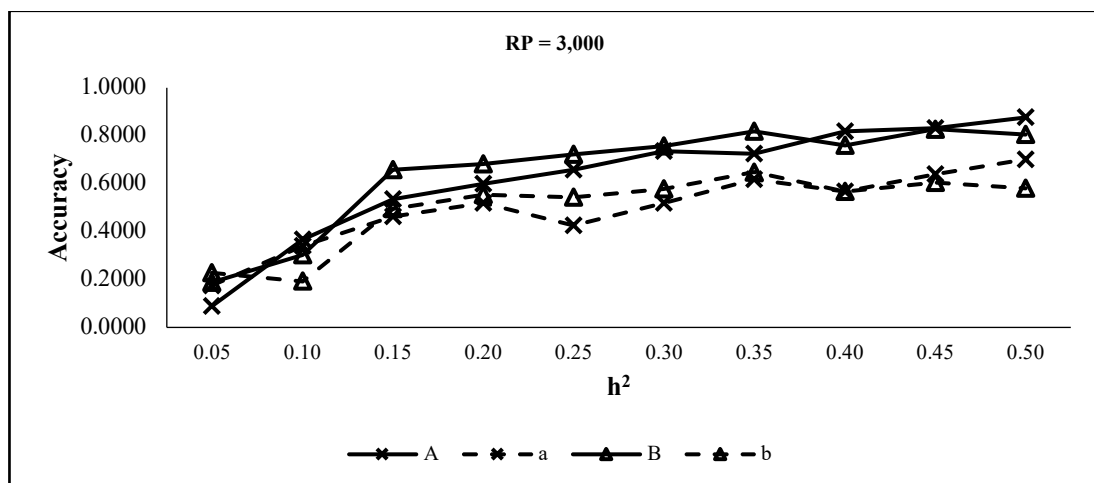


Figure 5. Accuracy of GEBV at the number 20K and 40K of SNPs in 3,000 CS.

(A = accuracy of CS 2,000 animals on 20K SNPs, a = accuracy of VS from CS 2,000 animals on 20K SNPs, B = accuracy of CS 2,000 animals on 40K SNPs, b = accuracy of VS from CS 2,000 animals on 40K SNPs).

The standard error (SE) of accuracy

The standard error (SE) from simulation found that the SE values of the CS of 2,000 animals with SNPs 20K and 40K ranged from 0.1064 to 0.0865 and 0.0889 to 0.0220, respectively. The CS of 3,000 animals with SNPs 20K and 40K ranged from 0.0259 to 0.0082 and 0.1051 to 0.0301, respectively, as shown in Table 2.

DISCUSSION

A study of the historical population of the dairy cattle population of Northern Thailand from 1964 to 2020 found that the size of the dairy cattle population has increased. This is consistent with a study by Gerdsook (2016), who reported that the dairy cattle population of Northern Thailand from 1952 to 2014 has increased and is on the trend of increasing. Numerous studies have reported the influence of historical populations on accuracy. For example, a study by Nwogwugwu et al. (2020) reported the accuracy of a cattle population in Korea by simulating the historical population with a constant size of 1,000 animals up to a generation of 1,000, which decreased to 200 animals in the next 95 generations. The accuracy was found to be 0.563, 0.735, and 0.808, with h^2 values of 0.1, 0.3, and 0.5, respectively. Consistent with the Atefi et al. (2016) study, the historical population was simulated. The size was constant at 1,000 animals until 100 generations and gradually decreased until the remaining 500 animals in the 200th generation. The accuracy was found to be 0.57, 0.70, and 0.77, with h^2 0.15, 0.30, and 0.45, respectively. The large historical population sizes indicate greater genetic diversity, which is helpful for accurately estimating genetic parameters and genetic markers associated with various traits. However, other factors, such as the quality and quantity of phenotypic data, the genetic structure of the trait, and the statistical methods used in the study, should also be taken into account to influence the accuracy of the assessment of GEBV.

The accuracy of GEBV by using simulation and data from the dairy cattle population of northern Thailand. The results showed that the accuracy of the CS was higher than that of the VS. Consistent with Bouwman et al. (2014), they estimated the accuracy of GEBV from simulations using genotyping data from relatives. They found that using genotype data from relatives and offspring can increase accuracy, especially in the VS. Similar to Calus et al. (2013), they used genomic technology to estimate genetics and evaluate the accuracy of the VS by predicting from the CS data that it has good genetic and

phenotypic information. The results showed highly accurate breeding values. Boison et al. (2017) evaluated the accuracy of GEBV in Gyr (*Bos indicus*) dairy cattle using different VS sizes. It was found that the accuracy of the production traits ranged from 0.28 to 0.49. However, the VS is a population that does not have direct phenotypic data but is derived from predicting animal data in the population with known phenotypes. As a result, the accuracy is lower than that of animals with known phenotypes.

When considering the effect of CS on the accuracy of GEBV, it was found that increasing the CS can improve accuracy. Several studies have reported that CS affects accuracy. The accuracy of GEBV is higher as the CS increases. Increasing the CS will increase genetic diversity, resulting in high accuracy. However, an appropriate CS must be considered due to the high cost of genome selection. This study shows that the CS of 2,000 animals is sufficient to achieve an accuracy of more than 0.4 for the dairy cattle population of northern Thailand with h^2 of 0.15. Similarly, Takeda et al. (2021) reported that the CS of 4,000 animals was sufficient to achieve a GEBV accuracy of carcass traits in Japanese black cattle of more than 0.4. Zhang et al. (2023) reported that using the CS of 6,000 animals could increase the accuracy of GEBV for the production traits of Chinese Holstein cattle by greater than 0.40. It can be seen that the accuracy of GEBV is different when using different CS. This is because animals in each population have different relationships. Falconer et al. (1997) reported that increasing the number of offspring (progeny) per sire in the VS can reduce differences in accuracy estimation methods. However, the CS studied this time was similar, resulting in similar accuracy values. In the next study, a larger CS should be added to observe the accuracy trend further.

It was considering the influence of different levels of h^2 on the accuracy of GEBV. At low h^2 , the accuracy was relatively low. But while the h^2 is high, the accuracy of GEBV tends to increase. This is consistent with the study by Buaban et al. (2021), which reported that the accuracy values of milk yield traits of dairy cattle in Thailand ranged from 0.27 to 0.37. Similarly, Yan et al. (2022) reported that the accuracy (r) of GEBV by simulation in goats with h^2 values of 0.11 and 0.34 was 0.465 and 0.604, respectively. While Togashi et al. (2019) reported the reliability values (r^2) of the dairy cow population with h^2 of 0.1, 0.3, and 0.5, which were equal to 0.0769, 0.2000, and 0.2941, respectively, the accuracy values were lower than this study. However, it can be seen that when the h^2 value increases, the accuracy tends to increase. This is because accuracy and

h^2 are important factors affecting the response to selection. Traits with high h^2 are more responsive to selection than those with low h^2 , resulting in rapid genetic progress.

The effect of SNPs of 20K and 40K on the accuracy of GEBV, it was found that the accuracy values for both CS estimated from 40K SNPs were only slightly higher than those from 20K SNPs. The more informative SNPs, the higher the accuracy of GEBVs. However, using a larger number of SNPs can improve the accuracy of GEBV, but there may be little or no increase. Consistent with the study of Hayes et al. (2019), they reported that increasing the number of SNPs from 24K to 728K resulted in a slight increase in the accuracy of GEBV in three cattle breeds, with values of 0.22 and 0.24, respectively. They also reported that using many SNPs results in higher breeding costs. However, some studies reported that using a high-density SNP resulted in higher GEBV accuracy than using a low-density SNP (Bolormaa et al., 2015). This study showed that increasing the accuracy of GEBV in the dairy cattle population in northern Thailand can use low-density SNPs for selection. Using low-density SNPs results in lower selection costs. Consistent with the study of Cole et al. (2016), they studied the efficiency of genomic selection in a multi-breed dairy population using 777,962 SNPs. The study found that 50K SNPs were sufficient to increase the accuracy of genetic selection. Using a larger number of SNPs did not result in higher accuracy. Lopes et al. (2020) evaluated the accuracy of GEBV in US Holstein cattle using 777,962 SNPs. Increasing the number of SNPs improves the accuracy of GEBV. However, the accuracy tends to increase only slightly when the number of SNPs increases over 50K.

In the study of the standard error (SE) of the accuracy of GEBV, it was found that increasing the CS will result in a lower SE, especially for traits with low h^2 . Consistent with the study of Gerdsook (2016), the SE decreased from 0.10 to 0.06 for the trait with h^2 of 0.10 when the CS increased from 100 to 1,500 animals. Similarly, Yan et al. (2022) reported the SE of the trait with a h^2 of 0.11. The SE decreased from 0.0862 to 0.0210 when the CS increased from 500 to 3,000 animals.

Each research (historical population) produced different results, as evidenced by the above information. Therefore, further research is important by using other factors and different levels of CS and SNPs for more results.

CONCLUSIONS

Accuracy of GEBV from simulation using dairy cattle population data from northern Thailand. It was found that the accuracy of the CS tended to be higher than that of the VS. In contrast, the accuracy of the CS of 3,000 animals and the VS from the CS of 3,000 animals tended to be slightly higher than that of the CS of 2,000 animals and the VS from the CS of 2,000 animals. In addition, we found that the accuracy of traits with low h^2 tended to be unstable. This is because the SE is higher than traits with a high h^2 . Moreover, traits with low h^2 have low accuracy, and SE is relatively high. While traits with high h^2 have high accuracy and relatively low SE, the accuracy of traits with low h^2 can be increased by increasing CS. Moreover, it was found that the accuracy for the number of SNPs 20K and 40K was similar, but the SE of the number of SNPs 40K was lower than 20K. From the results of the study, it was found that using the CS of 3,000 animals and SNPs 40K was appropriate for estimating GEBV in the dairy cattle population in northern Thailand. This is because the accuracy of GEBV is high, and the SE is low. Additionally, for low h^2 traits, increasing the CS size can reduce the SE of the accuracy.

REFERENCES

- Atefi, A., Shadparvar, A.A., and Hossein-Zadeh, N.G. 2016. Comparison of whole genome prediction accuracy across generations using parametric and semi parametric methods. *Acta Scientiarum*. 38: 447–453.
- Boison, S.A., Utsunomiya, A.T.H., Santos, D.J.A., Neves, H.H.R., Carvalheiro, R., Mészáros, G., Utsunomiya, Y.T., do Carmo, A.S., Verneque, R.S., Machado, M.A., Panetto, J.C.C., Garcia, J.F., Sölkner, J., and da Silva, M.V.G.B. 2017. Accuracy of genomic predictions in Gyr (*Bos indicus*) dairy cattle. *J. Dairy Sci.* 100: 5479–5490.
- Bolormaa, S., Pryce, J.E., Zhang, Y., Reverter, A., Barendse, W., Hayes, B.J., and Goddard, M.E. 2015. Non-additive genetic variation in growth, carcass and fertility traits of beef cattle. *Genetics Selection Evolution*. 47: 1–12.
- Bouwman, A.C., Hickey, J.M., Calus, M.P.L., and Veerkamp, F.R. 2014. Imputation of non-genotyped individuals based on genotyped relatives: assessing the imputation accuracy of a real case scenario in dairy cattle. *Genetics Selection Evaluation*. 46: 1–11.
- Buaban, S., Prempee, S., Sumreddee, P., Duangjinda, M., and Masuda, Y. 2021. Genomic prediction of milk production traits and somatic cell score using single-step genomic best linear unbiased predictor with random regression test-day model in Thai dairy cattle. *J. Dairy Sci.* 104: 12713–12723.
- Calus, M.P.L., Haas, Y.D., Pszczola, M., and Veerkamp, R.F. 2013. Predicted accuracy of and response to genomic selection for new traits in dairy cattle. *Anim.* 7: 183–191.
- Cole, J.B., and da Silva, M.V.G.B. 2016. Genomic selection in multi-breed dairy cattle populations. *R. Bras. Zootec.* 45: 195–202.

- Corbin, L.J., Blott, S.C., Swinburne, J.E., Vaudin, M., Bishop, S.C., and Woolliams, J.A. 2010. Linkage disequilibrium and historical effective population size in the Thoroughbred horse. *Anim. Genet.* 41: 8–15.
- Daetwyler, H.D., Pong-Wong, R., Villanueva, B., and Woolliams, J.A. 2010. The impact of genetic architecture on genome-wide evaluation methods. *Genetics.* 185: 1021–1031.
- De los Campos, G., Hickey, J.M., Pong-Wong, R., Daetwyler, H.D., and Calus, M.P.L. 2013. Whole-genome regression and prediction methods applied to plant and animal breeding. *Genetics.* 193: 327–345.
- Falconer, D.S., and Mackay, T.C. 1997. *Introduction to quantitative genetics*, 4th ed. John Wiley & Sons, Hoboken, NJ.
- García-Ruiz, I., Quiñones, A., and Taborsky, M. 2022. The evolution of cooperative breeding by direct and indirect fitness effects. *Science Advance.* 8: 1–10.
- Gerdsook, N. 2016. Relationship between reference population size and accuracy of genomic breeding values of dairy cattle population in upper northern Thailand. Master's thesis, Chiang Mai University, Chiang Mai, Thailand.
- Goddard, M.E. 2009. Genomic selection: prediction of accuracy and maximization of long term response. *Genetica.* 136: 245–257.
- Guarini, A.R., Lourenco, D.A.L., Brito, L.F., Sargolzaei, M., Baes, C.F., Miglior, F., Tsuruta, S., Misztal, I., and Schenkel, F.S. 2019. Use of a single-step approach for integrating foreign information into national genomic evaluation in Holstein cattle. *J. Dairy Sci.* 102: 8175–8183.
- Hayes, B.J., Bowman, P.J., Chamberlain, A.J., and Goddard, M.E. 2009. Invited review: Genomic selection in dairy cattle: Progress and challenges. *J. Dairy Sci.* 92: 433–443.
- Hayes, B.J., and Goddard, M.E. 2010. Genome-wide association and genomic selection in animal breeding. *Genome.* 53: 876–883.
- Hayes, B.J., Corbet, N.J., Allen, J.M., Laing, A.R., Fordyce, G., Lyons, R., McGowan, M.R., and Burns, B.M. 2019. Towards multi-breed genomic evaluations for female fertility of tropical beef cattle. *J. Anim. Sci.* 97: 55–62.
- Henderson, C.R. 1975. Best linear unbiased estimation and prediction under a selection model. *Biometrics.* 31: 423–447.
- Hickey, J.M., Kinghorn, B.P., Tier, B., and Wilson, J.F. 2011. The impact of genetic architecture on genome-wide evaluation methods. *Genetics Research.* 93: 343–355.
- Lopes, M.S., Silva, F.F., Meuwissen, T.H., and Guimarães, S.E. 2020. Optimal number of SNP markers for genomic prediction under the genetic architecture of complex traits. *Bioinformatics.* 21: 1–17.
- Mehdi, S., and Flavio, S.S. 2019. Qmsim version 1.10. User's guide. Centre for Genetic Improvement of Livestock Department of Animal and Poultry Science University of Guelph, Canada.
- Meuwissen, T.H.E., Hayes, B.J., and Goddard, M.E. 2001. Prediction of total genetic value using genome-wide dense marker maps. *Genetics.* 157: 1819–1829.
- Meuwissen, T.H.E., Hayes, B.J., and Goddard, M.E. 2016. Genomic selection: A paradigm shift in animal breeding. *Animal Frontiers.* 6: 6–14.
- Nwogwugwu, C.P., Kim, Y., Choi, H., Lee, J.H., and Lee, S. 2020. Assessment of genomic prediction accuracy using different selection and evaluation approaches in a simulated Korean beef cattle population. *Asian-Australas J Anim Sci.* 33: 1912–1921.
- Sargolzaei, M. and Schenkel, F.S. 2009. QMSim: a large-scale genome simulator for livestock. *Bioinformatics.* 25: 680–681.
- Scheper, C. 2016. Technical note for QUALSim (usage in combination with QMSim). Department of Animal Breeding, University of Kassel, Germany.
- Takeda, M., Inoue, K., Oyama, H., Uchiyama, K., Yoshinari, K., Sasago, N., Kojima, T., Kashima, M., Suzuki, H., Kamata, T., Kumagai, M., Takasugi, W., Aonuma, T., Soma, Y., Konno, S., Saito, T., Ishida, M., Muraki, E., Inoue, Y., Takayama, M., Nariai, S., Hideshima, R., Nakamura, R., Nishikawa, S., and Uemoto, Y. 2021. Exploring the size of reference population for expected accuracy of genomic prediction using simulated and real data in Japanese Black cattle. *BMC Genomics.* 22: 1–11.
- Togashi, K., Adachi, K., Kurogi, K., Yasumori, T., Tokunaka, K., Ogino, A., Miyazaki, Y., Watanabe, T., Takahashi, T., and Moribe, K. 2019. Effects of preselection of genotyped animals on reliability and bias of genomic prediction in dairy cattle. *Asian-Australas J Anim Sci.* 32: 159–169.
- VanRaden, P.M., VanTassell, C.P., Wiggans, G.R., Sonstegard, T.S., Schnabel, R.D., Taylor, J.F., and Schenkel, F.S. 2008. Invited review: Reliability of genomic predictions for North American Holstein bulls. *J. Dairy Sci.* 92: 16–24.
- Wientjes, Y.C.J., Veerkamp, R.F. and Calus, M.P.L. 2013. The effect of linkage disequilibrium and family relationships on the reliability of genomic prediction. *Genetics.* 193: 621–631.
- Yan, X., Zhang, T., Liu, L., Yu, Y., Yang, G., Han, Y., Gong, G., Wang, F., Zhang, L., Li, W., Yan, X., Mao, H., Li, Y., Du, C., Li, J., Zhang, Y., Wang, R., Lv, Q., Wang, Z., Zhang, J., Liu, Z., Wang, Z., and Su, R. 2022. Accuracy of genomic selection for important economic traits of cashmere and meat goats assessed by simulation study. *Frontiers in Veterinary Science.* 9: 1–13.
- Zhang, Z., Shi, S., Zhang, Q., Aamand, G.P., Lund, M.S., Su, G., and Ding, X. 2023. Improving genomic prediction accuracy in the Chinese Holstein population by combining with the Nordic Holstein reference population. *Animals.* 13: 1–12.

Effect of extraction time on the amounts of neurotransmitters and amino acids in chicken essence

Sauwanit Wutthikrairat¹, Yi-Chen Chen², Patcharaporn Tinchan³, Arsooth Sanguankiat⁴
and Sasitorn Nakthong^{3*}

¹Research and Development Program, Faculty of Agriculture at Kamphaeng Saen, Kasetsart University, Kamphaeng Saen Campus, Nakhon Pathom 73140, Thailand

²Department of Animal Science and Technology, National Taiwan University, Taipei City 8 106, Taiwan

³Department of Food Safety Innovation, Faculty of Agriculture at Kamphaeng Saen, Kasetsart University, Kamphaeng Saen Campus, Nakhon Pathom 73140, Thailand

⁴Department of Veterinary Public Health, Faculty of Veterinary Medicine, Kasetsart University, Kamphaeng Saen Campus, Nakhon Pathom 73140, Thailand

*Corresponding author: agrsas@ku.ac.th

Received: November 15, 2023. Revised: December 15, 2023. Accepted: December 16, 2023.

ABSTRACT

This study aimed to quantify yields of chicken essence, neurotransmitters, and amino acid concentrations in chicken essence. Kasetsart University, Thailand, bred three chicken lines to improve carcass percentages, and we used the chicken lines as the sources for chicken essence preparation. The selected chicken lines were Betong chicken (KU line), Tapaotong Kasetsart, and KU-Phuparn. Treatments were different extraction times for 1.0, 1.5, and 2.0 hours at 100 degrees Celsius. The results showed that Betong chicken (KU line) yielded higher amounts of chicken essence when employing 1.5 and 2.0 hours of extraction time compared to others from the Tapaotong Kasetsart and KU-Phuparn lines. Also, the concentration of each neurotransmitter in chicken essence with different extraction times was significantly different ($P < 0.05$). In addition to extraction time, Betong chicken (KU line) carcasses as the source of chicken essence preparation generated the highest amounts of anserine, carnosine, and creatine, followed by KU-Phuparn and Tapaotong, Kasetsart, respectively. Like neurotransmitters, extending extraction time improved the contents of amino acids. Compared to chicken essence extracted from Betong chicken (KU line) and Tapaotong Kasetsart, chicken essence originating from the KU-Phuparn line tended to generate a higher concentration of amino acids. The findings suggest that chicken lines and extraction affected chicken essence yields and amounts of neurotransmitters and amino acids in chicken essence.

Keywords: chicken essence (golden soup), endogenous compound, Betong chicken (KU line), Tapaotong Kasetsart line, KU-Phuparn line

INTRODUCTION

Nowadays, everybody emphasizes good health without any diseases, and the changed lifestyle, especially among people living in urban areas, causes physical fatigue. Good health begins with eating nutritious food and exercising regularly. Chicken meat is popular among consumers since it is considered an inexpensive meat compared to others (Sujiwo et al., 2018). Also, it is nutritious and contains high protein but low cholesterol. In 2022, the global consumption of chicken meat had grown at a rate of 2.09 percent per year, while domestic consumption accounted for 66.26% of total production (OAE, 2023). Thai native chickens have been raised either free- or semi-range. The advantages of Thai native chicken lines are tolerance to various environmental conditions and diseases, easy nurture, and low cost. Moreover, their meat textures are tough, soft, tender, and good taste, suitable for both cooking and human consumption.

Therefore, the demand for poultry meat is high in markets. However, there are a few disadvantages due to its low carcass percentages (Jaturasitha et al., 2008).

Three Thai native chicken lines, namely Betong chicken (KU line), Tapaotong Kasetsart, and KU-Phuparn, were bred by Kasetsart University, with many advantages. Betong is a famous broiler chicken line in lower southern Thailand; it was bred in Betong District, Yala, Thailand. The breed originates in the Laeng Chan line in Guangdong Province, China. Betong is usually raised in rubber plantations for 7 to 8 months before slaughtering. The particular characteristics of their carcass meat are that it is delicious, tender, soft, low fat, and has a good odor, which makes Betong chicken meat popular among Thai people. However, the Betong chicken line has a low breeding rate and lacks scientific information support, so the number of raising the Betong chicken line has declined. For this reason, the Betong chicken

(KU line) was bred at Luang Suwan Wachakasikit Poultry Farm, Department of Animal Science, Faculty of Agriculture, Kasetsart University, Bang Khen campus, Bangkok, Thailand, with the new character of fast-growing, with light brown to dark brown hair appearance (Sopannarath et al., 2015), raised for only 16 weeks (Sopannarath et al., 2015; Putsakul et al., 2010), and weights range from 962 to 2,949 grams. Males usually are heavier than females, and the mean live weights of males and females are 2,282.63 and 1,625.86 grams, respectively (Bungsrisawat et al., 2018). For the Tapaotong chicken line, Thai people with Chinese ethics call it Tapaotong due to its golden hair. The Tapaotong chicken line is significant in body size, with big breasts and much meat. Later, researchers of the Department of Animal Science, Faculty of Agriculture, Kasetsart University, Kamphaeng Saen Campus, Nakhon Pathom, Thailand, bred the Tapaotong Kasetsart chicken line to increase their tolerance to environments, and more resistant to diseases with good shape appearance, including hybrids of the stone crest and chakra crest with golden hair, yellow beak, and yellow skin. Its meat is soft, tender, and good taste. Black bone chicken is famous in China; the Chinese believe that black bone chicken can remedy many diseases, such as diabetes and anemia. Based on medical studies, black bone chicken has antioxidant capacities, strengthening muscle enhancers, wrinkle reducers, and carnosine, an abundant non-protein nitrogen-containing meat compound, resulting in high domestic demand. For these reasons, the KU-Phuparn chicken line, a black bone chicken, was bred by Kasetsart University, Chaloe Phrakiat Campus, Sakon Nakhon, Thailand. The unique characteristics are white hair, black meat and skin, chakra crest, black bone, and fast growth. According to the study, results show that males usually are heavier than females due to hormones affecting growth and better feed conversion ratio in males. Markets prefer chickens that average 1.2 kilograms in weight and are raised only ten weeks (Khumpeerawat, 2016).

Chicken essence is a dark brown drink extracted from chicken meat. Therefore, it is categorized as a functional food popular in Asia, especially South East Asia. Generally, chicken essence is a supplement that improves exercise performance, ameliorates physical fatigue, reduces stress, vanishes worry, enhances memory, and improves student learning (Jiang and Groen, 2000). Vertebrate animal meat is composed of anserine (a methylated product of carnosine; β -alanyl-L-methyl-L-histidine), carnosine (a dipeptide; β -alanyl-L-histidine), and creatine (a metabolite of arginine, glycine, and methionine). They are known as bioactive compounds (Li et al., 2012). Most animals, except humans and plants, possess anserine, carnosine, and creatine. These dietary nutrients are beneficial for preventing and treating obesity,

cardiovascular dysfunction, and aging-related disorders, as well as inhibiting tumorigenesis, improving skin and bone health, and ameliorating neurological abnormalities. Furthermore, by improving the metabolism and operations of immune system cells, such as monocytes, macrophages, and others, they may enhance people's immunological defense against infections by microorganisms (Jung et al., 2013).

The chicken carcasses of Betong chicken (KU line), Tapaotong Kasetsart, and KU-Phuparn lines were the benefit source for chicken essence production since Kasetsart University bred these lines for increasing carcass percentages. The objectives of this study were to observe the effect of extraction time on yields of chicken essence, neurotransmitters, and amino acids.

MATERIALS AND METHODS

Sources of samples

The selected chicken lines in this study were as follows: Betong chicken (KU line), Tapaotong, Kasetsart, and KU-Phuparn lines. Betong chicken (KU line) carcasses were obtained from Luang Suwan Wachakasikit Poultry Farm, Department of Animal Science, Faculty of Agriculture, Kasetsart University, Bang Khen campus, Bangkok, Thailand, while Tapaotong Chicken Farm, Song Phi Nong District, Suphan Buri Province, Thailand, supported Tapaotong Kasetsart chicken carcasses. Khun Tam Farm, Bangkok, Thailand, provided KU-Phuparn chicken carcasses. The weight of all chicken carcasses was between 1.0 and 1.5 kilograms. The prices of Betong chicken (KU line), Tapaotong Kasetsart, and KU-Phuparn chicken carcasses are 190, 130, and 210 Baht per kilogram, respectively.

Chicken essence preparation and experimental design

The method was modified by Wu (2020). The whole carcasses were thawed at 4 degrees Celsius in a refrigerator for 24 hours. The carcasses were washed with water and cut into pieces, and bone parts were smashed. Then, carcasses were weighed and steamed. The outer pot contained approximately 33% water (v/v), while the inner pot had pores to let chicken essence drip into the bottom. The experiment was assigned using the randomized complete block design (RCBD). Treatments were three times extraction conditions: 1.0, 1.5, and 2.0 hours at 100 degrees Celsius, respectively. Each treatment consisted of three replications. The chicken essences were filtered by using a cotton sheet and weighed. Yields were calculated using Equation 1.

$$\text{Yield(\%)} = \frac{\text{weight chicken essence}}{\text{weight of chicken carcass}} \times 100 \quad (1)$$

Quantitative analysis of neurotransmitters

The methods of anserine, carnosine, and creatine quantification were modified by Li et al. (2012). One gram of chicken essence was homogenized with 7.5 mL of 0.01 N HCl at $1,130 \times g$ for one minute, and then the homogenate was centrifuged at $17,030 \times g$ for 15 min at 4 degrees Celsius. The 2.5 ml supernatant was mixed with 7.5 ml of acetonitrile and centrifuged at $17,030 \times g$ for 15 min at 4 degrees Celsius. The clear supernatant was filtered through a $0.22 \mu\text{m}$ syringe filter, and 10 μl of samples were injected into the HPLC instrument (Waters 600E). The HPLC instrument consisted of a HILIC silica column ($4.6 \text{ mm} \times 150 \text{ mm}$, $3 \mu\text{m}$; Millipore) and a diode array detector (Waters 2487 HPLC UV/VIS Detector) at 214 nm to measure carnosine, anserine, and creatine contents. The mobile phase A was 0.65 mM ammonium acetate in water- acetonitrile mix (25:75 vol/vol, pH 5.5), while the mobile phase B was 0.65 mM ammonium acetate in water- acetonitrile mix (70:30 vol/vol, pH 5.5). The mobile phase B was supplied at 1.2 mL/min for 16 min with a linear gradient from 0 to 100%. The contents of carnosine, anserine, and creatine were calculated using standard linear regression, and the standards were purchased from Sigma Company (St. Louis, MO, USA). Neurotransmitter quantification was replicated at least three times on three independent occasions. The means and standard deviation of neurotransmitter amounts were reported.

Quantitative analysis of amino acids

The amino acid measurement was performed at the Institute of Food Research and Product Development, Kasetsart University, Bangkok, Thailand. Based on Journal of Chromatography B (2014) 116–127, The in-house Method WI-TMC-06 Dong et al. (2014) was used to quantify amino acids. Eighteen amino acids were measured as follows: alanine, arginine, aspartic acid, cystine, glutamic acid, glycine, histidine, isoleucine, leucine, lysine, methionine, phenylalanine, proline, serine, threonine, tryptophan, tyrosine, and valine.

Data analysis

All data were analyzed for variance (Analysis of Variance: ANOVA) according to the randomized complete block design, and the mean differences were compared by Duncan's New Multiple Range Test (DMRT) using the statistical package SPSS version 26.0 (IBM Corp, 2019).

RESULTS AND DISCUSSION

Yields of chicken essence

In the current study, we set 100 degrees Celsius as extraction temperature and varied extraction times of 1.0, 1.5, and 2.0 hours. When we increased the processes of chicken essence preparation from 1.0 to 1.5 hours, it enhanced the yield of chicken essence, as shown in Figure 1. However, increasing extraction time did not cause higher yields after 1.5-hour extraction time. In addition, chicken meat from Tapaotong Kasetsart and KU-Phuparn lines generated equal amounts of chicken essence at every extraction time. In contrast to the chicken essence originating from Tapaotong Kasetsart and KU-Phuparn meat, chicken carcasses of Betong chicken (KU line) gave higher percentages when extracting for 1.5 and 2.0 hours. Extraction time affects the contents of chicken essence because heat denatures myosin and actin (Lin et al., 2016). Over a longer time, the heating process denatures myosin, and actin expels sarcoplasmic fluid from muscle fibers (Dai et al., 2014). Finally, meat tissue loses water.

Quantitation of neurotransmitters in chicken essence

The current study measured amounts of anserine, carnosine, and creatine, as shown in Tables 1 to 3. The approximate concentrations of anserine, carnosine, and creatine ranged from 669–1,150, 104–336, and 316–545 mg/100g, respectively. Different extraction times yielded significant contents of anserine, carnosine, and creatine ($P < 0.05$). When a 2-hour extraction time was employed, we measured the highest concentration of anserine, carnosine, and creatine. According to chicken lines, the highest concentration of anserine, carnosine, and creatine was observed in chicken essence extracted from Betong chicken (KU line) meat, followed by chicken essence originating from Tapaotong Kasetsart and KU-Phuparn meat, respectively.

Table 1. Anserine concentrations in chicken essence (mg/100g) extracted from three Thai native chicken lines

Items	Extraction time		
	1.0 hour	1.5 hours	2.0 hours
Betong chicken (KU line)	691.00 ± 51.21 ^c	924.20 ± 27.82 ^{ba}	1,150 ± 48.21 ^{aa}
Tapaotong Kasetsart	669.33 ± 61.64 ^b	751.93 ± 22.65 ^{abc}	839.94 ± 39.09 ^{ab}
KU-Phuparn	676.01 ± 60.65 ^c	830.40 ± 51.53 ^{bb}	937.10 ± 35.92 ^{ab}

^{abc}Means in the same row with different superscripts are significantly different ($P < 0.05$).

^{ABC}Means in the same column with different superscripts are significantly different ($P < 0.05$).

Table 2. Carnosine concentrations in chicken essence (mg/100g) extracted from three Thai native chicken lines

Items	Extraction time		
	1.0 hour	1.5 hours	2.0 hours
Betong chicken (KU line)	198.86 ± 18.64 ^{ca}	265.86 ± 9.50 ^{ba}	336.42 ± 11.06 ^{aa}
Tapaotong Kasetsart	103.86 ± 19.78 ^{cb}	169.89 ± 8.25 ^{bb}	205.18 ± 16.89 ^{ac}
KU-Phuparn	198.69 ± 14.34 ^{ca}	251.16 ± 18.02 ^{ba}	273.56 ± 11.93 ^{ab}

^{abc}Means in the same row with different superscripts are significantly different ($P < 0.05$).

^{ABC}Means in the same column with different superscripts are significantly different ($P < 0.05$).

Table 3. Creatine concentrations in chicken essence (mg/100g) extracted from three Thai native chicken lines

Items	Extraction time		
	1.0 hour	1.5 hours	2.0 hours
Betong chicken (KU line)	346.67 ± 20.08 ^c	450.97 ± 9.87 ^{ba}	545.09 ± 13.99 ^{aa}
Tapaotong Kasetsart	319.89 ± 32.89 ^b	367.91 ± 10.29 ^{ab}	399.67 ± 21.76 ^{ab}
KU-Phuparn	316.09 ± 16.13 ^c	366.28 ± 20.81 ^{bb}	413.87 ± 12.64 ^{ab}

^{abc}Means in the same row with different superscripts are significantly different ($P < 0.05$).

^{ABC}Means in the same column with different superscripts are significantly different ($P < 0.05$).

Our study found different amounts of anserine and carnosine compared to previous studies, as shown in Tables 5 and 6. Many studies show that various factors, particularly chicken lines (Dai et al., 2014), cause different amounts of neurotransmitters, such as diverse types of meat, chicken lines, genders, and cooking conditions (Qi et al., 2018). For example, commercial chicken's edible meat delivers more anserine and carnosine contents than bones (Maikhunthod, 2003). In general, fresh breast meat of five lines of Korean native chickens consists of more anserine and carnosine than fresh thigh meat of the same Korean native chicken lines (Li et al., 2012). In addition to depending on the type of meat, most fresh meat of different Korean native chicken contains significant variations of anserine, carnosine, and creatine (Li et al., 2012). Like different kinds of meat and chicken lines, most fresh breast and thigh meat of the same Korean native chicken lines from females is composed of significantly higher amounts of anserine and carnosine (Li et al., 2012). The results disagreed with a report that prolonging extraction time at 105 and 115 degrees Celsius adversely influences anserine and carnosine concentration (Dai et al., 2014). Due to divergent chicken lines in these studies and the lack of scientific information on creatine, we could not compare these neurotransmitter amounts with other chicken essence (Dai et al., 2014). The chicken essence originating from the breast meat of Thai native chicken generates the highest

concentration of carnosine, followed by the others extracted from hybrid Thai native chicken lines and broilers, respectively (Qi et al., 2018).

Amino acid profiles of chicken essence extracted from three chicken lines

We determined amino acid quantification in chicken essence, as shown in Table 4. For chicken essence generated from chicken carcasses of Betong chicken (KU line) and Tapaotong Kasetsart lines, shifting extraction time from 1.5 to 2.0 hours resulted in increasing amounts of all amino acids, except proline and tryptophan. However, most amino acids in chicken essence derived from Betong chicken (KU line) and Tapoundthong Kasetsart line were equal between 1.5 and 2.0 hours of extraction time. Commonly, when we extended extraction time from 1.0 to 1.5 hours, all amino acids in chicken essence originating from chicken carcasses of the KU-Phuparn line increased. In contrast to others, chicken essence extracted from KU-Phuparn carcasses contained higher amounts of most amino acids, except valine, cysteine, and leucine, when we employed a 2.0-hour extraction time.

When we compared amino acids in our chicken essence with others reported in previous studies, as shown in Table 7. The concentration of most amino acids is similar to the others extracted from the Taiwanese native chicken line, except

aspartic acid, arginine, methionine, cystine, isoleucine, and phenylalanine (Dai et al., 2014). In our study, extending extraction time enhanced the increasing amount of amino acid in chicken essence. In agreement with our results, shifting from 4 to 6 hours with 115 degrees Celsius incubation improved most amino acids in chicken essence (Dai et al., 2014). Like the amounts of neurotransmitters, amino acid concentration in chicken essence possibly depends on the chicken line. For instance, Wu and Shiao (2002) demonstrated that chicken essence extracted from divergent chicken lines contains significantly different amounts of amino acids.

The requirements of carnosine and creatine for a 70-kg healthy adult are 606 and 1,700 mg per day, respectively (Jung et al., 2013). According to Jung et al. (2013), arginine, glycine, and methionine

are the precursors of creatine synthesis via the cooperation of multiple organs, and a 70-kg healthy adult releases 1.7 g creatine per day as the excretion of urine; on the other hand, the production of 1.7 g creatine needs 2.3 g arginine, 1.0 g glycine, and 2.0 g methionine (Jung et al., 2013). Possibly, the amounts of neurotransmitters in chicken essence may not meet human physiological requests. Therefore, we recommend that people should eat meat as an alternative source of these dietary nutrients.

Table 4. Amino acid profiles of chicken essence extracted from KU Betong, Tapaotong Kasetsart, and KU-Phuparn meat (mg/100 g) with 1.0-, 1.5-, and 2.0-hour extraction time

Items	Chicken line	Betong chicken (KU line)			Tapaotong Kasetsart			KU-Phuparn		
		Extraction time (hour)	1.0	1.5	2.0	1.0	1.5	2.0	1.0	1.5
Amino acid	Taste									
Aspartic acid	Umami	167.78	168.68	205.52	156.00	156.59	185.97	175.37	201.93	204.62
Glutamic acid	Sour	465.26	468.98	546.86	461.71	451.28	520.55	526.9	589.92	583.03
Total		633.04	637.66	752.38	617.71	607.87	706.52	702.27	791.85	787.65
Serine	Sweet	100.07	99.35	121.04	97.60	99.49	115.65	113.29	128.32	126.74
Threonine		77.22	77.80	92.09	77.66	75.04	88.32	83.93	96.09	94.68
Glycine		501.99	522.8	642.39	505.74	460.00	520.67	489.47	583.56	608.62
Alanine		240.18	247.55	298.85	246.59	226.7	261.05	251.41	289.63	295.27
Tyrosine		34.59	33.49	38.11	21.88	31.54	36.67	36.47	39.25	39.50
Proline		193.95	232.77	188.95	204.80	154.84	203.95	135.03	177.12	238.66
Total		1,148	1,213.76	1,381.43	1,154.27	1,047.61	1,226.31	1,109.6	1,313.97	1,403.47
Histidine	Bitter	144.03	140.54	151.31	91.38	140.50	148.23	132.95	136.81	154.75
Arginine		185.34	181.81	236.12	185.67	172.93	200.57	195.47	226.40	236.25
Valine		68.35	70.33	85.75	71.47	63.47	81.81	72.84	86.72	50.00
Methionine		56.26	60.53	71.74	60.11	56.91	70.01	70.14	76.97	75.70
Cystine		317.79	338.07	414.6	327.72	301.89	341.51	313.89	382.83	384.95
Isoleucine		47.65	48.86	59.74	49.93	43.61	55.35	49.73	59.39	56.81
Phenylalanine		67.00	68.27	83.79	67.20	64.88	74.76	68.60	80.85	82.19
Tryptophan		4.44	4.59	2.94	3.91	3.78	3.66	3.85	3.73	4.50
Leucine		105.41	106.99	127.8	108.63	103.88	123.90	114.58	183.35	129.67
Lysine		150.26	152.12	179.16	129.77	136.43	165.09	163.57	183.35	180.33
Total		1,146.53	1,172.11	1,412.95	1,095.79	1,088.28	1,264.89	1,185.62	1,420.40	1,355.15
Total amino acid		2,927.57	3,023.53	3,546.76	2,867.77	2,743.76	3,197.72	2,997.49	3,526.22	3,546.27

Table 5. Anserine concentrations in chicken essence (mg/100g) detected in this study and reported in previous studies

Source for chicken essence preparation	Anserine concentration (mg/100g)	Reference
Hybrid Thai native chicken	669–1,150	This study
Commercial chicken	36–437	Wu and Shiau, 2002
Taiwanese native chicken	377–518	Lin et al., 2016
Taiwanese native chicken	3,419–6,304	Lin et al., 2017

Table 6. Carnosine concentrations in chicken essence (mg/100g) detected in this study and reported in previous studies

Source for chicken essence preparation	Carnosine concentration (mg/100g)	Reference
Hybrid Thai native chicken	104–336	This study
Thigh meat from many chicken lines ¹	6–11	Maikhunthod, 2003
Breast meat of many chicken lines ¹	18–33	Maikhunthod, 2003
Commercial chicken	8–162	Wu and Shiau, 2002
Taiwanese native chicken	139–172	Lin et al., 2016
Taiwanese native chicken	2,525–3,263	Lin et al., 2017

¹In this study, they prepared chicken essence from Thai native chicken, hybrid Thai native chicken lines, and broiler.

Table 7. Amino acid profiles in chicken essence (mg/100g) detected in this study and reported in previous studies

Items Amino acid	Source for chicken essence preparation			
	Hybrid Thai native chicken	Taiwanese native chicken	Taiwanese native chicken	Commercial chicken
Aspartic acid	168–205	212–307	172–214	4.4–34.1
Glutamic acid	451–589	484–665	536–710	13–107
Serine	97–128	100–136	249–333	3.4–43
Threonine	75–96	73–106	155–175	3–28
Glycine	460–642	101–671	219–249	8–383
Alanine	226–298	296–426	382–413	10–59
Tyrosine	21–39	26–38	53–75	4–18
Proline	135–239	217–358	118–151	4–23
Histidine	91–155	127–156	41–63	1–10
Arginine	172–236	593–758	128–176	3–28
Valine	50–86	96–127	111–152	8–23
Methionine	56–76	10–30	45–63	4–11
Cystine	301–414	0–16	1–2	-
Isoleucine	43–59	19–78	65–89	2–12
Phenylalanine	64–83	74–107	66–88	4–14
Tryptophan	3–4	14–54	-	-
Leucine	103–183	111–170	136–178	4–23
Lysine	129–183	179–256	170–250	5–36
Reference	This study	Lin et al., 2016	Lin et al., 2017	Wu and Shiau, 2002

CONCLUSIONS

According to Betong chicken (KU line), Tapaotong Kasetsart, and KU-Phuparn chicken lines as the sources of chicken essence preparation in the present study, the information of prices, yields of chicken essence, and amounts of neurotransmitters and amino acids could be the guideline for producing chicken essence. The clear results showed that Betong chicken (KU line) carcasses gave the highest chicken essence yield when we applied with either 1.5 or 2.0-hour extraction time at 100 degrees Celsius. Many factors, especially chicken lines,

affected neurotransmitter amounts. Chicken essence generated from the Betong chicken (KU line) line provided the highest amounts of anserine, carnosine, and creatine, followed by others extracted from KU-Phuparn and Tapaotong Kasetsart, respectively. Amounts of each neurotransmitter in chicken essence extracted from three chicken lines significantly depended on extraction time ($P < 0.05$). To maintain physiological regulations, people should eat animal meat since chicken essence may contain insufficient amounts of neurotransmitters. Extraction time influenced amounts of amino acids in chicken essence. When we increased extraction time, a higher concentration of most amino acids in chicken essence was observed.

ACKNOWLEDGMENTS

This research was supported by research grant No. 73970 administered by the National Research Council of Thailand.

REFERENCES

- Bungsrisawat, P., Tumwasorn, S., Loongyai, W., Nakthong, S., and Sopannarath, P. 2018. Genetic parameters of some carcass and meat quality traits in Betong chicken (KU line). *Agriculture and Natural Resources*. 52(3): 274–9. <https://doi.org/10.1016/j.anres.2018.09.010>.
- Dai, Z., Wu, Z., Jia, S., and Wu, G. 2014. Analysis of amino acid composition in proteins of animal tissues and foods as pre-column o-phthalaldehyde derivatives by HPLC with fluorescence detection. *Journal of Chromatography B*. 964: 116–27. <https://doi.org/10.1016/j.jchromb.2014.03.025>.
- Dong, X-b., Li, X., Zhang, C-h., Wang, J-z., Tang, C-h., and Sun, H-m. 2014. Development of a novel method for hot-pressure extraction of protein from chicken bone and the effect of enzymatic hydrolysis on the extracts. *Food Chemistry*. 157: 339–46. <https://doi.org/10.1016/j.foodchem.2014.02.043>.
- IBM Corp. 2019. IBM SPSS Statistics for Windows, Version 26.0. Armonk, NY.
- Jaturasitha, S., Srikanchai, T., Kreuzer, M., and Wicke, M. 2008. Differences in carcass and meat characteristics between chicken indigenous to northern Thailand (Black-boned and Thai native) and imported extensive breeds (Bresse and Rhode Island Red). *Poultry Science*. 87(1):160–9. <https://doi.org/10.3382/ps.2006-00398>.
- Jiang, X., and Groen, A. 2000. Chicken breeding with local breeds in China—a review. *Asian-Australasian Journal of Animal Sciences*. 13(10): 1482–98.
- Jung, S., Bae, Y.S., Kim, H.J., Jayasena, D.D., Lee, J.H., and Park, H.B. 2013. Carnosine, anserine, creatine, and inosine 5'-monophosphate contents in breast and thigh meats from 5 lines of Korean native chicken. *Poultry Science*. 92(12): 3275–82. <http://dx.doi.org/10.3382/ps.2013-03441>.
- Khumpeerawat, P. 2016. KU-Phuparn is an alternative source for farmers. *Kasetsart extension journal*. 61(1): 53–58. (*in Thai*).
- Li, Y., He, R., Tsoi, B., and Kurihara, H. 2012. Bioactivities of chicken essence. *Journal of food science*. 77(4): R105-R10. <https://doi.org/10.1111/1750.3841.2012.02625x>.
- Lin, Y., Chen, C., and Tan, F. 2016. Influences of different heating conditions on the quality of native chicken essence. In: *Proceedings of the 62nd International Congress of Meat Science and Technology*, 14–19 August 2016, Bangkok.
- Lin, C., Wu, C., Lin, H., Rau, Y., and Fu, W. 2017. Effects of extraction conditions and chicken raw materials on the characteristics of dripped chicken essence. *Taiwanese Journal of Agricultural Chemistry and Food Science*. 55(5/6): 262–9. [https://doi.org/10.6578/TJACFS.201710_55\(5&6\)](https://doi.org/10.6578/TJACFS.201710_55(5&6)).
- OAE. Situation of important agricultural products and trends in 2023. Office of Agricultural Economics, [accessed on July 16, 2023].
- Maikhunthod, B. 2003. Extraction and antioxidant activity of carnosine from native, hybrid native and broiler chicken meats. M.S. Thesis. Suranaree University of Technology.
- Putsakul, A., Bunchasak, C., Chomtee, B., Kao-ian, S., and Sopannarath, P. 2010. Effect of dietary protein and metabolizable energy levels on growth and carcass yields in Betong chicken (KU Line). In: *Proceedings of the 48th Kasetsart University Annual Conference*, Kasetsart, 3–5 March, 2010, Bangkok.
- Qi, J., Hu-hu, W., Zhang, W-w., Deng, S-l., Zhou, G-h., and Xu, X-l. 2018. Identification and characterization of the proteins in broth of stewed traditional Chinese yellow-feathered chickens. *Poultry Science*. 97(5): 1852–60. <https://doi.org/10.3382/ps/pey003>.
- Sopannarath, P., and Bunchasak, C. 2015. Betong chicken (KU line) or KU Betongchicken. *Kasetsart Extension Journal*. 61: 13–21.
- Sujiwo, J., Kim, D., and Jang, A. 2018. Relation among quality traits of chicken breast meat during cold storage: correlations between freshness traits and torymeter values. *Poultry Science*. 97(8): 2887–94. <https://doi.org/10.3382/ps/pey138>.
- Wu, G. 2020. Important roles of dietary taurine, creatine, carnosine, anserine and 4-hydroxyproline in human nutrition and health. *Amino Acids*. 52(3): 329–60. <https://doi.org/10.1007/s00726-020-02823-6>.
- Wu, H.C., and Shiau, C.Y. 2002. Proximate composition, free amino acids and peptides contents in commercial chicken and other meat essences. *Journal of Food and Drug Analysis*. 10(3): Article 8.

Effect of ozone micro-nano bubbles on longan shelf life extension

Panadda Kidtuengkun^{1*}, Preuk Choosung¹, Parinyawadee Sritontip² and Chiti Sritontip^{1,2}

¹Faculty of Science and Agricultural Technology, Rajamangala University of Technology Lanna, Lampang, 52000, Thailand

²Agricultural Technology Research Institute, Rajamangala University of Technology Lanna, Lampang 52000, Thailand

*Corresponding author: PanaddaKidtuengkun@gmail.com

Received: May 11, 2023. Accepted: July 11, 2023.

ABSTRACT

This study aimed to evaluate the effects of micro/nano ozone bubbles (O₃ MNBs) water on extending longan shelf life. The experiment was assigned using a completely random design (CRD), which consisted of 4 treatments, including soaking with 1) distilled water for 5 minutes (control), 2) 10 minutes of ozone micro nanobubbles (O₃ MNBs) water, 3) 20 minutes of O₃ MNBs water, and 4) 30 minutes of O₃ MNBs water. All treatments contained four replications. Then, they were stored at 5°C with 80% relative humidity for fifteen days for further examination. The results revealed that the control had the highest weight loss than other treatments, especially 6 to 9 days after being treated with O₃ MNBs water. Moreover, longans with the O₃ MNBs water treatments were more significant in the L* and b* color indexes than the untreated fruit on longans outside the pericarp. In addition, the control appeared to have pericarp browning after storage for nine days and found fungal on the fruit twelve days after treatment.

Keywords: ozone, micro/nanobubbles, longan

INTRODUCTION

Longan (*Dimocarpus longan* L.) is a commercial fruit commonly grown in Thailand, the largest exporter of longan in the world. Longan can be induced flowering in the off-season and has a year-round supply, contributing roughly 141.42 million USD in 2022. The production area in the year 2022 was 279,845.92 hectares, which yielded approximately 1,567,087.36 metric tons (Sritontip et al., 2005; OAE, 2022). Although production export levels have increased, longan has a concise shelf life, deteriorating easily and quickly within 3 to 4 days at room temperature (Jiang et al., 2002). The short shelf life of fresh longan fruit is a common issue. In deteriorated longan, fruit shells turn from yellow-brown to dark brown into black color caused by dehydration, cooling damage, and microbes. For microbes damaged, it may result from microbial invasion before or after the harvesting process (Pan, 1994). It is not easy to store longan in good condition even for short periods. The main crucial postharvest losses are microbes, fungus spoilage, and pericarp browning of longan. The pericarp browning reaction can be associated with dehydration, heat stress, senescence, chilling injury, or disease of the longan fruit (Apai, 2010). At present, sulfur dioxide (SO₂) fumigation is a commercially accepted method to solve the problems of postharvest losses in longan,

but it risks consumer health and safety concerns. (Drinnan, 2004; Sevilai et al., 2020). For this reason, there is a need to develop effective methods to replace the protocol using SO₂ fumigation to be less harmful to humans and the environment, such as using ozone and Micro-nanobubbles (MNBs) technology as an alternative method.

In Thailand, MNBs are a novel technology. The MNBs produce little gas bubbles between 50 micrometers and 200 nanometers in diameter, raising the gas or oxygen concentration in water. Moreover, MNBs can help as a filter for wastewater to eliminate pesticide and microbe residues from crops and promote seed germination and vegetative growth of plants (Oshita and Liu, 2013; Sritontip et al., 2019). Due to their extended stay in aqueous solutions and huge specific surface area, MNBs are used extensively in environmental engineering, environmental remediation, agriculture, agronomy, horticulture, aquaculture, and hydroponics. Reactive oxygen species (ROS) produced by MNB can also purify wastewater, eliminate persistent organic contaminants from food, and inactivate infections in water (Marcelino et al., 2022; Seridou and Kalogerakis, 2021; Zhang et al., 2022).

Ozone (O₃) is triatomic oxygen and is widely used to control microorganism growth (bacteria, fungi, viruses, and protozoa) and chemical

residue in various food industries as well as in the exportation of vegetable and fruit produce (Kim et al., 1999). Aslam et al. (2021) report that aqueous ozone treatment was effective in reducing the microbial population, maintaining quality parameters, and extending the shelf life of fresh-cut onion slices. This agrees with Chamnan et al. (2021), who reported that the longan exposed to ozone gas at 8,500 ppm for 5 min was considered a suitable treatment to extend shelf-life up to 35 days, which is 57% longer than the shelf-life of non-ozonated longan. Yang and Chen (2022) report that the preservation technology of ozone micro-nano bubble treatment has improved the preservation of fruits and vegetables by 12%. Therefore, this study aimed to investigate the effect of ozone micro-nanobubble applications on reducing pericarp browning and disease incidence to extend the shelf-life of longan and sulfur residue reduction.

MATERIALS AND METHODS

In this study, non-infected, mature fresh longan fruit of the Daw variety from the off-season was employed. The fruit poles of longans were chopped to a maximum length of 0.5 cm after they were chosen for their identical size and skin tone. The skins of the fruits were cleaned with 200 mg/L of

sodium hypochlorite (NaClO) solution. Then, longan fruits were soaked in the NaClO solution for two minutes and dried at room temperature before further processes. The experiment was assigned using a completely randomized design. It included four treatments with four replications, i.e., 1) soaking longan fruits in distilled water for 5 minutes or control, 2) soaking longan fruits in O₃ MNBs water for 10 minutes, 3) soaking longan fruits in O₃ MNBs water for 20 minutes, and 4) soaking longan fruits in O₃ MNBs water for 30 minutes. There were 50 mature logan fruits in each replication.

The MNBs generator model KVM-25 used in this study was modified by the Faculty of Engineering, Rajamangala University of Technology Lanna, Thailand, to produce O₃ MNBs water for the experiment. The O₃ MNBs water had an oxidation-reduce potential (ORP) level at 600 mV. The total bubble distribution was $2.7388 \times 10^{11}/\text{mL}$, with a median size of 38.67 nm, mode size of 62 nm, and average size of 66.43 nm, measured by Horiba-960A laser scattering particle size distribution analyzer®. This could support a water flow rate of 25 L/minute, an airflow rate of 2 L/minute, an operating pressure of 0.25–0.4 MPa, and a 0.75 KW pump (Figure 1).

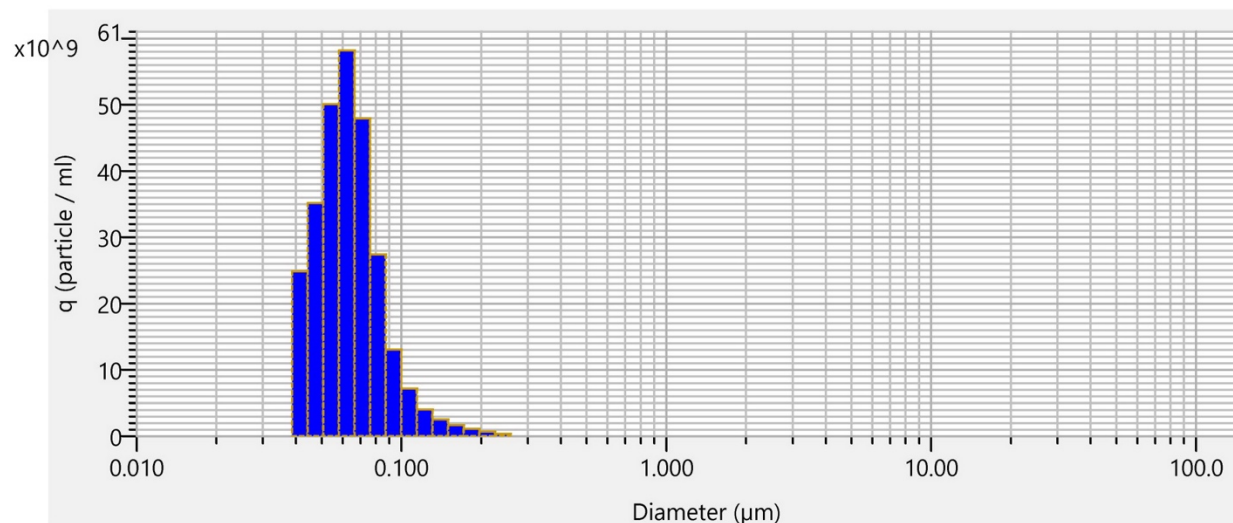


Figure 1. The analysis of the diameter of micro-nano bubbles produced by KVM-25 detected by Horiba-960A.

Longan fruit samples were soaked in according to treatment protocols simultaneously, then packed into a transparent box of perforated fruits and stored in the refrigerator at 5°C temperature and 80% relative humidity. Data were recorded every three days at a time for 15 days, or the longan fruits were counted until a fungal growth covering more than 25% of the longan fruit's surface was discovered or the level of change in pericarp browning was more

than 50 %. Weight loss in each treatment was recorded every three days from the first day until the end of the experiment using an electrical balance (Ohaus, model PX3202, Maximum 3,200 g, USA). The formula for determining the percentage of water loss was:

$$\text{Percentage of weight loss} = (A - B)/A \times 100$$

Where: A = sample weight on the first day of experimentation (g)

B = Sample weight, date of measurement (g).

The firmness of the fruit pulp was measured using the force gauge (RS232 Output Model 840060). The longan peel was removed, and the firmness of the fruit pulp was measured by pressing down at the center of the longan's fruit pulp. Skin color changes of the outer shell and fruit pulp were measured using the 3NH brand machine model NR200. The values are expressed as color brightness (L*), green (a*), and yellow (b*). The percentage of disease and total soluble solids using a hand refractometer were also recorded. The data were analyzed for variance, and the average was compared with Duncan's New Multiple Range Test (DMRT) at a significant level of 0.05.

RESULTS AND DISCUSSION

Weight loss percentage

Longan samples lost weight throughout the retention period, which lasted 15 days after the treatment. The highest weight loss percentage was found in the distilled water (control) treatment 6–9 days after treatment (Figure 2).

Fruit firmness

The changes in the fruit firmness tester showed a non-statistical difference among treatments after being treated with distilled water and O₃MNBs (Figure 3).

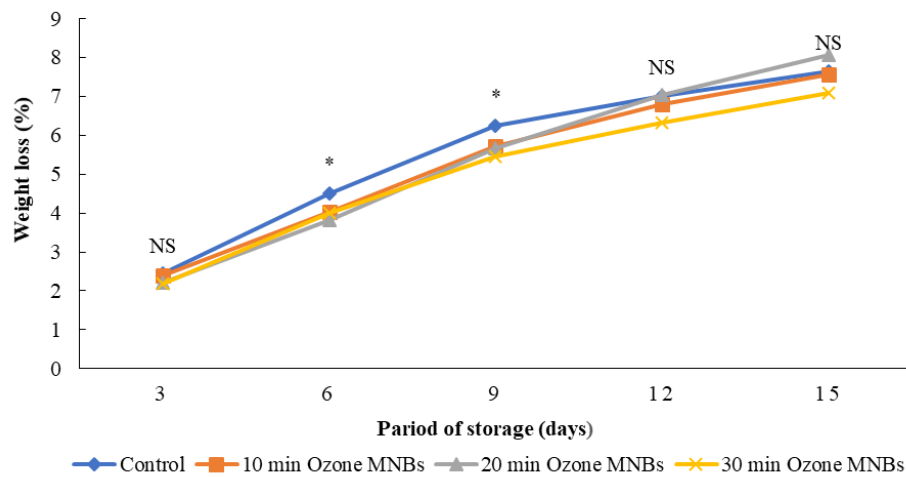


Figure 2. Weight loss of longan fruit after being treated and storage
NS = non-significant and * = significant differences at $P < 0.05$.

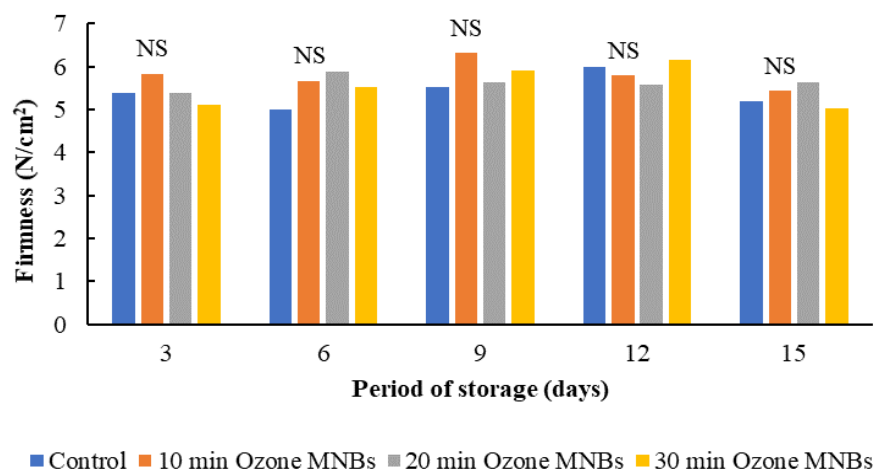


Figure 3. Firmness of longan fruit after being treated and storage
NS = non-significant.

Changes in the color of the outside of the pericarp and fruit pulp

The brightness value (L^*) of the control had been reduced on days 3, 6, and 15 following the storage period, according to alterations in the color values of the outside of the pericarp. Moreover, the a^* value in the control treatment was greater than in

the O_3 MNBs, although the b^* value suggested a lower value in the control treatment (Table 1).

After storage at a cool temperature, changes in the color value of the pulp revealed that the brightness value (L^*) and b^* values did not significantly differ. In contrast, the a^* value changed unforeseen (Table 2).

Table 1. Effects of O_3 MNBs on the L^* , a^* , and b^* values of the outer shell in longan fruits

Treatments	Period of storage (days)						
	0	3	6	9	12	15	
L^*	Control	55.98	48.10 ^b	48.01	46.10 ^b	44.25	39.93 ^c
	10 min O_3 MNBs	55.94	51.37 ^a	50.71	48.05 ^{ab}	44.55	45.27 ^b
	20 min O_3 MNBs	55.54	51.59 ^a	49.53	47.96 ^{ab}	45.92	49.76 ^a
	30 min O_3 MNBs	55.98	49.96 ^a	49.14	49.37 ^a	46.76	47.88 ^{ab}
	F-test	NS	**	NS	*	NS	**
a^*	Control	11.07	11.64	11.48	11.55	11.86	13.03 ^a
	10 min O_3 MNBs	11.30	11.18	11.44	11.76	11.56	12.10 ^{ab}
	20 min O_3 MNBs	10.99	10.61	10.35	11.68	11.46	11.29 ^b
	30 min O_3 MNBs	11.07	10.74	11.34	11.31	11.55	11.85 ^b
	F-test	NS	NS	NS	NS	NS	**
b^*	Control	24.93	26.59	28.70	24.37 ^c	22.98 ^b	21.43 ^b
	10 min O_3 MNBs	24.93	26.49	29.42	27.30 ^b	25.61 ^a	25.71 ^a
	20 min O_3 MNBs	24.96	26.20	28.74	28.64 ^{ab}	26.13 ^a	28.43 ^a
	30 min O_3 MNBs	24.93	25.45	28.46	29.94 ^a	24.11 ^{ab}	27.12 ^a
	F-test	NS	NS	NS	**	*	**

*Means within the column followed by the same superscript were not significantly different at $P > 0.05$ by DMRT, NS = non-significant, * = significant differences at $P < 0.05$, ** = significant differences at $P < 0.01$ according to the DMRT test.

Table 2. Effects of O_3 MNBs on the L^* , a^* , and b^* values of the pulp in longan fruits

Treatments	Period of storage (days)						
	0	3	6	9	12	15	
L^*	Control	31.36	31.22	30.77	36.98	33.04	32.82
	10 min O_3 MNBs	30.54	32.54	31.89	37.42	33.63	34.11
	20 min O_3 MNBs	30.86	32.23	31.26	35.84	33.05	33.39
	30 min O_3 MNBs	31.36	32.40	31.80	37.78	32.99	33.37
	f-test	NS	NS	NS	NS	NS	NS
a^*	Control	0.04	0.03	-0.01	0.02	0.16 ^b	0.02 ^b
	10 min O_3 MNBs	0.01	-0.09	-0.04	-0.01	0.18 ^b	0.06 ^b
	20 min O_3 MNBs	0.08	-0.17	-0.08	0.06	0.00 ^b	0.34 ^a
	30 min O_3 MNBs	0.04	-0.10	-0.03	0.15	0.62 ^a	0.07 ^b
	f-test	NS	NS	NS	NS	*	**
b^*	Control	-0.95	-1.03	-1.37	-0.82	-0.55	-0.65
	10 min O_3 MNBs	-1.11	-0.97	0.03	-0.44	-0.62	-0.37
	20 min O_3 MNBs	-1.03	-1.32	-0.84	-0.32	-0.63	-0.44
	30 min O_3 MNBs	-0.95	-1.59	-1.12	-0.26	-0.09	-0.52
	F-test	NS	NS	NS	NS	NS	NS

*Means within the column followed by the same superscript were not significantly different at $P > 0.05$ by DMRT, NS = non-significant, * = significant differences at $P < 0.05$, ** = significant differences at $P < 0.01$ according to the DMRT test.

Pathogenesis

After low-temperature storage, disease incidence in longan fruit was risen. The fruit's surface fungus started to develop during the period of storage. Only with the control approach did symptoms begin to appear on the 12th day of

the experiment. The occurrence of the two treatments was then discovered on the experiment's fifteenth day, with the control therapy having the highest incidence and using 10-minute O₃MNBs. In contrast, 20 and 30 minutes of O₃MNBs were not found in the disease (Figure 4).

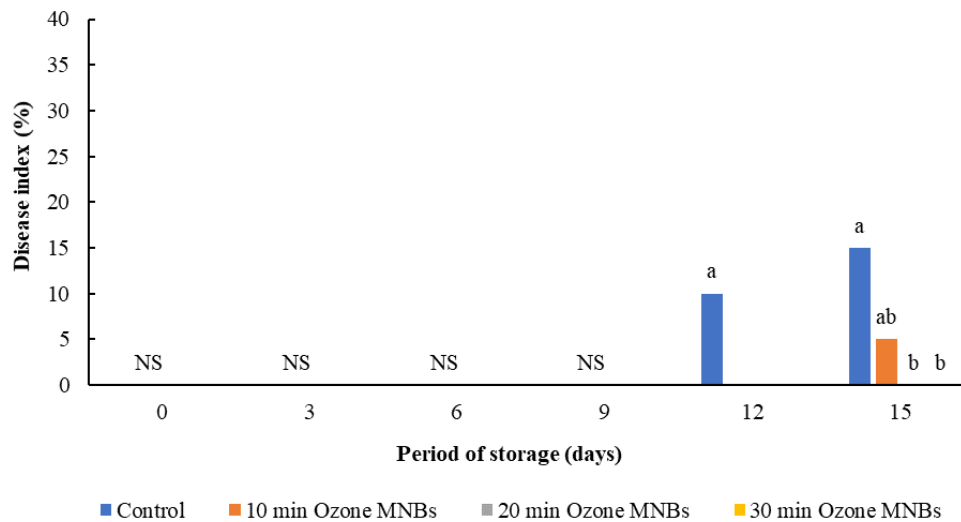


Figure 4. The effect of treatments on pathogenesis in longan fruit after storage.

NS = non-significant, * = significant differences at $P < 0.05$, according to the DMRT test.

Total soluble solids

It was found that the total amount of soluble solids in longan fruit tends to decrease gradually throughout the storage period compared to

the default. However, the differences were found during the 15 days of the treatment. The control treatment was the greatest in total soluble solid contents (Figure 5).

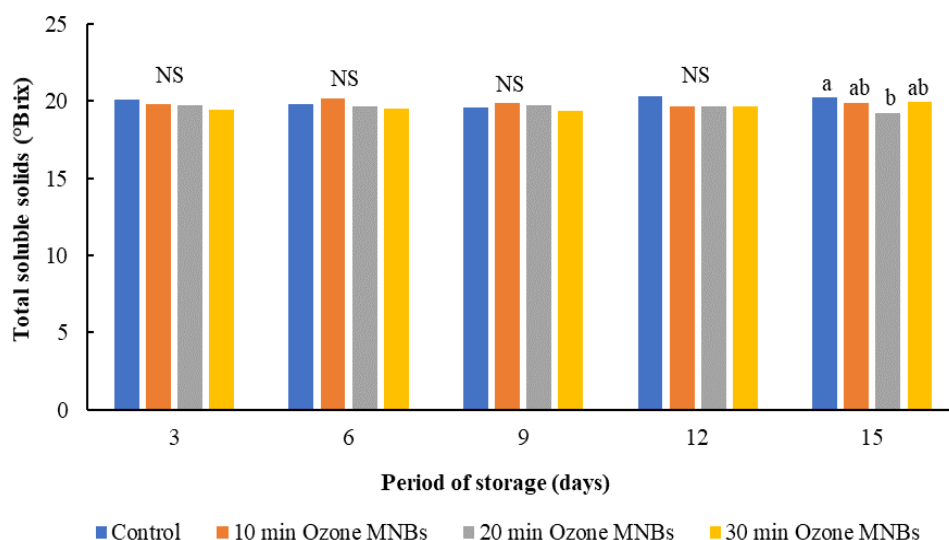


Figure 5. Effects of treatments on total soluble solid in longan fruits

NS = non-significant, * = significant differences at $P < 0.05$, ** = significant differences at $P < 0.01$ according to the DMRT test.

To increase shelf life and decrease disease, this study examined the impact of washing fresh longan fruits with O₃MNBs water on their quality. The outcome showed that longans were stored at a cool temperature for longer than the control. O₃ MNBs water has an impact on the fruit quality. The O₃ MNBs could lower the proportion of weight loss by reducing microbial infection regarding the spread of diseases. The L* and b* color indices of the longan fruit skin showed that the O₃ MNBs water treatments outperformed the untreated fruit.

A study of the effects of using ozone microbubbles (O₃ MBs) to reduce chlorpyrifos and anthracnose in sweet pepper has been reported. The sweet peppers were washed with O₃ MBs at each temperature and during each exposure period to O₃ MBs. Furthermore, O₃ MNBs affected the control of anthracnose caused by *Colletotrichum capsica* by about 96%, while the control unit was reduced by only 14.3% (Tamjapo et al., 2017). Lee et al. (2016) reported that chestnuts were washed with MNBs in combination with ozone for 10 minutes and found to reduce rot disease. This method could also extend the shelf life of chestnuts after harvesting. Moreover, the residual activity and ozone disinfection capacity could be significantly increased by O₃ MNB. When ozone ultra-fine bubbles were combined with high mechanical action in acidic electrolyzed water to wash fresh vegetables, the lowest viable bacterial count was detected, compared to other treatments, such as sodium hypochlorite. The effectiveness of ozone microbubbles in disinfecting *F. oxysporum* f. sp. melonis spores was investigated, and the results showed that they were more effective than macrobubbles. (Seridou and Kalogerakis, 2021; Ushida et al., 2017). In this study, the O₃ MNBs could extend the shelf life of logan while disinfecting microorganisms because O₃ can damage the enzymes of the DNA and RNA of microbial cells because it has two methods for suppressing bacteria. It is created by ozone molecules that oxidize compounds found in microbial cells or by unrelated substances that direct them to kill membrane cells and other internal cells in the cell. Microbial cells' cytoplasm, proteins, and lipid layers produce intracellular leakage, leading to cell disintegration. (Leowchavalit et al., 2003; Restainno et al., 1995; Victorin, K. 1992).

CONCLUSIONS

The soaking of O₃ MNBs for about 10 to 30 minutes could prolong the life of treatment and slow down the occurrence of diseases that may cause adverse effects on longan. The optimum O₃ MNBs soaking time in this experiment was 20 minutes.

REFERENCES

- Apai, W. 2010. Effects of fruit dipping in hydrochloric acid then rinsing in water on fruit decay and browning of longan fruit. *Crop Protection*. 29: 1184–1189.
- Aslam, R., Shafiq, M. A. and Kaur, P. 2021. Comparative study on efficacy of sanitizing potential of aqueous ozone and chlorine on keeping quality and shelf-life of minimally processed onion (*Allium Cepa* L.). *Ozone Science & Engineering*. 44(2): 196–207. <https://doi.org/10.1080/01919512.2021.1904204>.
- Chamnan, S., Varith, J., Jaturonglumlert, S., Phimphimol, J. and Sujinda, N. 2021. Effects of high concentration ozone gas fumigation on the quality and shelf-life of longan fruit. *Ozone science & engineering*. 44(1): 105–116. <https://doi.org/10.1080/01919512.2021.1948387>.
- Drinnan, J. 2004. Longans postharvest handling and storage. Australian Government. Rural industries research and development corporation. RIRDC Project No DAQ-249A. p 19.
- Jiang, Y., Zhang, Z., Joyce, D. C., and Ketsa, S. 2002. Postharvest biology and handling of longan fruit (*Dimocarpus longan* Lour.). *Postharvest biology and technology*. 26: 241–252.
- Kim, J.G., Yousef, A.E., and Dave, S. 1999. Application of ozone for enhancing the microbiological safety and quality of foods: A Review. *Journal of food protection*. 62(9) : 1071–1087.
- Lee, U., Joo, S., Klopfenstein, N.B., and Kim, M.S. 2016. Efficacy of washing treatments in the reduction of postharvest decay of chestnuts (*Castanea crenata* 'Tsukuba') during storage. *Plant Science*. 96: 1–5.
- Leowchavalit, K., Researchworakit, S., Tuytemwong, K., and Tuytemwong, P. 2003. Decontamination performance comparison of trisodium phosphate, chlorine, and ozonation. In: Academic Conference of Kasetsart University 41st, February 2003, Bangkok. p. 230–235.
- Marcelino, K. R., Ling, L., Wongkiew, S., Nhan, H. T., Surendra, K. C., Shitanaka, T., and Khanal, S. K. 2022. Nanobubble technology applications in environmental and agricultural systems: Opportunities and challenges. *Critical Reviews in Environmental Science and Technology*. 53 (14): 1378–1403. <https://doi.org/10.1080/10643389.2022.2136931>.
- OAE. 2022. Agricultural statistics of Thailand 2022. Office of Agricultural Economics. [Online] available. 14 February 2022. <https://www.oae.go.th>.
- Oshita, S., and Liu., S. 2013. Nanobubble characteristics and its application to agriculture and foods. In: Proceedings of AFHW 2013. International Symposium on Agri-Foods for Health and Wealth, August 2013. Golden Tulip Sovereign Hotel, Bangkok. p.5–8.
- Pan, X.C. 1994. Study on relationship between preservation and microstructure of *Euphoria longan* fruit. *Journal of Guangxi Agricultural University*. 13: 185–188.
- Restainno, L., Frampton, E.W., Hemphill, J.B., and Palnikar, P. 1995. Efficacy of ozonated water against various food-Environ. *Applied and Environmental Microbiology*. 61(9): 3471–3475.
- Seridou, P., and Kalogerakis, N. 2021. Disinfection applications of ozone micro-and nanobubbles. *Environmental Science: Nano*. 8(12): 3493–3510.
- Sevilai, R., Varith, J., Kanchanawong, P., Pimpimol, J., and Aroonsrimorakot, S. 2020. Factors influencing adoption of vertical forced-air sulfur dioxide fumigation technology of fresh longan exporters in Thailand. *Interdisciplinary Research Review*. p. 22–27.

- Sritontip, C., Dechthummarong, C., Thonglek, V., Khaosumain, Y., and Sritontip, P. 2019. Stimulation of seed germination and physiological development in plants by high voltage plasma and fine bubbles. *International Journal of Plasma Environmental Science & Technology*. 12(2): 74–78.
- Sritontip, C., Khaosumain, Y., Changjeraja, S., and Poruksa, R. 2005. Effects of potassium chlorate, sodium hypochlorite and calcium hypochlorite on flowering and some physiological changes in ‘Daw’ longan. *Acta Horticulturae*. 665: 269–274.
- Tamjapo, A., Uthaibutraand, J., and Whangchai, K. 2017. Effect of microbubble ozone on reduction of chlorpyrifos residue and growth of *Colletotrichum capsica* causing bell pepper anthracnose. *Agricultural Science Journal*. 48(3): 101–104.
- Ushida, A., Koyama, T., Nakamoto, Y., Narumi, T., Sato, T., and Hasegawa, T. 2017. Antimicrobial effectiveness of ultra-fine ozone-rich bubble mixtures for fresh vegetables using an alternating flow. *Journal of Food Engineering*. 206: 48–56.
- Victorin, K. 1992. Review of the genotoxicity of ozone. *Mutation Research/Reviews in Genetic Toxicology*. 277(3): 221–238.
- Yang, Y., and Chen, Q. 2022. The application of ozone micro-nano bubble treatment vegetable fresh-keeping technology in air logistics transportation. *Advances in Materials Science and Engineering*. 2022: 1–10. Article ID 4981444. <https://doi.org/10.1155/2022/4981444>.
- Zhang, Z. H., Wang, S., Cheng, L., Ma, H., Gao, X., Brennan, C. S., and Yan, J. K. 2022. Micro-nano-bubble technology and its applications in food industry: A critical review. *Food Reviews International*. 39(7): 4213–4235. <https://doi.org/10.1080/87559129.2021.2023172>.

Effects of humic acid on growth and development of melon in nutrient solution culture

Pimrumpa Samran^{1*}, Parinyawadee Sritontip² and Chiti Sritontip^{1,2}

¹Faculty of Science and Agricultural Technology, Rajamangala University of Technology Lanna, Lampang 52000, Thailand

²Agricultural Technology Research Institute, Rajamangala University of Technology Lanna, Lampang 52000, Thailand

*Corresponding author: Pimrumpa.sam@gmail.com

Received: March 6, 2023. Revised: September 29, 2023. Accepted: October 24, 2023.

ABSTRACT

A study on the effects of humic acid on vegetative growth and physiological changes of melon (*Cucumis melo* L.) was investigated. The melon seedlings were grown in nutrient solution culture and established in the greenhouse from December 2022 to February 2023 at the Agricultural Technology Research Institute, Rajamangala University of Technology Lanna, Lampang, Thailand. The experiment was carried out using a completely randomized design (CRD) with six treatments and ten replications, including 0 (control), 25, 50, 100, 150, and 200 mg/L of humic acid, respectively. The result showed that humic acid treatments affected the vegetative growth of melons. The application of humic acid at 50 mg/L gave greater plant height, leaf width, and leaf length than other treatments. The 25 and 50 mg/L humic acid enhanced leaf green color index (SPAD) and chlorophyll fluorescence of melon trees. However, increasing humic acid at 100–200 mg/L reduced vegetative growth and chlorophyll fluorescence.

Keywords: melon, humic acid, hydroponic system

INTRODUCTION

Melon, scientifically known as *Cucumis melo* L. is an annual crop that ripens when it gives off a sweet fruity odor. Melon is a nutritious fruit that is a rich source of vitamins A and C, minerals, fiber, and polyphenols with antioxidant and anti-inflammatory properties. Melon also has a high water content (about 90%) and is low in calories (Britannica, 2023). Melon is also considered a potential crop that can generate income for farmers who grow this fruit plant species under the greenhouse system either in the ground or in bags using planting material (Fhoythaworn and Agkhadsri, 2021). In 2016, the melon planting area in Thailand was about 85.28 hectares in 17 provinces. The main planting areas are Ayutthaya, Nonthaburi, Chanthaburi, and Nakhon Ratchasima provinces (DAE, 2017).

The largest supply of lignite coal and a significant amount of leonardite is found at the Mae Moh mine in Thailand's northern Lampang province. Leonardite is a naturally occurring raw material from which humic acid, fulvic acid, and humin can be produced (Jomhataikool et al., 2017). Base-acid treatment of soil and sediment involves the precipitation of humin, humic acid, and fulvic acid fractions using strong bases and strong acid solutions. (Garcia and Abad, 1996) Leonardite from the Mae Moh mine had a significant concentration of humic

acid between 34.7 and 61.58% (Ratanaprommanee and Shutsrirung, 2014).

Humic acid, which originates from different materials and can be found naturally-available in the soil, has many advantageous effects on various aspects and parameters of plant growth. Humic acids have influential roles in soil, such as improving structure, texture, water-holding capacity (WHC), and microbial population (Nardi et al., 2002; Fuentes et al., 2018; Shah et al., 2018). These organic acids also increase crop growth by increasing plant growth promoting auxin hormones with significant effects on both root and shoot growth and increasing photosynthesis (Canellas et al., 2020). Jomhataikool et al. (2019) reported that comparing humic acid to the control, the investigation on rice berries revealed that it was advantageous to leaf and root growth. According to the results of the tomato experiment, humic acid applications between 80 and 240 mg/L can stimulate microbial activity and root growth but should be avoided in soils that are highly contaminated with the pathogens that cause root rot (*Fusarium* spp.) (Yigit and Dikilitas, 2008). Moreover, Humic acid was also observed to boost nutrient uptake efficiency, growth, and yield in the maize experiment. In order to lessen the amount of fertilizer used in the maize growing process, humic acid chemical fertilizer can be used (Ngennyoy et al., 2014)

Growing plants using a hydroponic system approach uses water and non-soil components, or nutrient solutions is an effective system that can improve yield and crops safely and reliably; it can grow vegetables even when it is impossible to put crops in conventional soil (Sritontip et al., 2017). Melon also can be developed hydroponically. This method's unique selling point is the rapid development of root systems and effective absorption of crucial nutrients from the culture solution, which leads to greater yield and quality (Tung and Sritontip, 2022). The melon grown in a nutrient solution shows a greater leaf area index (LAI) than coconut media. Moreover, melon produced in U and double U containers offer higher fresh fruit weight and quality (Fatahian et al., 2013). Although melon can be grown in a culture system using nutritional solutions, it is difficult to regulate the output quality; the value of total soluble solids is unpredictable. Humic acid is a growth stimulant that can promote healthy melon development and fruit quality. This research aimed to evaluate the efficiency of humic acid concentrations in nutrient solutions on vegetative growth and physiological changes in melon.

MATERIALS AND METHODS

This study was established in the greenhouse from December 2022 to February 2023 at the Agricultural Technology Research Institute, Rajamangala University of Technology Lanna, Lampang, Thailand. The experimental design was assigned using a completely randomized design (CRD) with six treatments as the following: (1) control, (2) 25 mg/L humic acid, (3) 50 mg/L humic acid, (4) 100 mg/L humic acid, (5) 150 mg/L humic acid and (6) 200 mg/L humic acid, respectively. There were ten replications of each treatment with one plant each. Melon seeds were germinated in 104-cell nursery seedling trays and used plant media from Known-You Seed (Thailand) Co., Ltd. When seedlings were 14 days of age, they were transplanted into a hydroponics system. Seedlings of melon were grown in nutrient solution under a deep-flow technique (DFT) hydroponic system. The U-shaped PVC containers were sized 35 cm in width, 3 m in length, 12.5 cm in height, and 200 liters for nutrient solution containers (Figure 1) (Thichuto et al., 2022). The nutrient solution formula altered from Huett (1993) and Sritontip et al. (2017), the 1 liter of solution fertilizers consisted of stock fertilizers A and B. The stock A fertilizer contained 128 g $\text{Ca}(\text{NO}_3)_2 \cdot 4\text{H}_2\text{O}$ and 56 g Fe-EDTA and the stock B fertilizer had 8.7 g $\text{NH}_4 \cdot \text{H}_2\text{PO}_4$, 13.60 g KH_2PO_4 , 133 g KNO_3 , 51.80 g MgSO_4 , 0.30 g MnSO_4 , 0.20 g ZnSO_4 , 0.035 g CuSO_4 , 0.55 g HBO_3 , and 0.0175 g

$(\text{NH}_4)_2\text{MoO}_4$. The pH of the nutrient solution was maintained within the range of 6.5 with the addition of sulfuric acid. The humic acid solution was added in 200 liters for nutrient solution containers.

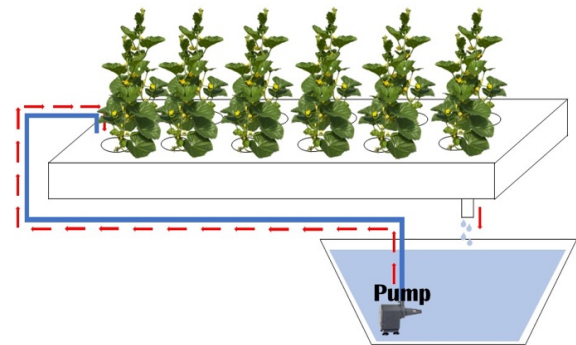


Figure 1. Hydroponic system model for growing of melon.

The physiology characteristics of melon were measured, including the number of leaves, stem height (cm), the diameter of trunk (mm), canopy width (cm), leaf width (cm), leaf length (cm), and stem diameter (mm). Changes in the greenness of the leaf were detected using the Konica Minolta model SPAD-502 plus®. In addition, changes in the chlorophyll fluorescence of melon leaf were measured by using Handy PEA+® (Hansatech instruments, England), and were recorded every week after growing into a hydroponics system. Data were analyzed for Analysis of Variance (ANOVA) which statistical differences with P-values less than 0.05 were considered significant. Then, means were compared by Duncan's Multiple Range Test (DMRT). The statistical model was: $Y_{ij} = \mu + \tau_i + \varepsilon_{ij}$ where: Y_{ij} is the j^{th} observation of the i^{th} treatment, μ is the population mean, τ_i is the treatment effect of the i^{th} treatment, and ε_{ij} is the random error (Steel et al., 1997).

RESULTS AND DISCUSSION

The vegetative growth parameters of melon grown in a hydroponic system were compared after being treated with different humic acid concentrations from 7 to 35 days. The results showed that the humic acid concentrations at 25, 50, and 150 mg/L in nutrient solution significantly increased plant height (Figure 2a). In addition, the canopy width of the 50 mg/L humic acid treatment was greater than the other treatments (Figure 2b). The 200 mg/L humic acid treatment yielded the lowest canopy width. The leaf width and leaf length showed that the humic acid at 50 mg/L treatment increased both parameters while the concentration at 100 and 200 mg/L treatments decreased on both (Figure 2c and d).

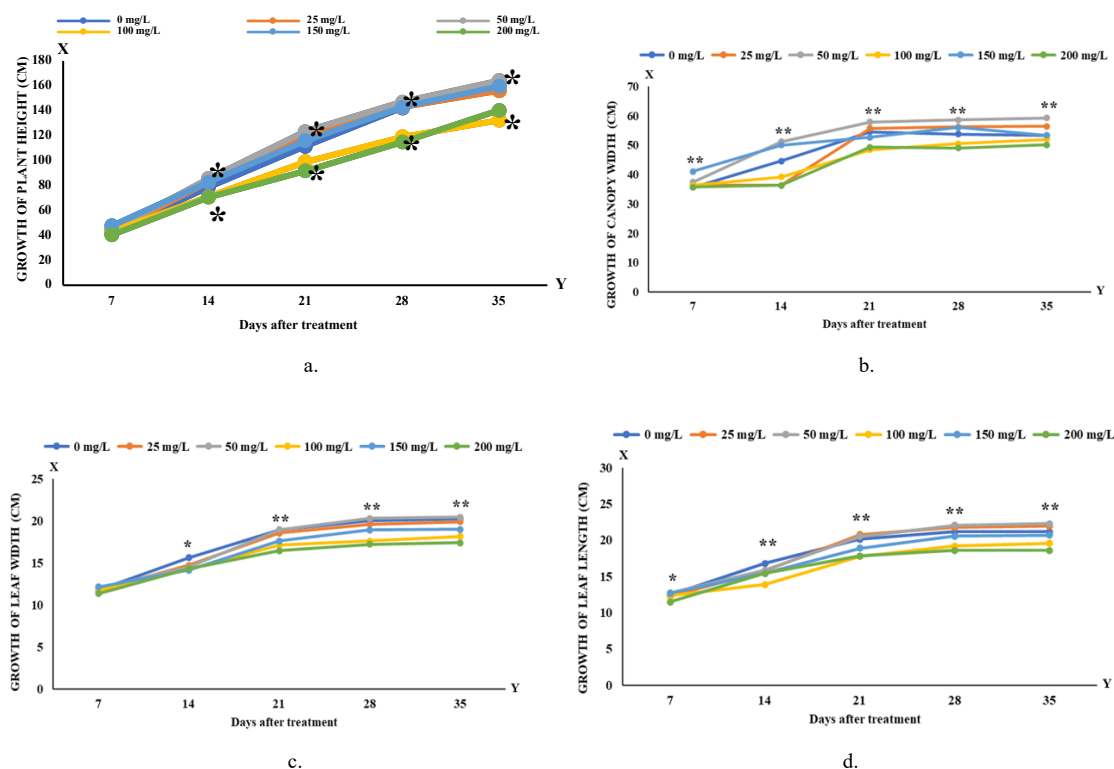


Figure 2. Effect of humic acid on vegetative growth of melon at 7 to 35 days after transplant (a) plant height, (b) canopy width, (c) leaf width, (d) and leaf length.

The physiological characteristics at day 14 found that the stem diameter of 150 mg/L humic acid plants gave the highest (8.74 mm), which was significantly different from those of 50–100 mg/L.

However, the leaf number per vine and leaf green color index were not significantly different. Moreover, humic acid at 100–200 mg/L resulted in chlorophyll fluorescence reduction (Table 1).

Table 1. Effect of humic acid on physiological characteristics of melon at 14 days after treatments

Treatments	Leaf number (leaves)	Leaf green color index (SPAD)	Chlorophyll fluorescence (Fv/Fm)	Stem diameter (mm)
Control	10.70	41.80	0.732 ^{ab}	8.22 ^{ab}
Humic acid 25 mg/L	11.80	43.46	0.745 ^a	8.06 ^{ab}
Humic acid 50 mg/L	11.70	41.68	0.740 ^a	6.92 ^c
Humic acid 100 mg/L	10.90	41.35	0.683 ^b	7.91 ^b
Humic acid 150 mg/L	12.50	41.44	0.702 ^b	8.74 ^a
Humic acid 200 mg/L	11.60	41.66	0.686 ^b	8.19 ^{ab}
F-test	ns	ns	*	**

The values with the same superscript within a column are statistically non-significant by Duncan’s test at $P > 0.05$. The asterisk indicates significantly different means (*for $P \leq 0.05$, **for $P \leq 0.01$), otherwise not significant (ns).

At 35 days after treatment, the results indicated that leaf number was significantly different among the treatments. The number of leaves of control, 50 and 150 mg/L humic acid treatments were significantly higher than that of 100 mg/L humic acid. Moreover, the leaf green color index values (SPAD) of control, 25 and 50 mg/L treatments were

significantly higher than other treatments, while the 200 mg/L humic acid plants gave the lowest. Humic acid factors did not affect melon stem diameter at 35 days after treatment. On the other hand, increasing humic acid concentrations lowers chlorophyll fluorescence (Table 2).

Table 1. Effect of humic acid on physiological characteristics of melon at 14 days after treatments

Treatments	Leaf number (leaves)	Leaf green color index (SPAD)	Chlorophyll fluorescence	Stem diameter (mm)
Control	26.80 ^a	57.80 ^a	0.840 ^{ab}	8.89
Humic acid 25 mg/L	25.70 ^{ab}	56.03 ^a	0.843 ^a	8.71
Humic acid 50 mg/L	26.00 ^a	56.10 ^a	0.842 ^a	8.69
Humic acid 100 mg/L	24.30 ^b	51.66 ^b	0.839 ^{ab}	8.64
Humic acid 150 mg/L	26.70 ^a	50.11 ^b	0.838 ^b	9.34
Humic acid 200 mg/L	25.40 ^{ab}	45.74 ^c	0.826 ^c	9.09
F-test	*	**	**	ns

The values with the same superscript within a column are statistically non-significant by Duncan's test at $P > 0.05$. The asterisk indicates significantly different means (*for $P \leq 0.05$, **for $P \leq 0.01$); otherwise not significant (ns).

The application of humic acid of 25 and 50 mg/L resulted in better plant growth, including stem height, canopy width, leaf width, leaf length, leaf greenness (SPAD), and chlorophyll fluorescence than the application of humic acid at 100, 150, and 200 mg/L.

The vegetative growth of melon increased after the plants were treated with humic acid at 25 and 50 mg/L when compared with the control, especially in plant height, canopy width, leaf width, and leaf length to the hormones auxin which promotes growth of plant roots and shoots. The results from this experiment agreed with Rzepka-Plevnes et al. (2011), who reported that the growth of strawberries cultured on a medium supplemented with IBA and humic acid was greater than that of cultured on a medium containing only auxin. Wongwaiwiriakit (2013) reported that 25 mg/L of humic acid in $\frac{1}{4}$ MS medium enhanced the growth of eggplant seedlings. Nevertheless, exceeding optimum concentrations of humic acid might not be appropriate for plant growth. Obsuwan et al. (2011) also reported that $\frac{1}{4}$ MS supplemented with humic acid at concentrations higher than 50 ppm decreased the growth of the eggplant seedlings. This research indicated that the growth of melons was positively impacted by applying humic acid in low quantities. However, a higher concentration of humic acid had an adverse effect.

CONCLUSIONS

Applying 25 and 50 mg/L of humic acid positively affected plant height, canopy width, leaf width, leaf length, leaf green color index, and chlorophyll fluorescence of the melon plant. However, increasing humic acid at 100 to 200 mg/L

reduced leaf width, leaf length, leaf green color index, and chlorophyll fluorescence.

ACKNOWLEDGMENTS

We thank Mae Moh Power Plant Public Relations, Electricity Generating Authority of Thailand (EGAT), for providing humic acid for being used in this experiment.

REFERENCES

- Britannica, T.E.E. 2023. Watermelon. Encyclopedia Britannica, <https://www.britannica.com/plant/watermelon>. Accessed 24 September 2023.
- Canellas, L. P., Canellas, N. O. A., Luiz Eduardo, L. E. S., Olivares, F. L., and Piccolo, A. 2020. Plant chemical priming by humic acids. *Chemical and Biological Technologies in Agriculture*. 7: 12.
- DAE. 2017. Department of Agriculture Extension: Cantaloupe in 2016. Available Source: <http://www.agriinfo.doae.go.th/year60/plant/roitor/veget/18.pdf>.
- Fatahian, V., Halim, R.A., Ahmad, I., Chua, K., Teh C.B.S., and Awang, Y. 2013. Melon production using four hydroponic systems. *Acta Horticulturae*. 1004 (85–92)
- Fhoythaworn, J., and Agkhadsri, D. 2021. Melon nutrient requirements in highland areas. <https://www.hrdi.or.th/Articles/Detail/1474Highland> Research and Development Institute (Public Organization).
- Fuentes, M., Baigorri, R., González-Gaitano, G., and García-Mina, J. M. 2018. New methodology to assess the quantity and quality of humic substances in organic materials and commercial products for agriculture. *Journal of Soils Sediments*. 18: 1389–1399.
- Garcia, D., Cegarra, J., and Abad, M. 1996. A comparison between alkaline and decomplexing reagents to extract humic acids from low-rank coals. *Fuel processing technology*. 48(1): 51–60.
- Huett, D. O. 1993. Managing nutrient solutions in hydroponics. NSW Agriculture and Horticultural Research & Development Corporation. Wollongbar, New South Wales.

- Jomhataikool, B., Kuboon, S., Kraithong, W., and Eiad-ua, A. 2017. Humic substance extraction from leonardite, lignite Mae Mho Mine by base-acid treatment process. *The Journal of Applied Science*. 16 (Special issue): 26–32.
- Jomhataikool, B., Faungnawakij, K., Kuboon, S., Kraithong, W., Chutipaichit, S., Fuji M., and Eiad-uai, A. 2019. Effect of humic acid extracted from Thailand's leonardite on rice growth. *Journal of Metals, Materials and Minerals*. 29(1): 1–7.
- Nardi, S., Pizzeghello, D., Muscolo, A., and Vianello, A. 2002. Physiological effects of humic substances on higher plants. *Soil Biology and Biochemistry*. 34: 1527–1536.
- Ngennyoy, S., Jutamane, K., Rungmekarat, S., and Kaokaew, S. 2014. Effect of humic substance and chemical fertilizer application on plant nutrient, growth and yield of maize (*Zea mays* L.). In: *Proceedings of 52nd Kasetsart University Annual Conference: Plant*, 4–7 Feb 2014. Kasetsart University, Bangkok. p.252–259.
- Obsuwan, K., Namchote, S., Sanmanee, N., Panishkan, K., and Dharmvanij, S. 2011. Effect of various concentrations of humic acid on growth and development of eggplant seedlings in tissue cultures at low nutrient level. *International Scholarly and Scientific Research & Innovation*. 5(8): 494–496.
- Ratanaprommanee, C., and Shutsrirung, A. 2014. Chemical properties and potential use in agriculture of leonardite from different sources in Thailand. In: *Proceedings of the 5th National and International Hatyai Conference*. May 16, 2014. Hatyai University, Hat Yai, Songkhla. p. 1236–1246.
- Rzepka-Plevnes, D., Kulpa, D., Gołębiewska, D., and Porwolik, D. 2011. Effects of auxins and humic acids on in vitro rooting of strawberry (*Fragaria x ananassa* DUCH.). *Journal of Food, Agriculture & Environment*. 9(3&4): 592–595.
- Shah, Z. H., Rehman, H. M., Akhtar, T., Alsamadany, H., Hamooh, B. T., and Mujtaba, T. 2018. Humic substances: determining potential molecular regulatory processes in plants. *Frontiers in Plant Science*. 9: 263.
- Sritontip, C., Changjeraja, C., Khaosumain, Y., Panthachod, S., Sritontip, P. and Lasak, S. 2017. *Low-cost soilless cultivation* (1st ed). Rajamangala University of Technology Lanna, Chiang Mai.
- Steel, R.G.D., Torrie, J.H. and Dickey, D.A. 1997. *Principles and procedures of statistics: A biometrical approach*. McGraw Hill Book Company, New York.
- Thichuto, S., Sritontip, P., Thonglek, V., and Sritontip, C. 2022. Effects of electrical conductivity and micro/nanobubbles in nutrient solutions of hydroponics on growth and yield of cherry tomato. *Journal of Science and Agricultural Technology*. 3(2): 29–36.
- Tung, L.Q., and Sritontip, C. 2022. Effects of micro/nano-bubble on growth and development of Muskmelon using hydroponic system. *Vietnam Journal of Science, Technology and Engineering*. 64(2): 18–23.
- Wongwairiyakit, R. 2013. Study of humic acid at various concentration in substitution with chelating agent on growth and development of eggplant seedling at low nutrient level in tissue culture. Master's thesis. Silpakorn University.
- Yigit, F., and Dikilitas, M. 2008. Effect of humic acid application on the root-rot diseases caused by *Fusarium* spp. on tomato plant. *Plant Pathology Journal*. 7(2): 179–182.

INSTRUCTION FOR AUTHORS

1. Types of articles and formats

Manuscripts may be submitted to JSAT in the form of Review Articles or Research Articles and must be clearly and concisely written in English with appropriate pages.

2. Preparation of manuscripts

All manuscripts must be prepared and submitted as single Word file (.docx) (Word 2010 or higher). For English font, please use “Time New Roman” with text size of 12 point. Please prepare your manuscript in double-space on A4-sized page. Line number must be used continuous numbering in manuscript. The submitted manuscript should be organized as follow:

2.1) Title

The title of manuscript should be supplied with enough information to catch the attention of readers.

2.2) Author names and affiliations

Please clearly indicate the given name(s) and family name(s) of each author and check that all names are accurately spelled. Indicate the corresponding author by “*”. If authors have different addresses, numbered superscripts are required to refer to each address provided. The format of authors’ affiliations should be: 1. Department, University, City name, State name, Postal code and Country. Corresponding author must inform email.

2.3) Abstract and keywords

Abstract - A concise abstract with maximum of 200 - 250 words identifying the new and significant results of the study must be provided for all manuscripts.

Keywords: – At least 3 to 5 keywords must be given below abstract and use “comma (,)” to separate each.

2.4) Introduction

Author should prepare the introduction with suitable length and keep it as short as possible.

2.5) Materials and methods

This section contains details about materials, techniques, apparatuses, experimental design, and environment. Sufficient detail should be provided to permit the reader to repeat the experiments. For the manuscript reports the utilization of chemical, please provide the purity of all chemicals used in this part.

2.6) Results and discussion

In this part, the results and discussion can be combined or separated depends on author design. Please use tables, graphs, diagrams, and photographs to provide a clear understanding of the results. Quantitative measures of significance (P-values) should be presented. Authors may use either absolute P-values or a defined significance level as long as usage is consistent. Discussion contains the interpretation of the results into existing literature. It should be clear and concise, address the related mechanisms and their significance.

2.7) Conclusions

Clear and significant conclusions should be provided and related to the results and objectives of your work.

2.8) Acknowledgments

In this section, financial and material support should also be mentioned. Authors should list all funding sources in this acknowledgments section. The names of funding organizations should be written in full. List those individuals who provided support during the research

2.9) References

2.9.1) In text citations, please use name-year system such as:

a. Before texts: Smith (2018)...., Tsuji and Hayate (2012)...., Smith et al.(2019)...., Smith (2018); Tsuji (2012)...., Smith et al.(2018a); Smith et al.(2008b)....

b. After texts: (Smith, 2018), (Tsuji and Hayate, 2012), (Smith et al., 2019), (Smith, 2018; Tsuji, 2012), (Smith et al., 2018a; Smith et al., 2008b)

2.9.2) References list

Published literatures or unpublished works must be listed alphabetically by surname of author at the end of the manuscript. Each reference to a periodical publication must include, in order, the name(s) of the author(s), the year of publication, the full title of the article, the publication in which it appears, the volume and inclusive page numbers, and the digital object identifier (DOI), if available. Examples of references are listed as follow:

- Journal article

Halmilton, M.B., Pincus, E.L., Fion, A.D., and Fleischer, R. C. 1999. Universal linker and ligation procedures for construction of genomic DNA libraries enriched for microsatellites. *Biotechniques*. 27: 500-507. <https://doi.org/xx.xxxxxxxx>

Gupta, A.P., and Kumar, V. 2007. New emerging trends in synthetic biodegradable polymers-poly lactide: A critique. *European Polymer Journal*. 43: 4053-4074.

- Book

Carr, R.L. 1976. *Powder and granule properties and mechanics*. Marcel Dekker Publisher, New York.

- Chapter in book

Jackson, M.B. 1982. Ethylene as a growth promoting hormone under flooded conditions. In: Wareing, P.F. (ed) *Plant growth substance*. Academic Press, London. p.291-301.

- Proceeding, symposia etc.

Pratt, A., Gilkes, R.J., Ward, S.C., and Jasper, D.A. 2000. Variations in the properties of regolith materials affect the performance of tree growth in rehabilitated bauxite mine-pits in the Darling Range, SW-Australia. In: Brion, A., and Bell, R.W. (eds) *Proceeding of Remade Land 2000, the International Conference on Remediation and Management of Degraded Lands*. Fremantle, 30 Nov-2 Dec 2000. Promaco Conventions, Canning Bridge. p.87-88.

- Dissertation

Senthong, C. 1979. Growth analysis in several peanut cultivars and the effect of peanut root-knot nematode (*Meloidogyne arenaria*) on peanut yields. Ph.D. Dissertation. University of Florida, Gainesville, Florida, USA.

3. Equation, figure, table and unit of measurement

Equation

All equations presented in the text can be prepared by Equation editor from Microsoft word or Math Type.

Figure

Data presented in figure must be written in English. Color or gray scale figure should be prepared as TIFF format (.tif) with at least 600 dpi. Photograph should be prepared as TIFF (.tif) or JPEG (.jpg) format with at least 600 dpi. Figure with caption should be placed next to the relevant text, rather than at the bottom of the file.

Table

Data presented in table must be written in English. Table with caption and footnote should be placed next to the relevant text, rather than at the bottom of the file.

Unit

Author should use the International System of Units (S.I.)

4. Structure of manuscript

- Title
- Author names and affiliations
- ABSTRACT
- Keywords
- INTRODUCTION
- MATERIALS AND METHODS
- RESULTS AND DISCUSSION (The results and discussion can be combined or separated depends on author design)
- CONCLUSIONS
- ACKNOWLEDGMENTS (if any)
- REFERENCES

5. After acceptance

Authors would be asked to send the “Copyright Transfer Agreement” to JSAT.

6. Publication or processing fee

There is no publication or processing fee.

JSAT

<https://www.tci-thaijo.org/index.php/JSAT>

Vol. 4 | No. 2 | July - December 2023

